International Committee for Future Accelerators

Sponsored by the Particles and Fields Commission of IUPAP

Beam Dynamics Newsletter

No. 31

Issue Editor:
Y. Funakoshi

Editors in Chief:
W. Chou and J.M. Jowett

August 2003

Contents

1 Foreword

1.1 From the Chairman

John Jowett, CERN

mail to: John.Jowett@cern.ch

This issue of the ICFA Beam Dynamics Newsletter has been edited by Dr Yoshihiro Funakoshi who has chosen the special theme of High Luminosity e^+e^- Colliders. I believe that he has compiled a very interesting and timely survey that will be of interest for a long time to come. Back in the mid-1980s, e^+e^- collider rings were thought by some to be reaching fundamental or, worse, economic performance limits in energy and luminosity and that there was little left to be done with them. Early proposals for double-ring multi-bunch factories with luminosities of order $10^{33}cm^{-2}s^{-1}$ seemed, to some at least, to rely on optimistic extrapolations of doubtful schemes.

Since then, perceptions have changed! The machines that ran through the 1990s and into the present century have swept aside supposed limits to beam-beam parameters, beam current, energy, crossing angles, transverse and longitudinal polarization level and, most spectacularly, luminosity. And there are still good ideas that have yet to be fully exploited. Might there be, for example, a physics case for building a high luminosity Z-factory to collide longitudinally polarized beams? The potential of the e^+e^- collider ring technology is still far from being exhausted.

In recognition of this, the Beam Dynamics Panel has an active working group on High Luminosity e^+e^- Colliders (founded by Dr Funakoshi and now chaired by Dr Caterina Biscari) that brings together accelerator physicists working on the current generation of machines. The next ICFA Advanced Beam Dynamics Workshop (e+e- Factories 2003, to be held at Stanford on 13-16 October 2003) is also devoted to this evergreen topic.

The December 2003 issue of the Beam Dynamics Newsletter will be edited by Dr Jie Gao and will contain a special section on the topic of "Linacs for Future Linear Colliders". It will include contributions from our colleagues in the other ICFA Panel on Advanced and Novel Accelerators.

1.1.1 Changes in the Beam Dynamics Panel

ICFA has appointed Dr Jie Gao of the Laboratoire de L'Accélérateur Linéaire, Orsay, France, as a new Panel member. As previously announced, Dr Junji Urukawa of KEK has also now joined the Panel. On behalf of the Panel, I would like to welcome these new Panel members.

By now, most of us will have heard the very sad news of the death of Jean-Louis Laclare. Among his many achievements, he was formerly a very active member of our Panel and the founder of the Working Group on Future Light Sources. I would like to draw all readers' attention to the obituary by Anick Ropert available at the Working Group's new web site

http://www.aps.anl.gov/asd/ICFA/ICFA-FLS.html

or via the Panel's home page.

1.1.2 ICFA Advanced Beam Dynamics Workshops for 2004

In recent years, ICFA Advanced Beam Dynamics Workshops have been occurring at a steady rate of 3 or 4 per calendar year. I am pleased to announce that, at its meeting in Fermilab on 15 August 2003, ICFA approved three new proposals for Advanced Beam Dynamics Workshops in 2004. These are

- The 31st ICFA ABDW: Electron Cloud Effects "ECLOUD04", Berkeley, USA, 19-22 April 2004.
- The 32nd ICFA ABDW: High Current, High Brightness Electron Injectors and Energy Recovering Linacs for Future Light Sources and Colliders, USA, late spring 2004.
- The 33rd ICFA ABDW: High Intensity High Brightness Hadron Beams "HB2004", Mainz, Germany, September 2004.

Further information about these workshops will appear in this and the next newsletter and will always be available from the Panel's home page:

http://wwwslap.cern.ch/icfa/

As always, thanks are due to the organisers of these and previous workshops for the valuable service they give to the international Beam Dynamics community. Organizing a workshop from the initial planning through to final publication of proceedings is a considerable undertaking over many months.

1.2 From the Editor

Yoshihiro Funakoshi, KEK

mail to: yoshihiro.funakoshi@kek.jp

In this issue of the ICFA Beam Dynamics Newsletter, we have a special section which deals dedicatedly with the high luminosity e+ e- colliders. To focus discussions on common issues among the machines, we confined ourselves to issues of circular colliders. In this field, Working Group on High Luminosity e+ e- Colliders chaired by C. Biscari at LNF has been formed within the Beam Dynamics Panel and has been playing an important role. This issue aims at giving a reference or a basis for further discussions in future in this field. Also this issue includes some outcomes of the working group such as a database on machine parameters of each machine. A motivation of the editor of this issue consists in summing up our present knowledge of the most critical issues in these colliders from the viewpoint of beam dynamics, together with giving clear views of the present status of each machine and its future plan.

2 High luminosity e+ e- colliders

2.1 Beam-Beam Simulations for VEPP-2000

I. Koop, E. Perevedentsev, Yu. Shatunov, A. Valishev
mailto: valishev@inp.nsk.su

Budker Institute of Nuclear Physics
Lavrentyeva av. 11, 630090, Novosibirsk, Russia

2.1.1 Introduction

The round beam collider VEPP-2000 at Novosibirsk [1] is at the stage of construction at the moment. Although the machine design is fixed there is some freedom in the optics tuning which can have impact on the beam dynamics. One of the critical issues of the project are the beam-beam effects. The design goal of the beam-beam parameter for the round beam is 0.075 at energy of 1 GeV per beam and 0.1 (or higher) as an option to be tested.

Previous studies have shown strong dependence of the beam-beam phenomena in the round beam on the nonlinear betatron dynamics, e.g. due to sextupoles [2]. Hence, the beam-beam problem for VEPP-2000 was studied together with the choice of main optical parameters: betatron function at the interaction point, working point, sextupole chromaticity correction scheme.

In this report we give a summary of numerical simulations of beam-beam effects for VEPP-2000 to justify the choice of optics parameters. We used two approaches: the strong-strong simulation with a modified version of Ohmi's code [3]; and the weak-strong model where this code is compared with Shatilov's LIFETRAC [4].

2.1.2 Machine parameters

Here we briefly recall main parameters of the machine important for simulations. VEPP-2000 design consists of two symmetrical arcs with two diametrically opposite symmetrical Interaction Points. In the main regime the transverse betatron modes are rotated by the final focus solenoids by $+\pi/2$ in one IP and by $-\pi/2$ in another which results in equal emittances. Requirement of conservation of the longitudinal component of the particle's angular momentum results in equal β^*-functions and fractional betatron tunes. Both e^- and e^+ beams contain 1 bunch. Beam energy in simulations was 0.9 GeV. Table 1 shows the parameres of VEPP-2000 which resulted from optimization.

2.1.3 Strong-strong case

The strong-strong case presupposes solution of self-consistent problem for the system of two colliding beams. This model is more realistic compared to the weak-strong one but at the same time more difficult to realize and requires considerable computer resources. The computer code developed at KEK by Ohmi shows good agreement with experimental data for KEKB. It is described in detail in [3]. For our simulation we modified the part of the code responsible for arc transformation: sextupoles were introduced as thin elements with linear transformations between them and random excitation was changed to include the dynamical

emittance change [5]. Since the damping time for VEPP-2000 is 10 times larger than for KEKB, the tracking time increases in proportion. Hence, we used the 2-D version of the code with infinitely thin bunches, excluding longitudinal effects. For further reference we call this code 'BBSS'.

Table 1 Main parameters of VEPP-2000.

Parameter	Value
Circumference	24.38 m
Momentum compaction	0.036
Synchrotron tune	0.0035
Energy spread	6.4×10^{-4}
Beam emittances (x,y)	1.29×10^{-7} m rad
Dimensionless damping decrements (x,y,z)	$2.19\times10^{-5}, 2.19\times10^{-5}, 4.83\times10^{-5}$
Betatron tunes	4.05, 2.05
Betatron functions @ IP	10 cm

Initial design parameters were $\beta^* = 6.3$ cm, $\varepsilon = 2.2\times10^{-7}$ m rad and fractional betatron tune $\nu = 0.1$. Simulation without sextupoles has shown that values of ξ as high as 0.15 can be reached without degradation of luminosity. However, this optics has limited aperture, both dynamical and physical which is limited in the solenoids of the final focus. Limited dynamical aperture results in degradation of the beam life time at ξ higher than 0.06 even without beam size blow-up.

This problem initiated the search of new optics aimed at increasing the aperture. Increasing of the β^* value from 6.3 to 10 cm with simultaneous reduction of the beam emittance allows to conserve the beam size at IP and luminosity at constant bunch population. The betatron tune was changed to 0.05. Together with improvement of the phase relations between sextupoles this resulted in enhancement of the aperture. Figure 1 shows the simulated dependence of the beam size and luminosity on the nominal beam-beam parameter. With the new optics parameters no particle losses were detected in simulation up to $\xi = 0.1$.

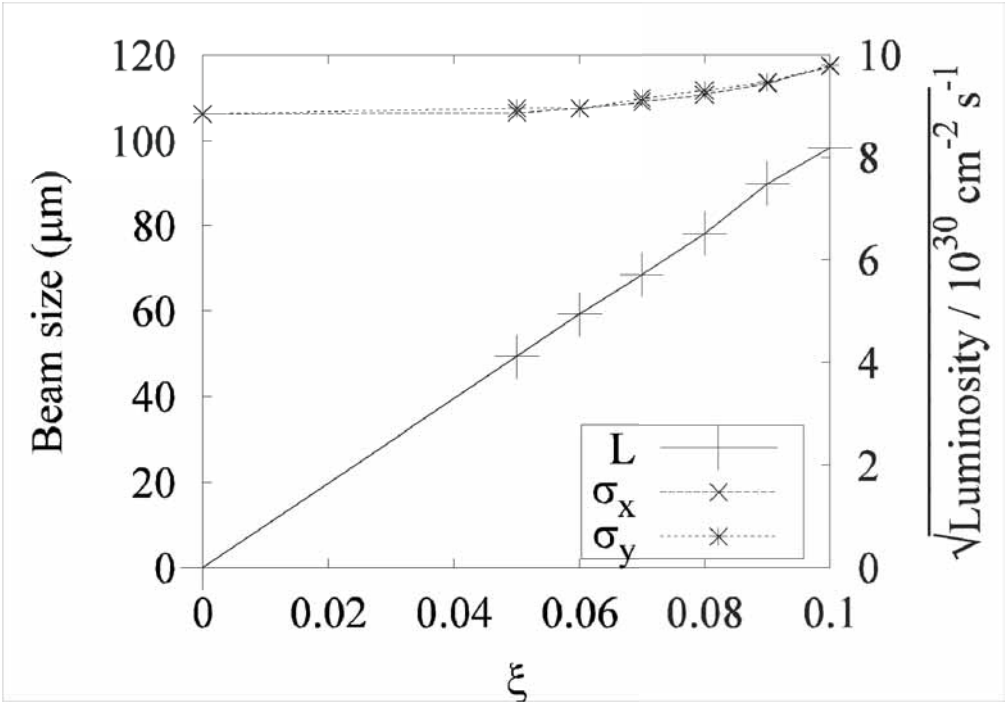

Figure 1 Beam size and luminosity vs. the beam-beam parameter. Strong-strong 2-D simulation.

2.1.4 Weak-strong simulation

Because of its speed, the weak-strong model is good for preliminary estimates. We have at our disposal a well-tested code LIFETRAC by D. Shatilov [4]. BBSS also can be run in quasi weak-strong mode when intensities of the bunches differ significantly (by several orders of magnitude) and it was a good test to compare the two codes. Figure 2 presents results of calculations with sextupoles switched off. At moderate ξ's the simulated emittances do not differ, while at high values of the beam-beam parameter BBSS exhibits bigger beam blow-up. The same situation is seen in Fig. 3, where a similar comparison is shown with sextupoles on. This difference can be explained by the 3-D effects which are excluded in the quasi weak-strong calculation (BBSS). Although the ratio of the bunch length σ_z and β^* is 0.25, the hourglass effect might act on the interaction. The next step of the comparison is to use the 3-D version of BBSS code which is available but very demanding to computer resources.

The weak-strong calculation does not exhibit a serious difference with the strong-strong one (see Fig. 3 which contains two points for the strong-strong case with the same parameters). As regards the beam life time, the threshold predicted by the weak-strong codes is higher – particles are lost from the beam at ξ's above 0.12 for BBSS and 0.15 for LIFETRAC.

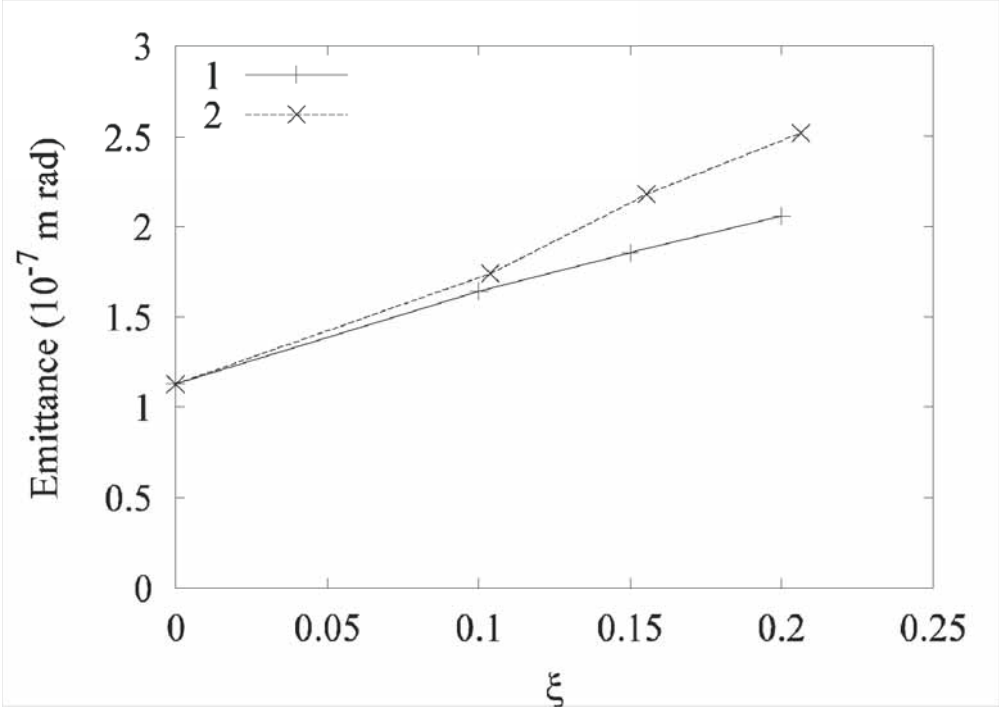

Figure 2 Emittance of the weak beam vs. the beam-beam parameter. Sextupoles off. 1 - LIFETRAC, 2 - BBSS in weak-strong regime.

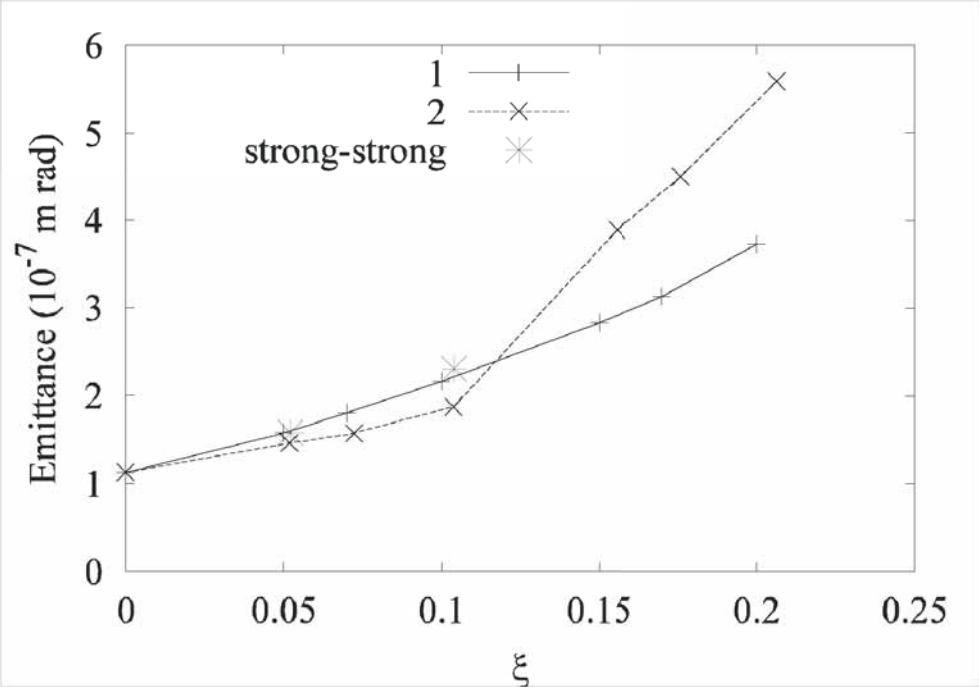

Figure 3 Emittance of the weak beam vs. the beam-beam parameter. Sextupoles on. 1 - LIFETRAC, 2 - BBSS in weak-strong regime.

2.1.5 Summary

Both weak-strong and strong-strong simulations of beam-beam interaction for round colliding beams at VEPP-2000 predict a possibility to reach the design luminosity of $1\times10^{32} cm^{-2}s^{-1}$ at 1 GeV. With unlimited dynamical aperture the beam-beam parameter can be as high as 0.2 without degradation of luminosity. Chromaticity correction sextupoles limit the dynamical aperture and lead to decrease of the beam life time at ξ's above 0.1. Meanwhile, sextupoles do not cause beam blow-up and do not set a beam-beam limit. Comparison of two weak-strong codes did not reveal a significant difference in the results. Existing discrepancy could be explained by 3-D effects, e.g. hourglass effect excluded in one of the codes.

Future efforts will be concentrated on the 3-D strong-strong simulation and on improvement of the arc tracking. Higher order nonlinearities such as cubic should be implemented, since the lattice of VEPP-2000 contains strong solenoids. Their fringe-fields might have a serious impact on the beam dynamics.

Acknowledgements

We are grateful to K. Ohmi and D. Shatilov for the codes and helpful discussions on their usage and development of the simulation. This work is supported by ISTC grant 1928.

References

1. Yu.M. Shatunov *et al.*, in *Proceedings EPAC'2000*, 439.
2. I. Nesterenko, D. Shatilov, E. Simonov, in *Proceedings PAC'1997*, 1762
3. K. Ohmi, Phys. Rev. E **59**, 7287 (2000)
4. D. Shatilov, Part. Accel. **52**, 65 (1996)
5. A. Valishev, E. Perevedentsev, K. Ohmi, in *Proceedings PAC'2003*.

2.2 Beam Dynamics Issues in DAΦNE e^+e^- Φ-Factory

M. Zobov

mail to: Mikhail.Zobov@lnf.infn.it

INFN-LNF
Via Enrico Fermi, 40 - 00044 Frascati, Italy

2.2.1 Introduction

The Frascati Φ-factory DAΦNE is an e^+e^- collider designed to provide very high luminosity at the energy of the Φ-resonance (1020 MeV in the center of mass) [1]. The most relevant DAΦNE parameters are summarized in Table 1. The layout of the collider is shown in Fig. 1.

The first experimental detector KLOE [2], aimed at the study of CP violation, has been installed in the Interaction Region 1 (IR1) of DAΦNE in March 1999. Since then the collider alternated machine study and physics data taking shifts. Later, a small non-magnetic experiment for the study of the properties of kaon atoms (DEAR [3]) was installed on the second IR. By collecting about 107 pb^{-1} of the integrated luminosity in 2002, the DEAR experiment has completed its experimental program on observation of the kaonic nitrogen and has made first experimental tests on the hydrogen target.

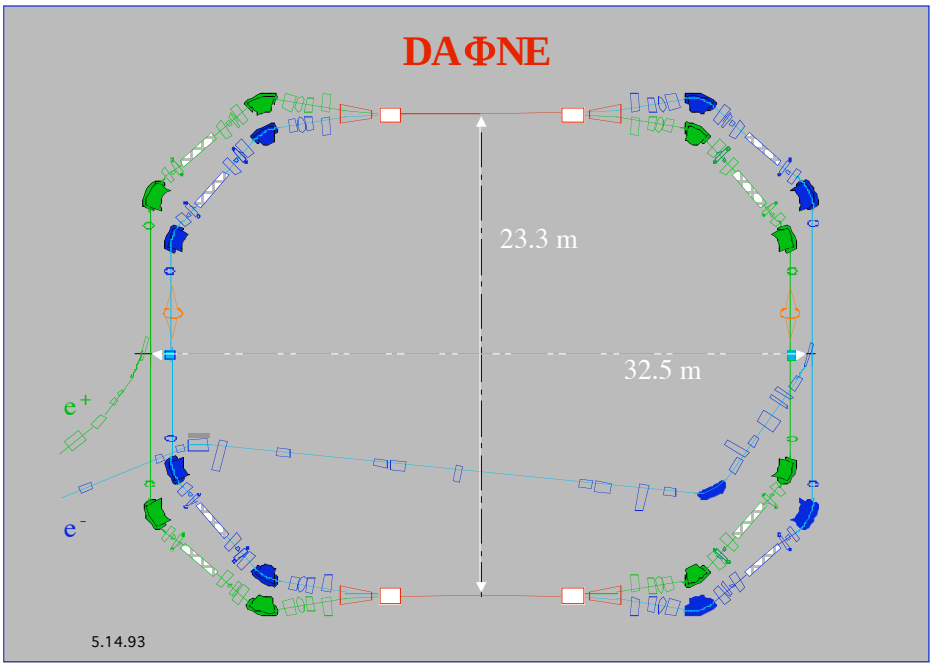

Figure 1: DAΦNE Magnetic Layout

Table 1: Main DAΦNE Parameters

Beam Energy [GeV]	0.51/ring
Circumference [m]	97.69
RF Frequency [MHz]	368.29
Harmonic Number	120
Momentum Compaction	0.02-0.03
RF Voltage [kV]	120-170 (present operation) 250 (nominal)
Natural Bunch Length [cm]	~1.4 (at 120 kV) ~1.0 (at 250 kV)
Damping Time [ms]	17.8 (longitudinal) 36.0 (transverse)
Emittance [mm mrad]	1.0 (design) 0.6 (present operation)
β_y/β_x at IP [m]	0.045/4.5 (design) 0.027/1.7 (present operation)
Coupling, %	1 (design) 0.2 (achieved)
Maximum Beam Current [A]	2.1 (electron ring) 1.3 (positron ring)
Design Luminosity [cm^{-2} s^{-1}]	$1.2x10^{32}$ (phase I) $5.0x10^{32}$ (phase II)
Achieved Luminosity at KLOE [cm^{-2} s^{-1}]	$0.8x10^{32}$
Achieved Luminosity at DEAR [cm^{-2} s^{-1}]	$0.7x10^{32}$
Integrated Luminosity at KLOE [day/pb]	4.8
Integrated Luminosity at DEAR [day/pb]	2.2

During the collider shut down in the first half of this year, the experimental detector FINUDA [4] has been rolled-in and now it is ready for data taking. The experiment is dedicated to the study of hypernuclei physics. During the four years of machine operation both the peak and the integrated luminosity have been steadily increasing, as shown in Fig. 2. The maximum peak luminosity for the KLOE experiment has achieved $0.8x10^{32}$ cm^{-2} s^{-1} with the maximum daily integrated luminosity of 4.8 pb^{-1}. The total integrated luminosity delivered so far to KLOE amounts to 530 pb^{-1}.

The maximum peak luminosity of $0.7x10^{32}$ cm^{-2} s^{-1} in the runs for DEAR has been obtained by trying the collider operation with 100 consecutive bunches (out of available 120) [5]. This has allowed almost doubling the daily integrated luminosity, from 1.1 pb^{-1} to 2 pb^{-1}, with respect to the operation with 50 bunches separated by 1 empty bucket, thus helping to complete the DEAR program.

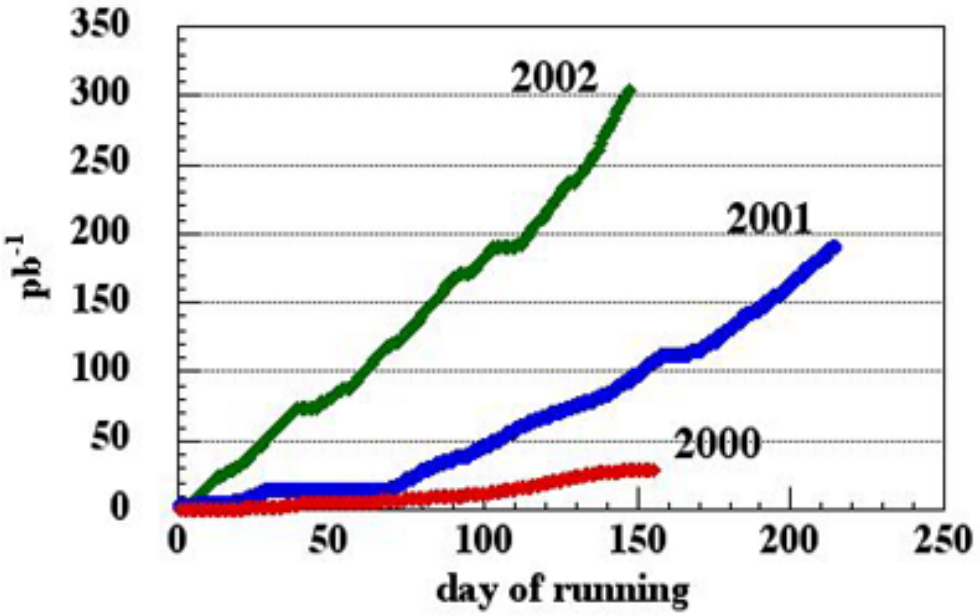

Figure 2: DAΦNE Integrated Luminosity.

This progress became possible due to continuous machine physics study. The major steps, which have led to the luminosity performance improvement, can be summarized as following:

- working point choice;
- coupling correction;
- nonlinear beam dynamics study;
- implementation of the "detuned" optics;
- reduction of both vertical and horizontal beta functions at the interaction point (IP);
- single- and multibunch instability cures;
- gradual collider parameter optimization.

Besides, a basis for further luminosity performance improvements has been created:

- a reliable linear optics model has been elaborated and successfully applied for the collider optimization. Substantial efforts have been invested to explore the machine nonlinear behavior since further luminosity improvement is impossible without knowledge of the nonlinear beam dynamics;
- intensive numerical simulations of beam-beam effects have revealed the importance of the working point choice, coupling, crosstalk between beam-beam effects and lattice nonlinearities and this has been proven in practice. The simulations have provided us with guidelines for future luminosity improvement;
- we have created tools, techniques and methods for deeper machine studies;
- analysis and cures of beam instabilities have allowed colliding stable beams with the world record level currents. There are no serious obstacles now to push the beam currents above 2 A.

In this paper we give a synthetic overview of the above listed activities. More details can be found in published papers quoted in References. We also discuss our proposals aimed at increasing the luminosity to meet the ultimate design goal and to exceed it.

2.2.2 Present Working Point

A systematic study of beam-beam effects in DAΦNE both analytical and numerical [6], started well prior to the collider commissioning. Among predicted best working points those at (0.09; 0.07), (0.10; 0.14) and (0.15; 0.21) were suggested. It has been shown that due to the long damping time (in terms of revolution turns) and weak noise, even rather high order beam-beam resonances can affect the collider performance. In particular, tune scans performed with BBC [7] and LIFETRAC [8] codes indicated that:

- the betatron resonances up to 6-8 order affect the beam core and lead to the beam blow up;
- the resonances up to 11-12 order influence the distribution tails and may limit the lifetime;
- the tail growth is sensitive to small tune variations of the order of ~ 10^{-3};
- the only working point on the tune diagram above the integers where the project parameters can be met is (0.09;0.07) and a limited area around this point;
- the beam-beam tune shift parameter of $\xi_{x,y} = 0.03$ (lower than the design value of 0.04) without core blow up can be reached at the point (0.15;0.21) and (0.10;0.14).
- for the working points (0.09;0.07), (0.15;0.21) and (0.10;0.14) the distribution tails are confined well within the dynamic aperture.

During "Day One" collider commissioning (without the experimental solenoidal detector) the working point (0.15; 0.21) was chosen for collisions instead of (0.09; 0.07). Despite reduction in expected luminosity in comparison with the point (0.09; 0.07), the chosen point has a number of advantages appreciable at the commissioning stage:

- the closed orbit is less sensitive to machine errors;
- easier coupling correction;
- larger dynamic aperture;
- smaller second order chromaticity term;
- etc.

An intensive numerical study has been carried out for the given working point [9], considering different factors affecting the collider luminosity performance such as the separation at the second interaction point (IP), vertical crossing angle, lattice nonlinearities, parasitic crossings, interaction with two IPs etc.

The luminosity of 1.6×10^{30} $cm^{-2}s^{-1}$ obtained in single bunch collisions was close to that estimated by BBC and LIFETRAC (2.2×10^{30} $cm^{-2}s^{-1}$). Experimental tune scan around (0.15; 0.21) showed that the beam-beam lifetime agreed well with LIFETRAC tail growth predictions [10]. That is why the commissioning with the installed experimental detector resumed at the same working point. However, it was found that the nonlinear beam dynamics was different for the electron and positron rings at this point. This fact pushed us to start studying the nonlinear dynamics more intensively and led to working point evolution during the commissioning.

The evolution of the working points in the two rings with reasons explaining the eventual changes is shown in Fig. 3.

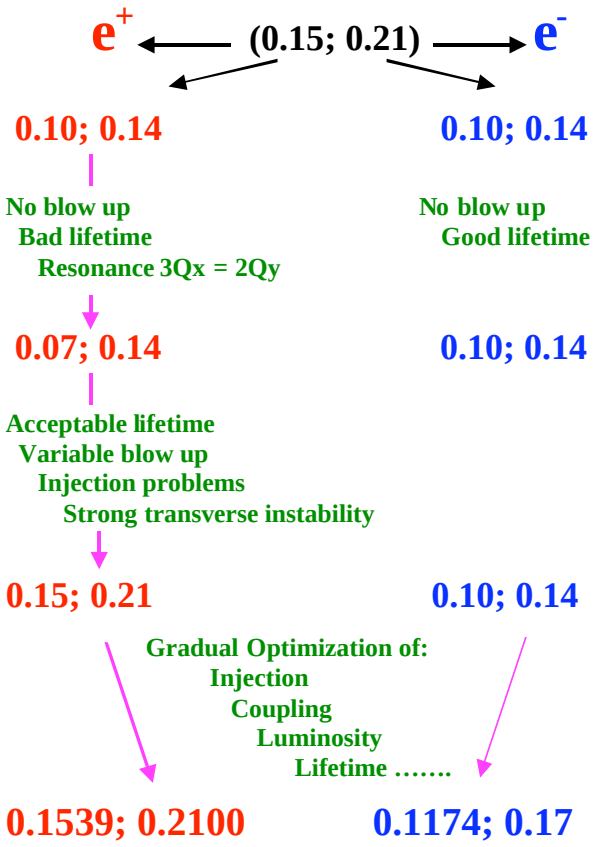

Figure 3: DAΦNE working point evolution.

At the beginning of the commissioning with KLOE we found out that the electron beam lifetime was very low in the vicinity of the working point (0.15; 0.21) even without beam-beam collisions. On the contrary, the positron beam lifetime was good.

As the first step, we changed the working point in the both rings from (0.15; 0.21) to (0.10; 0.14) which, according to simulations, also could provide an acceptable luminosity performance. The situation completely reversed for this case. In collisions there was no observable beam blow up for both the electron and for the positron beams up to 7-10 mA per bunch. However, the lifetime of the positron beam was bad, presumably due to the sextupole resonance $3Q_x = 2Q_y$, while the electron beam lifetime was good.

As an intermediate step, the working point (0.07; 0.14) situated at the resonance $2Q_x = Q_y$ was tried for positrons. The lifetime was improved for the point, but we encountered injection problems and also a strong transverse instability was observed there. Yet another negative feature of this point was variable beam blow up: at high currents per bunch the beam core tune was shifting far from the resonance $2Q_x = Q_y$ thus avoiding beam blow up due to that skew sextupole resonance. But for smaller currents the tune shift was decreasing and beam blow up due to the resonance was observable.

Finally, it was decided to run the collider at the asymmetric tunes, i. e. to return back to the working point (0.15; 0.21) for the positron ring and to move the electron ring at the point (0.10; 0.14). After gradual optimization of all collider parameters such as injection, luminosity, lifetime, coupling etc. the working points slightly drifted to (0.1539; 0.21) for e^+ ring and (0.1174;0.17) for the electron one. These tunes are used so far with possible small variations around them for further fine optimization either of the lifetime or the luminosity.

2.2.3 Coupling Correction

Usually, beam-beam interactions are simulated without considering what is an actual source of betatron coupling. One assumes a linear optics between collisions at the IP and coupling is introduced as a ratio between emittances in the vertical and horizontal planes, respectively.

In a real machine different sources can create the same coupling: skew magnets, residual vertical dispersion, solenoids, off-axis sextupole magnets etc. Depending on the coupling sources and their distribution along the ring, the normal betatron modes can propagate in a different way down to the IP. As a consequence, beams may interact differently at the IP resulting in different core blow up and tail growth.

In order to estimate how the design coupling of 1% can affect the luminosity of DAΦNE, we performed numerical simulations with LIFETRAC. For this purpose LIFETRAC was modernized to be able to match the lattice input from MAD with beam-beam simulations [11]. In this way we could simulate different sources of coupling [12]. In particular, as shown in Fig. 4, we compared the results of the simulations when 1% coupling was created by:

- one arbitrary skew quadrupole;
- all available skew quadrupoles;
- due to misalignment of the low β triplet in the KLOE interaction region;
- higher than nominal KLOE detector solenoid field;
- non explicit coupling (traditional way of simulations).

As we can see, the beam core blow up in both transverse planes varies in a wide range. The vertical blow up is small in case of non-explicit coupling and reaches a factor of 4.5 when all skew quadrupoles are adjusted to create 1% coupling. This was a clear indication of necessity to start machine coupling study and correction.

Details of the machine coupling study and consecutive correction are described elsewhere [13]. I just list principal steps that have led to notable coupling reduction:

- global coupling correction with skew quadrupoles;
- adjustment of the KLOE interaction region: KLOE detector solenoid and compensator magnet current variation;
- corrector strength minimization;
- residual vertical dispersion correction;
- nonlinear term minimization;
- working point fine tuning.

As a result, coupling was reduced down to 0.2% for both rings and the luminosity in single bunch collisions increased approximately by a factor of 2.

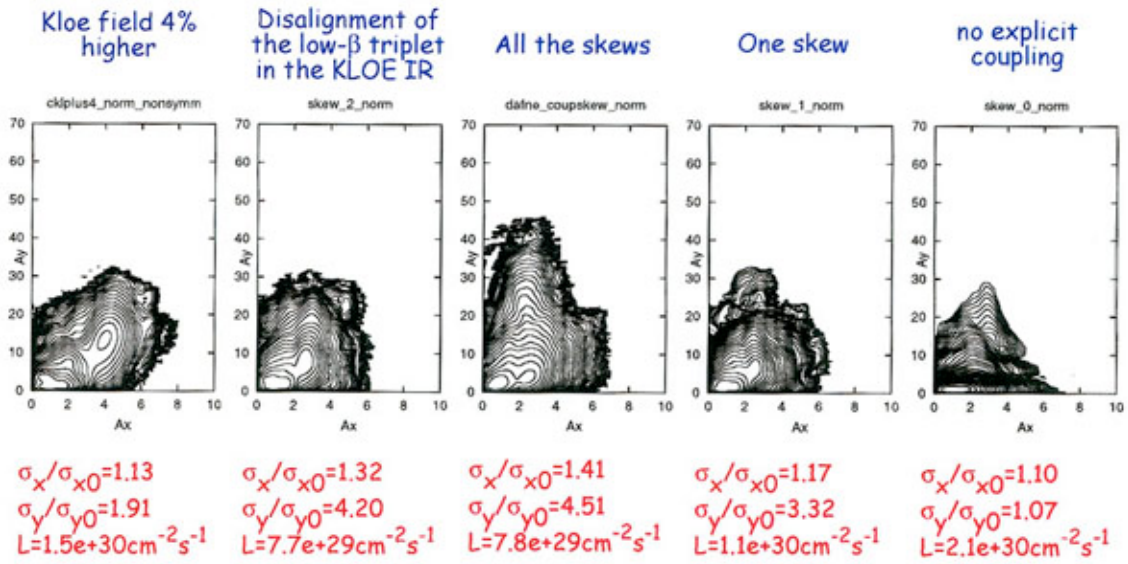

Figure 4: Beam-beam blow up [8] due to different coupling source.

2.2.4 Nonlinear Dynamics Study

As it is well known, lattice nonlinearities can affect significantly beam-beam performance. So, nonlinear dynamics study was considered as an important task for luminosity increase.

The following main techniques were used for that study and performance optimization:

- tune scan;
- dedicated orbit bumps inside incriminated magnetic elements;
- beam decoherence measurements;
- second order dispersion measurements and minimization;
- dedicated octupoles for the cubic nonlinearity and second order chromaticity correction.

The tune scan was used to define safe areas for beam-beam collisions on the tune diagram non affected by nonlinear lattice resonances. By changing the tunes we were observing the lifetime and blow up (roundness at the synchrotron light monitor) of a single bunch. We were surprised that for some tunes situated far from the principal sextupole resonances the beam was dying or beam blow up was observable even without beam-beam collisions.

By analyzing the result we found out that the lattice nonlinear resonances up to the 6^{th} order were responsible of the effect. For example, the resonances $2\Delta Q_x+4\Delta Q_y = 2$, $2\Delta Q_x - 4\Delta Q_y = 1$, $3\Delta Q_x - 2\Delta Q_y = 2$, $\Delta Q_x + 4\Delta Q_y = 1$, $4\Delta Q_x + 2\Delta Q_y = 3$, $4\Delta Q_x + \Delta Q_y = 2$ and others were clearly detectable. The tune areas near the resonance intercrosses were particularly dangerous driving beam blow up or leading to a dramatic beam lifetime reduction.

Since such resonances can be driven only by strong nonlinear lattice magnetic elements, dedicated orbit bumps were performed in order to recognize such elements. Tune shifts versus the closed orbit bump amplitudes were measured to estimate nonlinear contribution of the magnetic elements.

The localized bumps inside the wigglers and consecutive analytical study [14] have shown that the wigglers are sources of strong octupole-like terms providing dominating cubic nonlinearity in DAΦNE. Later this was confirmed by beam decoherence measurements. Besides, the wiggler are responsible of the nonlinear tune dependence on energy and, as it

has been found, their nonlinear behaviour is one of the main reasons of the dynamics aperture limitation, especially for off-energy particles.

By applying the orbit bumps it was also found that the "C" corrector magnets placed at both sides of each interaction region, used to vary the horizontal crossing angle and relative vertical position of the colliding beams, give substantial sextupolar contribution [15].

A decisive step ahead in reduction of the collider nonlinearity was the implementation of the new "detuned" lattice, the lattice that avoids exploiting the low beta insertion at the second interaction point [16]. The main advantages of the lattice can be summarize as follows:

- no low beta IR at the second IP allows to reduce strength of the sextupole magnets used for chromaticity correction or, instead, decrease the vertical beta function at the main IP without the sextupole strength increase;
- the beta functions in the wigglers are lower thus reducing their nonlinear contribution in beam dynamics;
- lower currents in "C" magnet can be used;
- it provides much larger separation of beams at the second "parasitic" IP;
- as consequence, the cubic nonlinearity of the lattice is substantially lower in comparison with "old" KLOE lattice (used before the detuned lattice implementation).

Effects of machine nonlinearity on particle motion were investigated using a dynamic tracking system implemented in the DAΦNE main rings [17]. A single bunch is excited horizontally by pulsing one of the injection kickers. The dynamic tracking system allows to store and to analyze turn-by-turn the position of the kicked bunch. The coherent betatron oscillation amplitude is recorded over 2048 turns providing information on trajectories in phase space and betatron tune shifts with amplitude. Analysis of the coherent oscillation amplitude decay due to nonlinear filamentation gives a possibility to estimate directly a cubic nonlinearity. In particular, we measured the coefficient c_{11} characterizing the strength of the horizontal cubic nonlinearity [18].

During a long machine tune up for collisions different kinds of lattices have been tried. For each lattice configuration the nonlinearity coefficient c_{11} was been measured with the dynamic tracking system. It has been found that c_{11} can change in a very wide range. Moreover, it even changes the sign when the wigglers are switched off. Briefly summarizing the experimental observations and measurements we can say that:

- the highest negative contribution to c_{11} comes from the wigglers and it depends strongly on beta functions at their locations. That is why, in comparison with the "old KLOE lattice", the detuned lattice with lower beta functions at the wiggler positions has weaker negative cubic nonlinearity. And, besides, c_{11} gets positive when the wigglers are completely switched off.
- for most settings the sextupoles give also negative contribution to c_{11}, but usually it is substantially smaller than that of the wiggler.
- we attribute the positive contribution to the cubic nonlinearity to fringing fields in quadrupole magnets.

The numerical simulations of beam-beam effects with LIFETRAC taking into account the measured cubic nonlinearities have shown that they have a dramatic impact on the collider luminosity performance [18]. The numerical results explain most of experimental observations made during collisions in both single and multibunch regimes.

In particular, the strong negative nonlinearity accounts for the low single bunch luminosity during collisions in the "old" KLOE lattice. Figure 5 shows an example of equilibrium distributions in the space of normalized betatron amplitudes for different values of c_{11}.

In the multibunch regime the maximum achievable luminosity is mainly limited by parasitic crossings reinforced by the nonlinearity, if other limiting factors, such as multibunch instabilities, ion trapping and uneven fill are eliminated. This is demonstrated in Fig. 6.

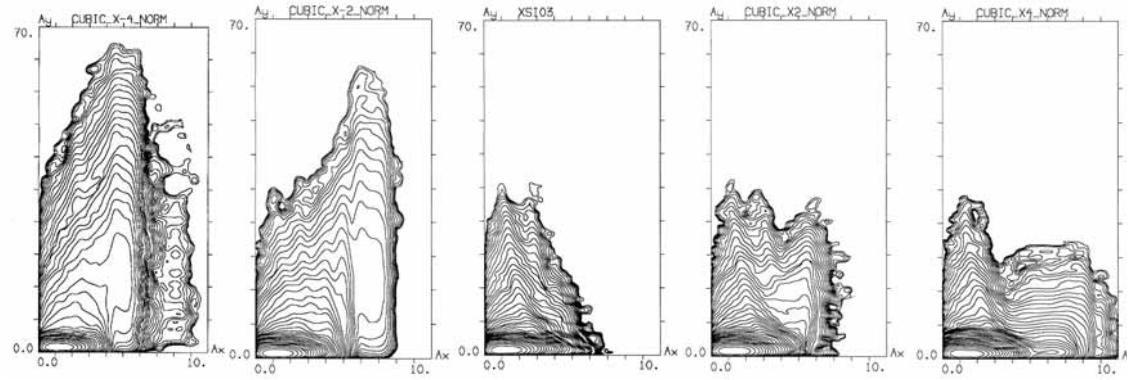

$C_{11} = -400$	$C_{11} = -200$	$C_{11} = 0$	$C_{11} = 200$	$C_{11} = 400$
$\sigma_x/\sigma_{x0} = 1.053$	$\sigma_x/\sigma_{x0} = 1.075$	$\sigma_x/\sigma_{x0} = 1.067$	$\sigma_x/\sigma_{x0} = 1.110$	$\sigma_x/\sigma_{x0} = 1.160$
$\sigma_y/\sigma_{y0} = 1.30$	$\sigma_y/\sigma_{y0} = 1.038$	$\sigma_y/\sigma_{y0} = 1.047$	$\sigma_y/\sigma_{y0} = 1.055$	$\sigma_y/\sigma_{y0} = 1.044$

Figure 5: Beam-beam blow-up and tail growth for different lattice cubic nonlinearities. Contour plates of density in the amplitude space are shown.

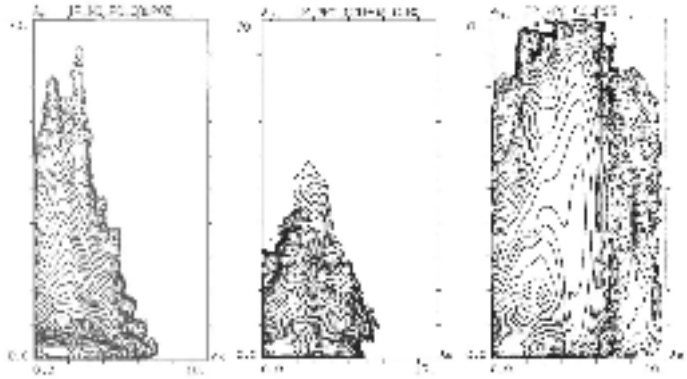

$\sigma_x/\sigma_y = 1.076$	$\sigma_x/\sigma_{x0} = 1.097$	$\sigma_x/\sigma_{x0} = 1.099$
$\sigma_y/\sigma_{y0} = 1.449$	$\sigma_y/\sigma_{y0} = 1.954$	$\sigma_y/\sigma_{y0} = 2.498$
$\tau = \infty$	$\tau = \infty$	$\tau = 36$ sec

Figure 6: Beam-beam blow-up with parasitic crossing and cubic nonlinearity.

According to the simulations, in order to decrease the nonlinearity effects to an acceptable level, its strength should be kept below $|c_{11}| < 200$. Indeed, the present luminosity record was achieved when c_{11} was reduced down to –60 for e^+ ring and to –170 for e^- one.

In order to provide a knob for compensating the cubic nonlinearities and the second order chromaticity correction, three dedicated octupoles were installed in each collider ring[19]. When colliding beams in the DEAR configuration it has been found experimentally that the octupoles adjustment gave about 15% lifetime improvement with bunches separated by 1 empty bucket and up to 40% improvement in 100 consecutive bunch operations.

2.2.5 Single- and Multibunch Instabilities

It is impossible to reach the high luminosity in DAΦNE without providing stable high current multibunch beams. At present the design single bunch current of 44 mA has been largely exceeded. About 200 mA were stored in a single bunch without observing any destroying instability. In the multibunch regime more than 2A were accumulated in the electron storage ring and about 1.5 A in the positron one.

This success has been achieved due to:

- careful study of the vacuum chamber coupling impedance [20] and innovative design of almost all the main vacuum chamber components. New ideas were incorporated in design of such components as RF cavities, longitudinal feedback kickers, shielded bellows, injection and transverse feedback kickers, beam position monitors, DC current monitors etc. [21-27].
- implementation of powerful feedback systems: longitudinal feedback systems, transverse vertical and horizontal feedback systems, 0 – mode feedback system.
- cures of high current instabilities on the basis of experimental observation and analysis of the instability threshold and their dependence of collider parameters: bunch pattern, RF voltage, momentum compaction, bunch length, orbits, feedback timing and many others

As far as single bunch instabilities are concerned, during the past three years we carried out the following measurements:

- measurements of the longitudinal impedance and bunch lengthening in both rings;
- turbulent mode coupling-transverse impedance measurements;
- analysis of the single electron bunch blow up and its dependence on the RF voltage and bunch current.
- identification of a source of the vertical multibunch instability in the positron ring;
- measurements and cures of the quadrupole instability in the electron ring.

The results of the impedance and bunch lengthening measurements [28] can be summarized as follows:

- in both rings for currents higher than about 10 mA bunches lengthen in the turbulent regime. In this regime the final bunch length does not depend on the momentum compaction and can be estimated quite precisely ;
- bunch lengthening in e^+ ring agrees well with numerical simulations based on impedance calculations carried out before the collider commissioning[29, 30];
- bunches in the electron ring are longer than those in the positron ring due to higher coupling impedance accounted for about 40 ion clearing electrodes.

The transverse broad-band impedance was evaluated by measuring the betatron tune shift versus bunch current. It was found that:

- the vertical transverse impedance is much higher than the horizontal one for both rings;
- the electron ring vertical impedance is slightly higher than that of the positron ring and is estimated to be 130 kΩ/m;
- the betatron tune shift at the design bunch current of 44 mA is about 7 kHz in both rings. This value is smaller than the synchrotron frequency in DAΦNE that is typically in the range 25-40 kHz. So, the transverse turbulent microwave instability should not be expected in DAΦNE.

It was also observed that for the working point (0.11; 0.17) a single electron bunch can be blown up for certain bunch currents and RF voltages. Analysis and the tune scan around the working point revealed that:

- the working point (0.11; 0.17) is situated in the vicinity of the betatron resonance $3Q_x = 2Q_y$;
- variation of the tunes with bunch current shifts the working point exactly on the resonance for some current leading to the coupling increase and the blow up;

– the fact that the blow up depends on the RF voltage shows that the synchrobetatron satellite resonance $3Q_x + Q_z = 2Q_y$ is also strong and may affect the beam-beam performance.

Lowering the RF voltage to 110-120 kV was a solution at that time to move the working point from the resonance to enhance the luminosity.

Among multibunch instabilities we paid much attention to the dipole vertical instability and to the quadrupole longitudinal instability.

In order to find a source of the vertical coupled bunch mode instability in the positron ring we carried out many dedicated experimental measurements:

– modal analysis, grow-damp measurements and instability observations for different bunch patterns helped us to discover that the coupled bunch modes 100 and 101 are unstable in both rings;
– in order to find vacuum chamber components where a higher order mode (HOM) driving the instability is trapped we performed local closed orbit bumps, tried latticed with different beta functions at the locations of the suspected vacuum chamber components, observed behavior of two counterrotaing beams to define weather the HOM is localized in the common interaction regions.

As a result it was concluded that the HOM trapped in the injection kickers at the frequency of about 60 MHz is the incriminated parasitic mode driving the instability. An RF feedback for this particular mode has been prepared and has been proven to rise the instability threshold. Unfortunately, the feedback was not effective enough for high currents, presumably due to beam loading problems. At present this instability is successfully damped by the transverse multibunch feedback.

The longitudinal quadrupole instability was limiting the maximum stable current in the DAΦNE electron ring at a level of ~700–800 mA/beam. In order to investigate the phenomenon, the instability threshold has been measured as a function of various machine parameters as radio frequency voltage, momentum compaction, number of bunches, fill pattern, etc. An unexpected interaction with the longitudinal feedback system, built to control the dipole motion, has been found and a proper feedback tuning has allowed increasing the threshold. The maximum stable beam current has now exceeded 1.9 A and it is no longer limited by the quadrupole instability [31].

2.2.6 100 Bunch Operation

During the last 2 months of 2002 in runs for the DEAR experiment, the DAΦNE collider was operating by filling 100 consecutive buckets with a gap of 20 empty buckets for ion cleaning [5]. Previously, the best results in KLOE runs were obtained with the bunch pattern composed by 47-50 bunches separated by 1 empty bucket and an ion clearing gap.

The passage to the 100 bunch pattern was dictated by the necessity to increase the luminosity. On the other hand, it was a good opportunity to study parasitic crossings effects, multibunch beam instabilities, some other aspects of the beam dynamics for closely spaced bunches (2.7 ns separation).

With the aim to bring into collision 100 contiguous bunches some modifications were implemented into the machine optics:

– the horizontal beta function at the IP was decreased down to 1.7 cm from the design value of 4.5 cm [32];
– the horizontal crossing angle was increased from 2x12.5 mrad to 2x14.5 mrad;
– the modified lattice had a smaller horizontal emittance.

With these modifications the bunch separation at the first parasitic crossing (at 40 cm from the IP) was increased from $5\sigma_x$ to $12\sigma_x$.

After careful adjustment of all the feedback systems, more than 2 Amperes were routinely stored in two beams with acceptable background and lifetime. No clear signs of the electron cloud instability in the positron ring either ion instability (fast or conventional) in the electron ring were observed.

During the operation with 100 bunches some increase in lifetime and luminosity sensitivity to tune variations has been observed. We attribute this fact to higher Piwinski's angle for the modified optics due to the smaller horizontal beam size and larger horizontal crossings angle. This is in an agreement with performed beam-beam simulations.

Yet another observation was a strong dependence of the lifetime in collisions to octupole settings, presumably due to the crosstalk between beam-beam effects and lattice nonlinearities enhanced by the parasitic crossings, as it has seen also in simulations [18]. The best sets for the two rings were found experimentally.

The collider has shown a very good reliability: in Fig. 7 the peak luminosity, beam currents and integrated luminosity are presented for one of the best 24 hour data taking period. With 100 bunches the DEAR peak luminosity of 0.7×10^{32} cm^{-2} s^{-1} has been achieved while with 50 bunches it was 0.45×10^{32} cm^{-2} s^{-1}. Respectively, the integrated luminosity has reached 2.0 pb^{-1} per day compared to 1.1 pb^{-1} in 50 bunch operation. This has allowed completing the physics program of the DEAR experiment.

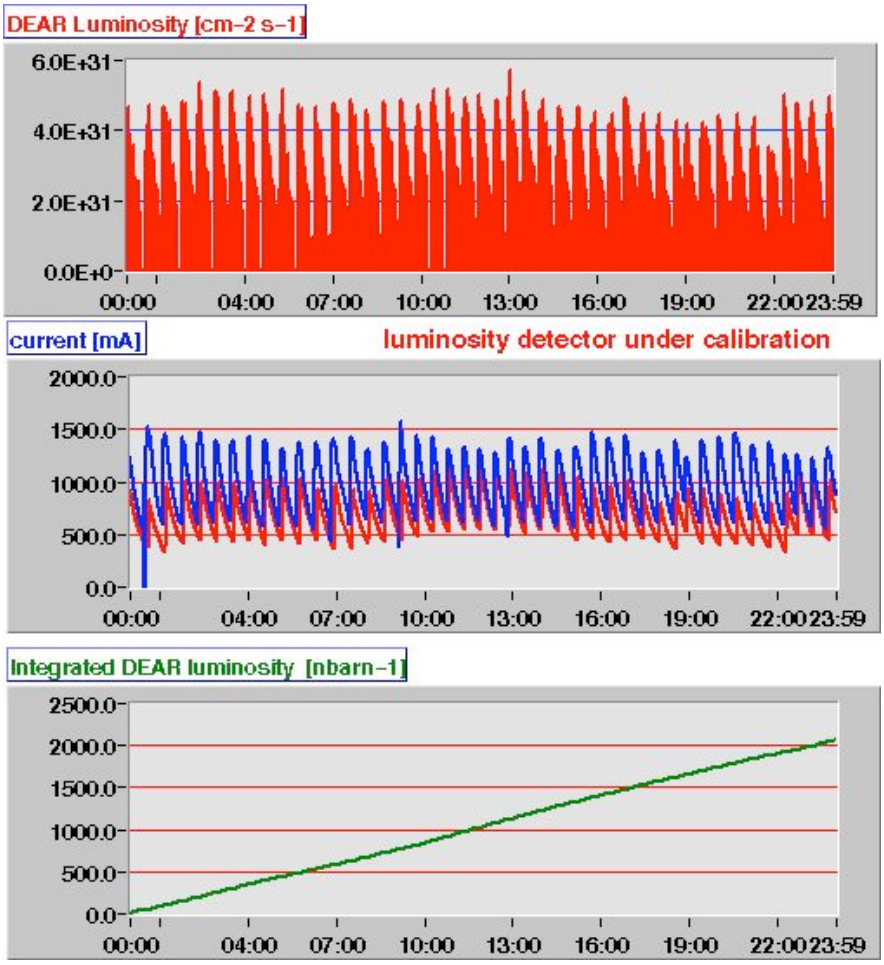

Figure 7: Peak and integrated luminosity in 24h (12/8/02).

These results were obtained with moderate bunch currents, < 15 mA in e^- bunches and < 12 mA in e^+ bunches. For comparison, about 20 mA/bunch were stored in 50 bunch pattern while running DAΦNE for the KLOE experiment. So, there is a margin for further luminosity improvement by increasing the single bunch current.

2.2.7 Luminosity Upgrade Plans

In three years from now all the current physical programs at DAΦNE are expected to be completed. The future long term programs are briefly described in [33] and will be discussed also in the forthcoming Workshop "e^+e^- in the 1-2 GeV Range: Physics and Accelerator Prospects" to be held in Alghero (Italy) on 10-13 September 2003 [34]. Our short term strategy for luminosity increase is based on the following steps:

- First of all, we plan to adopt 100 bunch operation mode as a routine one also for the KLOE and the FINUDA experiments. Since the maximum luminosity in KLOE of 0.8×10^{32} cm^{-2} s^{-1} was obtained with 50 colliding bunches having approximately 20 mA per bunch, we hope to double the luminosity in 100 bunch operation with the same current per bunch. However, the currents per every beam will be as twice as high imposing more severe requirements on the feedback systems in order to provide stable multibunch collisions. Besides, we also may need more experimental studies to handle beam-beam parasitic collisions.

- Profiting from a long shutdown of the collider in the first half of this year for the roll-in of a second large magnetic detector FINUDA, it was decided to modify the shape of the DAΦNE wiggler poles in order to reduce the effect of the field fall-off at large horizontal distance from the beam axis [35]. Numerical simulations taking into account the modified wiggler fields have revealed substantially larger on- and off-energy dynamics apertures [36]. This will allow shifting the collider working point closer to integers where, according to beam-beam simulations, we can gain yet another factor of 2 in the luminosity increase.

- The 3rd harmonic passive RF system is ready to be installed in both collider rings to improve the beam Touschek lifetime and the detector background[37, 38, 39]. For this purpose we plan to increase the energy acceptance of the machine by increasing the RF peak voltage and to lengthen the bunches at this high peak voltage by means of the harmonic voltage up to the limit imposed by the hour-glass effect in beam-beam collisions. We have evaluated that the use of the harmonic cavity in the lengthening regime can improve the Touschek lifetime up to 80% with respect to the present operating conditions. The simulations have shown that the microwave lengthening process is less pronounced in this case. Besides, we expect the enhancement of the Landau damping due to the large non-linearity of the harmonic voltage which should relax the single and multibunch dynamics. However, by analyzing the beam dynamics we have found that the harmonic system can introduce a few undesiderable effects. The presence of a gap in the bunch filling pattern will produce a large spread in parasitic losses and synchronous phases (thus modifying also the beam spectrum). As a consequence, different bunches will interact at different collision points near IP and the synchronization of the bunch-by-bunch feedback systems may be affected. Moreover, as we have seen in numerical simulations, the bunch charge distribution changes for different bunches along the train and the Touschek lifetime gain is not uniform over the train. The actual tolerability of such effects can not be exactly predicted since it depends on the eventual operating conditions (such as the gap width, for example). That is why we have foreseen the "parking option" (consisting in tuning the cavity away from the 3rd harmonic frequency and in-between two revolution harmonics) which allows recovering the operating condition before the harmonic cavity installation, and can be considered as a reliable back-up procedure.

- New interaction regions were installed during the 2003 year shut down providing IR quadrupoles rotation. We expect better coupling correction with the new IRs and a possibility of collisions at the second IP (FINUDA) with the KLOE detector solenoid switched off. Besides, new BPM are placed in the vicinity of the interaction point for better collision parameter diagnostics.

- The DAΦNE lattice is enough flexible to provide collider operation even with a negative momentum compaction [40]. There can be several advantages for beam dynamics and luminosity performance of DAΦNE with the negative momentum compaction:

    - The bunch length is shorter and the bunch distribution is more regular since the wake potential is focusing. This has already been demonstrated in numerical simulations taking into account DAΦNE vacuum chamber impedance. The shorter bunch length is preferable for both the peak luminosity increase and beam lifetime improvement since we can reduce the transverse beta functions at the interaction point (IP) and, besides, the Piwinski angle is lower in collisions with a crossing angle, as is in DAΦNE case.

    - Qualitative considerations confirmed by numerical simulations have shown that the lattice with the negative momentum compaction can ease the longitudinal beam-beam effects [41], improving beam lifetime and lowering beam size blow up.

    - Since the head-tail instability with the negative momentum compaction takes place with the positive chromaticity we can relax requirements on the sextupole strengths.

Numerical simulations of the beam-beam effects have indicated that by undertaking the following actions: shifting the working point close to integers, applying the negative momentum compaction and further decreasing the vertical beta function we have a possibility to push the DAΦNE luminosity to 10^{33} cm^{-2} s^{-1} level.

References

1. G. Vignola, “DAΦNE, The Frascati Φ-Factory”, in Proceedings of 1993 IEEE Particle Accelerator Conference (PAC 93), pp. 1993-1997; M. Serio et al., “Overview of DAΦNE, the Frascati Φ-Factory”, Int. J. Mod. Phys. Proc. Suppl. 2A: 115-117, 1993; M. Bassetti et al., “Status Report on DAΦNE”, Frascati Phys. Ser. 4: 19-30, 1996; M. Bassetti, “Status of DAΦNE Project”, Frascati Phys. Ser. 10: 39-47, 1998.
2. The KLOE Detector Collaboration, “KLOE: a General Purpose Detector for DAΦNE”, LNF-92/019 (IR), April 1992.
3. The DEAR Collaboration, “DAΦNE Exotic Atom Research”, LNF-95/055 (IR), 1995.
4. The FINUDA Collaboration, “FINUDA: a Detector for Nuclear Physics at DAΦNE”, LNF-93/021 (IR), May 1993.
5. A. Drago et al., “100 Bunches DAΦNE Operation”, to be published in Proceedings of 2003 IEEE Particle Accelerator Conference (PAC 2003).
6. K. Hirata, D. Shatilov and M. Zobov, “Beam-Beam Interaction Study for DAΦNE”, Frascati Phys. Ser. 10: 303-308, 1998.

7. K. Hirata, “Analysis of Beam-Beam Interaction with Large Crossing Angle”, Phys. Rev. Lett. 74: 2228-2231, 1995.
8. D. N. Shatilov, “Beam-Beam Simulation at Large Amplitudes and Lifetime Determination”, Part. Accel. 52: 65-93, 1996.
9. M. Zobov, M. Boscolo and D. Shatilov, “Beam-Beam Interactions at the Working Point (5.15; 5.21)”, DAΦNE Technical Note: G-51, Frascati, March 3, 1999. http://www.lnf.infn.it/acceleratori/dafne/NOTEDAFNE/G/G-51.pdf
10. M. E. Biagini et. al., “Beam-Beam Interactions in DAΦNE: Numerical Simulations and Experimental Results”, in KEK Proceedings 99-24, February 2000 (A), pp. 181-186.
11. D. Shatilov and C. Biscari, private communications.
12. D. Shatilov and M. Zobov, “Some New Results in Beam-Beam Simulations”, presented at Machine Advisory Committee, 4-5 May 2000.
13. C. Milardi et al., “Optics Measurements in DAΦNE”, in Proceeding of 7th European Particle Accelerator Conference (EPAC2000), pp. 1051-1053.
14. C. Milardi et al., “Effects of Nonlinear Terms in the Wiggler Magnets at DAΦNE”, in Proceedings of of 2001 IEEE Particle Accelerator Conference (PAC 2001), pp. 1720-1722.
15. G. Benedetti, “Sextupole in the “C” Corrector Magnet”, DAΦNE Technical Note: BM-5, Frascati, March 1, 2001. http://www.lnf.infn.it/acceleratori/dafne/NOTEDAFNE/BM/BM-5.pdf
16. C. Biscari, “Detuned Lattice for DAΦNE Main Rings”, DAΦNE Technical Note: L-32, Frascati, March 1, 2001. http://www.lnf.infn.it/acceleratori/dafne/NOTEDAFNE/L/L-32.pdf
17. A. Drago and A. Stella, “A Dynamic Tracking Acquisition System for DAΦNE e+e- Collider”, in Proceedings of 5th European Workshop on Diagnostics and Beam Instrumentation (DIPAC2001), pp. 213-215.
18. M. Zobov, “Crosstalk Between Beam-Beam Effects and Lattice Nonlinearities in DAΦNE”, DAΦNE Technical Note: G-57, Frascati, July 10, 2001. http://www.lnf.infn.it/acceleratori/dafne/NOTEDAFNE/G/G-57.pdf
19. C. Vaccarezza et al., “Preliminary Results on DAΦNE Operation with Octupoles”, in Proceedings of 8th European Particle Accelerator Conference (EPAC2002), pp. 1314-1316.
20. S. Bartalucci et al., “Broad-Band Model Impedance for DAΦNE Main Rings”, Nucl. Instrum. Meth. A337: 231-241, 1993.
21. S. Bartalucci et al., “Analysis of Methods for Controlling Multibunch Instabilities in DAΦNE”, Part. Accel. 48: 213-237, 1995.
22. A. Gallo et al., “A Waveguide Overloaded Cavity as Longitudinal Kicker for the DAΦNE Bunch-by-Bunch Feedback System”, Part. Accel. 52: 95-113, 1996.
23. F. Marcellini et al., “DAΦNE Broad-Band Button Electrodes”, Nucl. Instrum. Meth. A402: 27-35, 1998.
24. S. De Santis et al., “Coupling Impedance of a Hole in a Coaxial Beam Pipe”, Phys. Rev. E54: 800-805, 1996.
25. G. O. Delle Monache et al., “DAΦNE Shielded Bellows”, Nucl. Instrum. Meth. A403: 185-194, 1998.
26. A. Ghigo et al., “HOM Damping in the DAΦNE Injection Kicker”, in Proceedings of 7th European Particle Accelerator Conference (EPAC2000), pp. 1145-1147.
27. M. Zobov et al., “Measures to Reduce the Impedance of Parasitic Resonant Modes in the DAΦNE Vacuum Chamber”, Frascati Phys. Ser. 10: 371-378, 1998.
28. A. Ghigo et al., “DAΦNE Broadband Impedance”, in Proceedings of 8th European Particle Accelerator Conference (EPAC2002), pp. 1494-1496.

29. M. Zobov et al., “Collective Effects and Impedance Study for the DAΦNE Φ-Factory”, in KEK Proceedings 96-6, August 1996 (A), pp. 110 – 155.
30. M. Zobov et. al., “Bunch Lengthening and Microwave Instability in the DAFNE Positron Ring”, DAΦNE Technical Note: BM-3, Frascati, June 7, 1998. http://www.lnf.infn.it/acceleratori/dafne/NOTEDAFNE/BM/BM-3.pdf
31. A. Drago et al., “Longitudinal Quadrupole Instability and Control in the Frascati DAΦNE Electron Ring”, Phys. Rev. ST Accel. Beams 6: 052801, 2003.
32. C. Biscari et al., “Half ß*x at IP2”, DAΦNE Technical Note: BM-9, Frascati, April 11, 2002. http://www.lnf.infn.it/acceleratori/dafne/NOTEDAFNE/BM/BM-9.pdf
33. C. Biscari, this issue of ICFA Beam Dynamics News Letters.
34. http://www.lnf.infn.it/conference/d2/
35. M. Preger and C. Sanelli, to be published.
36. P. Raimondi, private communications.
37. M. Migliorati, L. Palumbo and M. Zobov, “Bunch Length Control in DAΦNE by a Higher Harmonic Cavity”, Nucl. Instrum. Meth. A354: 215-223, 1995.
38. D. Alesini et al., “The DAΦNE 3rd Harmonic Cavity”, in Proceedings of 2001 IEEE Particle Accelerator Conference (PAC 2001), pp. 885-887.
39. D. Alesini, “Longitudinal Beam Dynamics in the Frascati DAΦNE Collider with a Passive 3rd Harmonic Cavity in the Lengthening Regime”, Phys. Rev. ST Accel. Beams 7: 074401, 2003.
40. P. Raimondi, private communications.
41. V.V. Danilov, E. A. Perevedentsev and D. N. Shatilov, “Negative Momentum Compaction in the Longitudinal Beam-Beam Effects”, Int. J. Mod. Phys. Proc. Suppl. 2A: 1109-1111, 1993.

2.3 DAΦNE long term plans

C. Biscari for the DAΦNE team

mail to: Caterina.Biscari@lnf.infn.it

INFN-LNF
Via Enrico Fermi, 40 - 00044 Frascati, Italy

The future of DAΦNE after the completion of the present physics programs, which is expected in three years from now, is being discussed in the physics and accelerator community of the LNF and collaborating institutes.

DAΦNE is presently the only lepton collider working at the Φ resonance. Luminosity in the design range of 10^{32} $cm^{-2}sec^{-1}$ meets the physics requests by KLOE, FINUDA and DEAR experiments. In the LHC era, competitive experiments in this energy range ask for luminosities at least one order of magnitude higher which are not reachable with conservative designs with the present knowledges.

The DAΦNE passage from the factory to the superfactory regime needs major modifications in the collider design and huge R&D efforts. Different strategies are being investigated and some of them are briefly reported afterwards.

For a first evolution of the collider we are taking into account also the possibility of increasing the energy up to 2 *GeV* c.m., aimed at the measurement of the form factors of the nucleon and the QCD excited states in the 1.2 to 2–2.5 *GeV* c.m. energy range [1].

A first milestone on the definition of the DAΦNE future will come from the Workshop "e^+e^- in the 1-2 GeV Range: Physics and Accelerator Prospects" to be held in Alghero (Italy) on 10-13 September 2003, announced in this edition [2].

2.3.1 Super Φ Factory

The DAΦNE passage from the factory to the superfactory regime needs major modifications in the collider design. Experience has shown that powerful radiation damping is needed: simulations [3] indicate that roughly a reduction by a factor of 10 on the damping time would allow an increase of the b-b tune shifts by a factor of two. A normal conducting machine, with a circumference of the order of 100 m, must be almost completely filled by bending magnets for lowering the damping time to few msec.

Another crucial point is the squeezing of the vertical betatron function at the IP to the range of few millimeters, which implies rings in the regime of very short bunch lengths.

That being stated, the project study for a super Φ Factory at Frascati will not in principle be constrained by the present collider layout, even if it will be based on the utilisation of the existing infrastructures

One possibility is the idea of colliding beams of higher energies with large crossing angles [4]. The energy in the center of mass E_{cm} depends on the energy of the colliding beams and on their crossing angle. For example two 1.5 GeV rings colliding at 140° (meaning that beams travel in the same direction), produce Φ's with a boost such that K_s decays in length of 1 m, while K_L can be detected at distances up to 10 m, simplifying the problem of detector background shielding and asking for completely new approach in the detector design[5]. From the point of view of the accelerator the main advantage is the natural increase of radiation damping and of Touschek beam lifetime. Luminosity and beam-beam tune shift behaviour with large crossing angle are being studied[6]. The main disadvantage of this

scheme is the need of very short bunches in order to limit the geometrical decrease of luminosity with crossing angle.

Another scheme is based in the introduction of a "longitudinal low beta" at the IP. Tuning the R_{56} term along the ring should allow bunch length variation from a maximum value at the rf cavity location to a minimum at the IP [7].

This scheme needs a very large momentum compaction structure and high rf voltage. Using cells with alternating positive and negative radius of curvature dipoles a high negative momentum compaction is obtained, together with a total increase of radiation damping. Beam dynamics simulations, considerations about the longitudinal phase space behaviour in such regime, effect of wake fields on the longitudinal distribution, dynamic aperture computations, are being analised. A preliminary layout of the rings, compatible with the present DAΦNE hall and also with KLOE detector has been defined.

2.3.2 Light Quarks Factory

The upgrade of the energy of the collider by a factor of two is named DAFNE2 (Double Annular Frascati e^+e^- factory for Nice Experiments at 2 *GeV*) [8]. The requested integrated luminosity, of the order of some hundreds of pbarn^{-1}, is well within the reach of the present DAΦNE performance.

Luminosity in the range of 10^{32} cm^{-2} s^{-1} at the energy higher by a factor two with respect to the present situation could be reached with currents of the order of 0.5 A per ring, distributed in 30 bunches.

The main systems of DAΦNE (rf, vacuum, feedbacks) are already dimensioned for these parameters, while the main modification to the collider corresponds to the dipoles; they are being redesigned to fit the existing vacuum chambers while providing the necessary magnetic field. Upgrade of the Linac energy is foreseen to inject on energy.

References

1. R. Baldini, “Unknown for ever?”, Accelerator Division – LNF Seminar, Frascati, January 2003.
2. http://www.lnf.infn.it/conference/d2/, Forthcoming Beam Dynamics Event, this issue
3. M. Zobov, private communication.
4. P. Raimondi, private communication.
5. F. Bossi, private communication.
6. P. Raimondi, M. Zobov, "Tune Shift in b-b Collisions with a Crossing Angle", DAΦNE Tech. Note, G58 April 2003.
7. A. Gallo, M. Zobov, "Strong RF Focusing for Luminosity Increase", DAFNE Technical Note G60, August 2003.
8. G. Benedetti et al., " Feasibility study of a 2 GeV Lepton Collider at DAΦNE", Proceedings of PAC2003, in publication.

2.4 Accelerator Physics Design of BEPCII

P.D. Gu, Y. Luo, Q. Qin, J.Q. Wang, S. Wang, G. Xu, C.H. Yu
gupd@ihep.ac.cn, luoy@ihep.ac.cn, qinq@ihep.ac.cn, wangjq@ihep.ac.cn
wangs@ihep.ac.cn, xug@ihep.ac.cn, yuch@ihep.ac.cn
IHEP, Beijing, P.R. China

2.4.1 Introduction

The Beijing Electron-Positron Collider (BEPC) has been running for both high energy physics (HEP) and synchrotron radiation (SR) researches since 1989. Good performance of BEPC accomplishes a lot of achievements in the τ-charm region over the past decade, and in many fields of SR applications as well. As an upgrading scheme from BEPC, the BEPCII project was approved by the Chinese government in the early time of this year, with a micro-β scheme and multi-bunch collision in a double-ring machine installed in the current BEPC tunnel. The design work of the BEPCII, from linac to storage ring, from accelerator physics to every subsystem, is being carried on. This paper will describe the main progresses on the design of the BEPCII in the field of accelerator physics.

2.4.2 Beam-Beam Interaction

To achieve the high luminosity in the factory class collider, high beam currents and small beam sizes are necessary. These induce a stronger beam-beam interaction. The successful performance of KEKB and PEPII indicates that the beam-beam limit can be reached without any single bunch instability. This means the beam-beam interaction limits the peak luminosity. It is an important issue to study the beam-beam interaction in the design and performance of such a high luminosity collider.

The simulation studies are done by taking the advantages of the code BBC (Beam-Beam interaction with a Crossing angle) developed by K. Hirata [1]. BBC is a weak-strong simulation code in 6-D phase space, including the effect of crossing angle. Although the weak strong simulation can not investigate the coherent phenomena of beam-beam interaction, it is generally used during the design of a collider. Because of the CPU time consuming, the strong-strong simulation in a large scale tune scan so far has not been done.

The effect of a finite bunch length is taken into account by dividing a strong bunch into 5 slices longitudinally, and the weak one is represented by 50 randomly generated super particles, with a Gaussian distribution in 6-D phase space. The simulation is done for more than 5 radiation damping time.

The tune scan is performed for optimizing the tune from the viewpoint of high luminosity. Figure 1 shows the simulated luminosity on the tune grid (fractional part only) of $\delta\nu_x \in (0,1)$ and $\delta\nu_y \in (0,1)$ with a crossing angle of $\phi_c = 11$ mrad×2, in which the luminosity reduction factor L/L_0 is given instead of the luminosity itself. The mesh size is set as 0.02, which is smaller than the synchrotron tune $\nu_s = 0.034$. It indicates that the high luminosity region is just above the half integer in horizontal plane, and there is no significant difference between just above half integer and just above the integer in vertical plane. According to the commissioning experiences of KEKB and PEPII [2], a vertical tune above half integer is preferable because the orbit distortion is much stable than that of above an

integer. The high luminosity is expected at around $\delta\nu_x$=0.53 and $\delta\ \nu_y$=0.58, and these tune values are set as the design working points.

To achieve higher luminosity, a larger beam-beam parameter ξ_y is preferable. However, the maximum ξ_y is limited by beam-beam interaction. The simulation results show that the maximum ξ_y is decreased because of the large crossing angle of ϕ_c=11 mrad×2, but the design value of ξ_y = 0.04 is reasonable and reachable.

For BEPCII, the crossing angle of ϕ_c=11 mrad×2 is the basic requirements of the interaction region. From the viewpoint of beam-beam interaction, the crossing angle not only limits the maximum ξ_y, as described above, but also induces some additional luminosity reductions due to the geometric effects. The simulation shows that the luminosity reduction factor due to the finite bunch length effect and the crossing angle is about 80% while the luminosity reduction factor is 86% for the head-on collision. However, the crossing angle of ϕ_c = 11 mrad×2 is still acceptable. The simulation also indicates that the bunch length should be controlled carefully to avoid further luminosity reduction due to the finite bunch length effect.

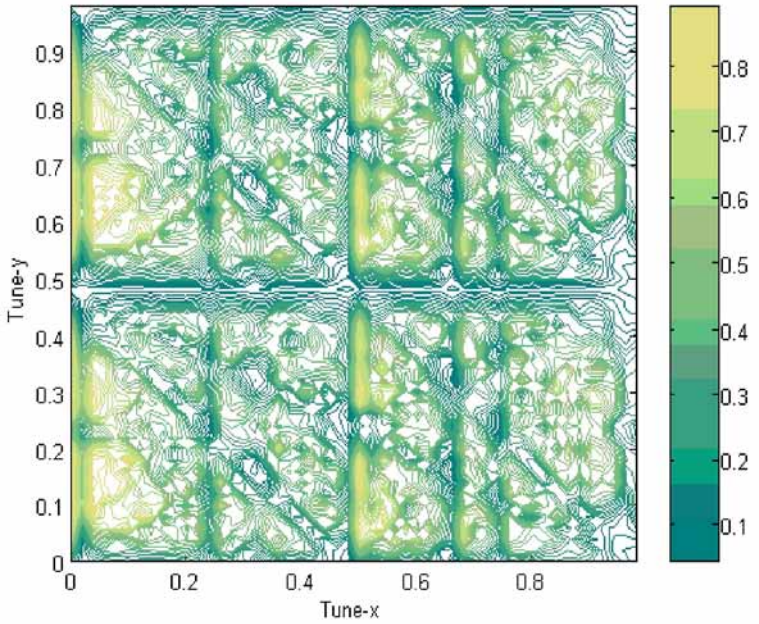

Figure 1 Luminosity survey with a crossing angle of ϕ_c= 11 mrad×2

2.4.3 Lattice Design of the BEPCII Storage Ring

With a new inner ring installed inside the old one in the existing BEPC tunnel, BEPCII will provide the colliding beams with the center-of-mass energy from 1.0 GeV×2 to 2.1 GeV×2 and also the dedicated synchrotron radiation beam at 2.5 GeV. For the colliding beams the luminosity is optimized at 1.89 GeV with the peak luminosity of 1×10^{33} $cm^{-2}s^{-1}$. As to the dedicated synchrotron radiation mode, the beam current reaches 250 mA with an emittance as low as possible.

There have been several beam-lines in the BEPC for the synchrotron radiation experiments, so the current bending magnets and insertion devices in the southern region have to be fixed at their present positions. In order to increase the average luminosity, the "top-off" injection scheme up to 1.89 GeV is adopted. This requires that the injection and collision optics be the same. The main parameters of the storage ring for both collision and SR modes are shown in Table 1.

Table 1 Main Parameters of the BEPCII storage ring

Parameters	Unit	Collision	SR (no wigglers)
Energy E	GeV	1.89	2.5
Circumference C	m	237.53	241.13
RF frequency f_{rf}	MHz	499.8	499.8
Harmonic number h		396	402
RF voltage V_{rf}	MV	1.5	3.0
Transverse tunes ν_x/ν_y		6.53/7.58	8.28/5.18
Damping time $\tau_x/\tau_y/\tau_E$	ms	25/25/12.5	12/12/6
Beam current I	A	0.91	0.25
Bunch number n_B		93	Multi
SR energy loss/turn U_0	keV	121	336
SR power P	kW	110	84
Energy spread σ_ε		5.16×10^{-4}	6.66×10^{-4}
Momentum compact α_p		0.0235	0.016
Bunch length σ_z	cm	1.5	1.18
Emittance $\varepsilon_x/\varepsilon_y$	nm·rad	144/2.2	–
Hori. natural emittance ε_{x0}	nm·rad	–	120
β-function β_x^*/β_y^*	m	1/0.015	–
Crossing angle at IP ϕ_c	mrad	11× 2	–
Bunch spacing s_b	m	2.4	–
Beam-beam ξ_x/ξ_y		0.04/0.04	–
Luminosity $\mathcal{L}$	$cm^{-2}s^{-1}$	1.0×10^{33}	–

1) Geometric design

Being upgraded from BEPC, BEPCII will use the old tunnel and keep the present beam-lines, so that the circumferences of "three rings" (two horizontally separated colliding rings and an SR ring) and the distance between the outer and inner rings are only adjustable in a few tens of centimeters. The RF frequency of the colliding rings is constrained by the linac frequency and the demands of the harmonic number from the data acquisition system of the BESIII detector. The final choice of the RF frequency is 499.8 MHz, which is 7/40 of the linac frequency 2856 MHz. Corresponding to this frequency, the harmonic numbers for the colliding and SR rings are 396 and 402, respectively. The distance between the outer and inner rings is 1.18 m. The north half ring of BEPC must be shifted 0.36 m northward.

Due to the space limit, the only way to separate the two beams is to use the crossing angle at the interaction point (IP). The crossing angle of BEPCII is chosen as 11 mrad × 2. Since the crossing angle cannot give a sufficient separation, the first pair of defocusing quadrupoles of the IR will deflect the beams further to 26 mrad × 2 and then a pair of septum magnets deflects the beam in the inner rings to 65.5 mrad, avoiding the SR background in the IR in the meantime. A bridge is needed in the SR mode connect the two half outer rings. Two superconducting dipole coils on both sides of the IP are used to accomplish this function. The beam will have 6 mm horizontal offset at the bending coils for the SR mode. In the RF region, the crossing angle of the particle trajectories is 154.7 mrad×2. Vertical local bumps will be used to separate two beams, so that the optics of two rings can be symmetric. In the operation of the SR mode, the bridges, which connect the inner and outer rings, will be powered off. Thus, the electron beam will go straight through the bending magnets. In this case, both of the RF cavities can provide the power to the electron beam. Fig. 2 shows the BEPCII complexity.

2) Optics design of the collision mode

The double-ring geometric structure of BEPCII causes each ring not to be a 4-fold symmetric structure, but the electron and positron rings are symmetric while the SR ring is east-west symmetric. Each colliding ring of BEPCII can be divided into four regions: IR, arc, injection, and RF regions.

In the IR region, two superconducting quadrupole (SCQ) are located at both sides of the IP to squeeze the β_y^*. It also bends the beams further from 11 mrad to 26 mrad. 5 warm bore quadrupoles are used for connecting the arc and IP. The first two warm quads, Q1a and Q1b, which have equal gradients for the inner and outer rings, are special dual aperture quadrupoles. A low field bending magnet is located at the beginning of the arc to decrease the synchrotron radiation to the IP. Since the longitudinal space in the IR is very tight, it is difficult to adopt a compensation scheme using skew quadrupoles. The best way is to compensate the coupling locally inside the detector with anti-solenoids and skew quadrupole coils.

In the RF region, there are seven quadrupoles to connect the arc regions of the inner and outer rings. Part of the RF region is dispersion free, and the β functions at the RF cavities in both vertical and horizontal planes are less than 15 m.

At the injection points, dispersion is zero as well as the same positions in the inner ring. The horizontal β function is larger than 20 m to reduce the sigma amplitude of the remnant oscillation of the injected beam. The phase advance between two kickers is π.

The main consideration of the optics in the arc region is to meet the designed emittance, momentum compaction factor and a sufficient dynamic aperture. The β functions in both vertical and horizontal planes are less than 25 m, and the dispersion is less than 2.5 m. The horizontal β functions at focusing sextupoles and the vertical β functions at defocusing sextupoles are as large as possible. Moreover, the limited vertical aperture at the insertion devices will lead to the constraint of vertical β function.

3) Chromaticity correction and dynamic aperture

A sufficient dynamic aperture is necessary, either for efficient beam injection or long beam lifetime under colliding in BEPCII. Though the requirements for the injection and the colliding beams are slightly different, we use the condition of the injection beam for both cases, which means a larger momentum acceptance ($\sim 10\sigma_\varepsilon$) and larger transverse apertures. For the tracking results evaluated here, the horizontal RMS beam size is taken from the natural horizontal emittance at 2.1 GeV (0.18 μm), and the vertical beam size σ_y from the fully-coupled emittance, i.e., half of the uncoupled horizontal emittance. In the dynamic aperture tracking with SAD [3] program, particles are launched at the IP with 1000 turns.

36 sextupoles are used to correct natural chromaticities ($\xi_{x0} = -12.5$ and $\xi_{y0} = -25.5$) in the BEPCII storage ring, powered by 18 power supplies. With these sextupoles, chromaticities of the BEPCII storage ring are corrected to 1.0.

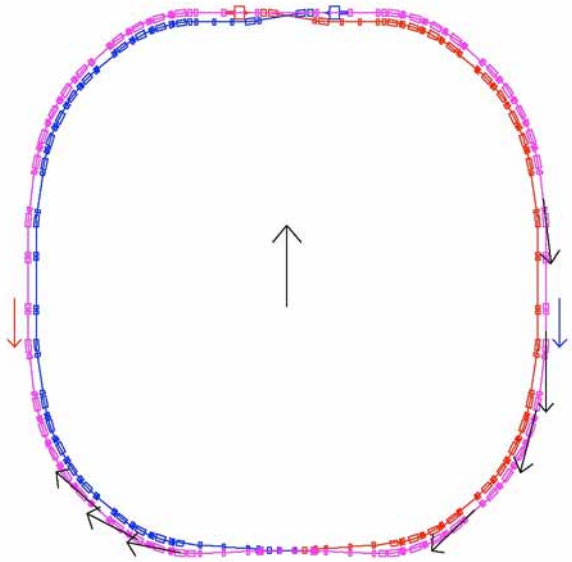

Figure 2 The BEPCII Complexity

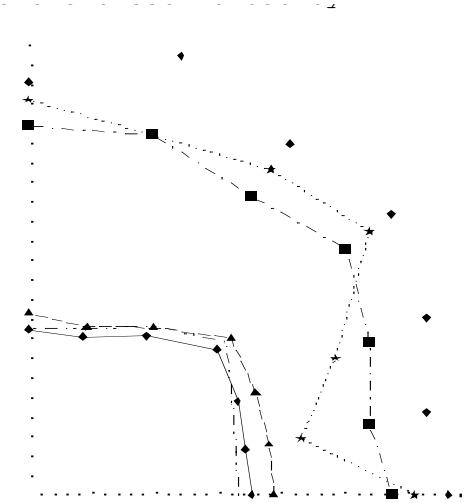

Figure 3 Dynamic aperture for BEPCII (3 most outer lines for bare lattice: solid one is on-momentum, dotted and dot-dashed ones $\pm 10\sigma_\varepsilon$ off momentum. 3 inner lines for the average of 20 random seeds w/ misalignment (after COD correction) and multiple errors w/o K_1: dashed line is on-momentum, solid and dot-dashed ones $\pm 10\sigma_\varepsilon$ off momentum.)

Fig. 3 shows the tracking results for the BEPCII dynamic aperture. One can see that the dynamic aperture will have a big reduction if errors from magnets are included. Studies show that the dynamic aperture is sensitive on K_1 errors for the dipoles and quadrupoles and more sensitive if the horizontal tune is closer to the half integer. This means the linear lattice must be well performed otherwise it will be difficult to operate the machine close to the half integer.

4) Optics design of the SR mode

In the BEPCII complex, there is another electron ring called SR ring, which can be used as a dedicated light source. The SR ring is formed by connecting two outer half rings of the electron and positron rings. The design goal of the SR mode is to operate electron beam at 2.5 GeV with a maximum beam current of 250 mA. The betatron tunes are chosen as ν_x/ν_y = 8.28/5.18. The emittance is thus 120 nm·rad at 2.5 GeV. The maximum beta functions β_x and β_y are smaller than 23 m. The maximum horizontal dispersion function D_x is about 1.65 m. The natural chromaticities are $\xi_{x0} = -11.6$ and $\xi_{y0} = -9.7$ for the horizontal and vertical planes, respectively. The dynamic aperture is larger than 25σ even with 0.8% energy spread.

2.4.4 Collective Effect

In BEPCII, to achieve the high luminosity, the micro-β scheme is adopted. This requires that the bunch length be well controlled to 1.5cm. However, bunch lengthening happens due to the potential well distortion and microwave instability. Normally, we chose the design bunch under the threshold of microwave instability. This corresponds to an impedance

threshold of 0.97 Ω at the design current of 9.8 mA. Calculation and beam measurement have shown that the broadband impedance of the present BEPC storage ring is about 4 Ω, thus a strict impedance budget has been made with an effort on designing and optimizing the main vacuum components to reduce impedance. With the main impedance generating elements being taken into account, the budget of $(Z/n)_0$ is estimated as 0.23 Ω. The longitudinal effective impedance is got from the Heifets-Bane broadband impedance model, and the threshold bunch current for the microwave instability is around 36 mA, that is about 4 times of the design current. At 9.8 mA, the bunch lengthens by about 5%.

The coupled bunch instabilities may arise from the high-Q resonant structures, such as the RF cavities and the resistive-wall impedance of the beam pipe. In BEPCII, superconducting cavities (SC) are adopted, so HOMs can be well damped. The up bound of the growth rates is firstly estimated by assuming symmetric filling pattern with 99 equally spaced bunches and each bunch has currents of 9.8 mA. Then it's confirmed by the multi-particle tracking results. The growth time of the fastest growing instability modes is at the same level of the synchrotron radiation damping time, so longitudinal feedback system will be considered. The growth rate of the most dangerous mode due to resistive-wall is of 4.3 ms, so this should be damped with bunch-to-bunch transverse feedback system.

To avoid ion trapping, a clearing gap is required with 5% of the total buckets unfilled, i.e., with one bunch train of 93 bunches. The Fast Beam-Ion Instability (FBII) has been studied with analytical formulae as well as tracking code, the growth time of FBII is about 3 ms which should be damped with the feedback system.

The electron cloud instability (ECI) may lead to the beam-size blow-up and luminosity degradation, which was observed in the two positron rings of KEKB and PEPII. With the existing formula [4], the threshold electron cloud density leading to transverse mode-coupled instability is higher than that of two B-factories. This may attribute to the smaller circumference of BEPCII. To guarantee the beam performance against ECI, antechamber with the inner surface of beam chamber TiN coated is used in the arc to reduce the primary and secondary electron yields, and in the straight section space may be reserved to wind solenoids to suppress the concentration of electrons near the beam axis. Besides, we are also investigating the possibility to install clearing electrodes to sweep out electrons. Preliminary simulations have shown that with antechamber and TiN coating, the EC density is substantially lower than the instability threshold, and feedback system is still needed to overcome the coupled bunch instabilities. Further study is under way and efforts are being made to improve the simulation code by including the effect of antechamber structure and clearing electrode.

In BEPCII, the beam lifetime is mainly determined by beam-beam bremsstrahlung during beam collision, which is calculated as 5.1 hours at the peak luminosity. Other limits are from the beam-gas scattering which gives beam lifetime of about 26 hrs at the vacuum pressure of 8×10^{-9} Torr, and the Touschek effect of about 7.1 hrs. So the total beam lifetime is around 3.0 hrs. With the top-off injection the maximum average luminosity is expected as 60% of the peak luminosity.

2.4.5 Interaction Region Design

The design of the interaction region (IR) has to accommodate competing and conflicting requirements from the accelerator and the detector. Many equipment including magnets, beam diagnostic instruments, masks, vacuum pumps, and experiment detector must coexist in a very small region. So the most difficult part of the design of a new collider is that of the IR.

The IR of BEPCII is about ±16 m long from the IP, in which about 20 main magnets need to be installed. The space is very tight. The design criteria for the BEPCII IR configuration are based on the experiences from other machines and some special requirements of the BEPCII. The two beams collide at the IP with a horizontal crossing angle of 22 mrad. The IR configuration provides an effective compensation scheme of high field detector solenoid. The aperture of vacuum chamber in the IR must be designed at least $2\times(14\sigma+2$ mm) for the beams (uncoupled in the horizontal plane and fully coupled in the vertical plane). And the background level of both synchrotron radiation and lost particles in the detector must be sufficiently low.

The BESIII detector consists of a cylindrical drift chamber, surrounded by an electromagnetic calorimeter, which is immersed in about 1 T magnetic field of a 3.7 m long superconducting solenoid. The geometry of the drift chamber requires that the accelerator components inside the detector should fit the conical space with an opening angle of 21.5°. The first accelerator component, which follows the central drift chamber, can only approach to 0.552 m on each side of the IP. The superconducting magnet SCQ and the septum bend magnet ISPB are fully located inside the detector boundary. The schematic layout of the IR is shown in Fig 4.

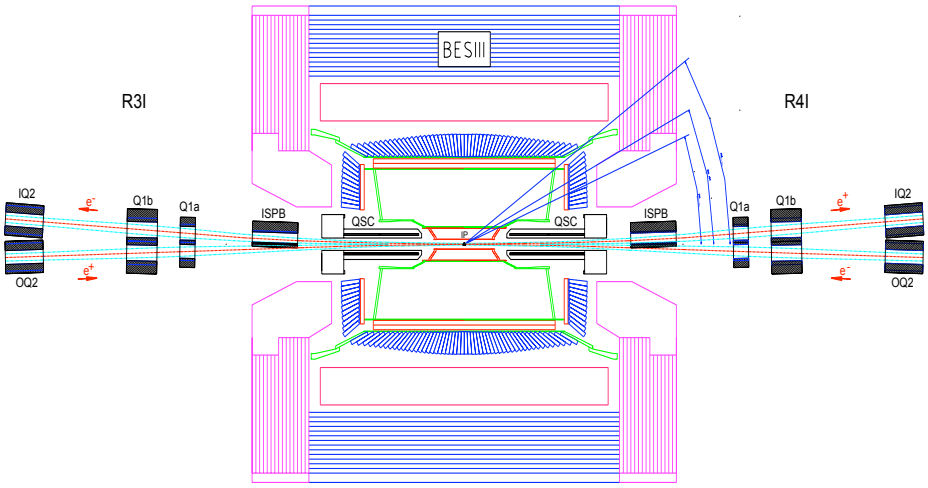

Figure 4 Schematic layout of the IR

In order to avoid the parasitic bunch crossing, a quick beam separation after collision is necessary. Our design choice is to introduce a horizontal crossing angle of 2×11 mrad at the IP and to incorporate with a horizontal bending magnet labeled ISPB for a larger separation between e– and e+ beams. The ISPB is a septum magnet with a narrow septum coil, located at 2.3 m away from the IP with a length of 0.6 m and the field strength of 4.6 kGs. It acts on the outgoing beam-line only.

On each side of the IP, a doublet of quadrupoles on each beam-line is used to provide the focusing optics needed at the IP (β_y^*=1.5 cm). The first vertical focusing quadrupole is a superconducting magnet (SCQ) shared by both beams. The SCQ package also includes compensation solenoid magnets, dipole magnets for SR mode and skew quadrupole coils. Its cryostat has a warm bore with an inner diameter of ϕ134 mm and an outer diameter of ϕ302 mm. The endcan of the cryostat has an outer diameter of ϕ635 mm. The second elements of the doublets are horizontal focusing quadrupoles Q1a and Q1b with a distance of 0.3m between them. In order to keep the symmetry for the two rings and save the space, Q1a and

Q1b are designed as a two-in-one structure and two separated beam channels for the incoming and outgoing beams with the same field strengths. These quadrupoles have to meet some special difficulties in design because the two beam pipes at their positions are still very close to each other. The next machine elements are quadrupoles Q2, Q3 and Q4, where the sufficient separation of the two beams is available to allow them to be installed side by side in the two rings. Those quadrupoles match the IR optics to that of the arc region.

2.4.6 Beam Injection

BEPCII will keep the BEPC's horizontal phase space multi-turn injection, and maintain its beam transport lines, which connect the linac and the collider. In order to achieve higher average luminosity, the beam injection rates have to be greatly improved, which are expected to be greater than 200 mA/min and 50 mA/min for e– and e+ beams, respectively. To ensure this high injection rates, for the positron beam, two-bunch injection scheme will be adopted with an adjustable injection repetition (12.5 Hz, 25 Hz, and 50 Hz).

The BEPC beam transport lines are upgraded in many aspects, such as replacing the old power supplies, adding four new independent power supplies to free some lattice matching constraints and installing new beam position monitors along the lines to keep close and real time control of the beam central orbits. In order to lessen the number of the particles lost in the ring, especially in the interaction region, collimators are needed in the beam transport lines to clean the larger amplitude and larger relative energy deviation particles. Instead of the BEPC's separate films and beam drifts in the air, the transport beam pipes will be directly connected to the storage ring to minimize the emittance dilution. So the vacuum situation in the end of the transport lines should be improved.

Two horizontal kickers with a phase advance of π are employed to create the horizontal closed orbit bump for the circular beam. The Lamberston septa of BEPC are still kept. Since the bunch spacing is changed, new kicker magnet power supplies and vacuum chamber are being studied. The physical apertures given by the IR are $14\sigma_{x,y,0}$ +2 mm (COD), which impose strict constraint to the beam injection path. The half aperture of collimators in the ring is designated to $\sim 12.5\sigma_{x,y,0}$. Simulations of the injection bunch's motion with collimators are carried out to decide the injection efficiency. Top-off injection will be adopted to achieve the higher average luminosity.

2.4.7 Linac

The main upgrading goals of the injector linac are the increase of the beam energy from 1.3 GeV to 1.89 GeV, the upgrade of the positron beam current from 2 mA to 40 mA, and the improvement of the operation reliability and stability. To meet these goals, besides the upgrades of the RF power system, new electron gun and new positron source, we have to find the new beam optics to establish the optics tuning and orbit correction systems to partially cure the beam blow-up due to chromatic/dispersive and wake field effects caused by the high current and machine errors, and hence to ensure the required beam transmission, the emittance and energy spread.

1) Studies on optimizing the beam optics

Electron beam leaves the bunching section with the solenoid focusing system, entering the main linac with the quadrupole focusing channel that consists of 15 triplet quads. These existing quadrupoles are divided into two groups according to their parameters, and are non-uniformly distributed along the linac. During the machine operation, any change of each

klystron output and/or the change of the stand-by klystron positions will cause changes of downstream beam optics. Therefore, to keep the optimum beam optics, we have to tightly control the power and phase instability of each klystron, and to adjust the downstream quad's strengths when the above changes happen.

Based on the existing lattice features, our studies with the code TRANSPORT have shown that one can optimize the optics by fitting the beam envelope σ_x and σ_y at each triplet. Due to the decrease of emittance with beam energy increase, the fitted σ_x and σ_y can be decreased along the linac too (say from 4.0 mm to 1.5 mm). The triplets' polarity arrangements of DFD-DFD and DFD-FDF have been studied respectively. The distributions of the magnetic gradients of the triplets along the linac are almost the same for these two lattices.

In the BEPCII-Linac, a 240 MeV, ~ 6 A primary electron beam is bombarded on the positron production target. There are two sets of triplets between the pre-injector exit (end of solenoid focusing) and the target. The beam modeling results show that one can confine the beam spot sizes (σ_x and σ_y) and the beam waists ($\alpha_x = \alpha_y = 0$) at the target by fitting the 4 valuable gradients of these two triplets.

To increase the positron yield, the studies on the primary electron beam spot size issue are carried out on the existing BEPC-Linac (140 MeV@target) and the minimization of the spot size for the BEPCII case (240 MeV@ target) is modeled and studied too.

The positron beam energy at the exit of the uniform solenoid (0.5 T, 7.0 m-long) is about 80 ~100 MeV. If only the existing triplets are used to focus the beam transversely, the positron beam envelopes will grow larger than beam tube bore radius in the first 500 MeV, due to its very large emittance and transverse momentum (given by EGS4 + PAMELA simulations) at the solenoid exit. Thus, an additional series of the large aperture quads "ridding" on the accelerating structures in this energy region is certainly needed to provide an additional focusing. On each of the first 5 accelerating tubes (A8-A12) after the positron target focusing solenoid, we will install 4 quads, and the rest 4 quads will be installed on the tubes of A13 and A14 to match the positron beam into the downstream focusing system that only consists of triplets. With this focusing lattice the positron beam envelopes can be kept within the bore radius of the accelerating tube. The polarities of the triplets are rearranged as DFD-FDF for both electron and positron beams.

An on-line optics correction loop has been preliminarily designed according to the lattices given above. The output RF power from each klystron (given by the measured voltage of each modulator and the prepared curves of klystron output vs. modulator voltage) is one of the input data for the correction loop to define the beam energy at each quad. The fitted gradient values of each quad and their corresponding power supplies' currents will be one of the output data of the loop to control/reset the quad's power supplies.

2) Orbit correction

In the BEPCII-Linac upgrade, a beam orbit correction loop will be established to partially cure the initial beam offset effects and the machine alignment error effects on the beam emittance growth and the orbit deviation. Both "1-to-1" and "global" orbit correction schemes are adopt. A stripe-line BPM is located in the upstream of each triplet, and a set of correctors (both for x and y directions) is "ridding" on the upstream accelerating structure. The prototypes of a BPM and a pair of correctors (for x and y) have been made and tested with good measurement results.

In the modeling, the initial beam offset, quads offset and accelerating structure offset have been taken into account with LIAR and PARMELA codes. The maximum electron bunch charge is 2.33 nC with its assumed energy spread of 2.5 MeV at the pre-injector exit (30 MeV). Besides the chromatic/dispersive effects in the quads induced by the above errors, the short and long–range wake effects in the structure have been calculated separately first, and then combined, with and without orbit correction. To have a minimum energy spread at the linac exit, the optimized accelerating phase of –3.5 is chosen to compensate the single-bunch beam loading effect.

In the case of positron beam, the large energy spread (_E = 12 MeV) induced chromatic/dispersive effects are dominated, while the wake effect for bunch charge of only 21 pC is negligible.

2.4.8 Conclusion

The BEPCII is being designed together with the subsystems like magnet, power supply, beam instrumentation, vacuum, control, RF, mechanism, etc, with an aim of 1×10^{33} $cm^{-1}s^{-2}$ for the peak luminosity. Challenges from not only accelerator physics, but also some key technologies like superconducting RF cavities and magnets, will be met in the construction of the whole machine. The project is expected to fulfill in five years.

References

1. K.Hirata, Phys. Rev. Lett. 74(1995).
2. K.Oide, Operation Experience and Performance Limitations in e^+e^- Factories, Proceedings of EPAC 2002, Paris,France, 2002.
3. http://www-acc-theory.kek.jp/SAD/sad.html
   K.Ohmi and F. Zimmermann, Phys. Rev. Lett. 85, 3821 (2000).

2.5 Beam Dynamics Activities at CESR-c

Michael Billing, James Crittenden, Mark Palmer, David Rice, David Rubin, David Sagan, Alexander B. Temnykh, *Laboratory for Elementary-Particle Physics, Cornell University,* Ithaca NY USA
Email: mgb@cesr10.lns.cornell.edu, critten@lns.cornell.edu, dhr1@cornell.edu, map36@cornell.edu, dlr@cesr10.lns.cornell.edu, dcs16@cornell.edu, abt6@cornell.edu

The CESR-c conversion to the Cornell Electron Storage Ring (CESR) extends the operating energy of the 768 m circumference e+e- storage ring down to 1.5 GeV beam energy. The total c.m. energy range now reaches from 12 GeV to 3 GeV, covering from the upsilon family of mesons down to the J/psi resonance.

The principal change to the machine for low energy operation is the addition of approximately 16 m of 2.1 T superferric wigglers to increase synchrotron radiation damping. A second change is providing higher voltage in the RF cavities to reduce bunch length to 1 cm to take full advantage of a small vertical beta function at the interaction point. The voltage requirements are increased because of the additional beam energy spread from the high field in the wigglers.

When final CESR-c design parameters are achieved, approximately 90% of the synchrotron radiation will take place in the wiggler magnets - a qualitatively different condition than in any electron storage ring to date. Studies with half the wigglers (80% synchrotron radiation from wigglers) have begun in August, 2003. The beam dynamics in such a machine have yet to be measured. This exploration and understanding will be a key component of CESR-c operation.

In both CESR and CESR-c a "pretzel" orbit provides separation at most of the 89 parasitic crossing points of the electron and positron beams. This horizontal closed orbit distortion, with opposite sign for electron and positrons, extends completely around the ring circumference and dominates optics design and many beam dynamics issues. For example, sextupoles become first order optics elements, but with opposite sign for the two beams. The small non-linearities in the wigglers (the mid-pole field profile is within ±0.1% over the horizontal beampipe aperture) have different effects for the two beams also. While many of the beam dynamics issues here are unique to CESR, others, as well as the calculation and analysis methods used, have general applicability.

Four papers follow. The first, "CESR-c Lattice Design and Optimization" describes the method of designing optics (including sextupoles) for the pretzeled CESR machine. The second, "A Magnetic Field Model for Wigglers and Undulators," describes both high accuracy and calculationally expedient methods used for modeling the wiggler beam dynamics. The third is "Beam Based Characterization of a New 7-pole Super-conducting Wiggler at CESR," comparing magnetic measurements and beam-based measurements of a prototype wiggler with field calculations. The last , "Recent Developments for Injection into CESR," describes a technique to measure and analyze the trajectories of injected (and stored) beams for improvement of optics and tuning.

2.6 CESR-c Lattice Design and Optimization

D. L. Rubin, M.J. Forster
Cornell University, Ithaca NY, USA
drubin@physics.cornell.edu

2.6.1 CESR-c Lattice

The 768m circumference CESR-c storage ring operates over the energy range of 1.5GeV/beam to 5.6GeV/beam. The lattice arcs are comprised of 94 quadrupoles and 76 sextupoles. The final focus quadrupoles, which are immersed in the 1T-1.5T field of the experimental solenoid, are a superconducting, permanent magnet hybrid. The quadrupole nearest to the interaction point is a 20cm long NdFeB permanent magnet vertically focusing quadrupole with 31.9 T-m gradient. A pair of vertically and horizontally focusing superconducting quadrupoles share a single cryostat complete the final focus. All of the interaction region quadrupoles are rotated 4.5^0 about their axis to compensate for the coupling introduced by the CLEO solenoid. Skew quadrupole windings, superimposed on the main quad windings of the superconducting quadrupoles are used to trim the compensation.

The counter rotating beams of trains of bunches share a common vacuum chamber. Four horizontal electrostatic deflectors are deployed in the machine arcs to generate a differential closed orbit distortion that separates the beams at parasitic crossing points of electrons and positrons. [3] The closed orbits intersect at the interaction point with a ±3 mrad crossing angle.

In preparation for operation in the J/ψ energy range (1.5-2.2 GeV/beam), we have begun to install superconducting wigglers in the machine arcs. [2] The wigglers will reduce the radiation damping time at low energy from about 500ms to 50ms. Six wigglers were installed during the spring of 2003 in the East arc of the machine. The remaining six will be installed in the West arc early next year. The introduction of the wigglers into the lattice, with their inherently strong vertical focusing and zero horizontal defocusing, significantly distorts the optical parameters. Furthermore, the approximate mirror symmetry of the guide field, with symmetry axis a diameter through the interaction point running north and south, is badly broken.

A consequence of the horizontal separation of the closed orbits of the electrons and positrons is that the beams are typically displaced in opposite directions in the sextupoles. The sextupole feed down distorts the linear optics differentially. With mirror symmetry, most of the sinister distortions are compensated globally. As a result of the now broken symmetry, optical parameters for the two beams can be very different including, β-functions, dispersion, damping partition numbers, emittance, etc.

All of the guide field quadrupoles and sextupoles are independently powered, giving enormous flexibility to the design of the lattice. The design objectives include equality of relevant optical parameters for the electron and positron beams.

2.6.2 Lattice design

The lattice parameters are defined by the distribution of the variables, namely the quadrupole, sextupole and horizontal separator strengths. For any given distribution we compute β-functions, solenoid compensation, emittance, dispersion, etc. In addition we quantify the cumulative effect of the multiple parasitic crossings in terms of the long range beam beam tune shifts and the "B_parameter." [5] The B_parameter depends on beam sizes as well as separation at the parasitic crossing points and the local β. The implementation of an accurate map for the wigglers is critical to design process. We represent the 2.1T, 1.3m long wigglers with a fifth order Taylor series in order to properly include the nonlinearities. The coefficients for the Taylor map are based on a fit to a field profile generated with a finite element code [4]. The variables are manipulated to minimize a figure of merit that is zero when all of the design goals have been achieved.

Typically the optimization proceeds in steps. We begin by minimizing the figure of merit exclusively with quadrupoles as variable elements. Next a sextupole distribution is determined that yields the desired chromaticity and simultaneously minimizes amplitude and energy dependence of β-functions. [1] The nonlinear aperture of the optics is characterized by the amplitude dependence of the Jacobian of the one turn map which is computed by tracing trajectories with a range of starting points through a single turn. Finally we return to optimization with quadrupoles and iterate as necessary.

2.6.3 Lattice parameters

The lattice functions for a preliminary design of a 6 wiggler optics are shown in Figure 1. The β-functions and closed orbits for positrons are in red (solid lines) and for electrons in blue (dashed lines). From left to right is the interaction point, the west arc, the east arc and finally the interaction point again. The 6 superconducting wigglers are in the east.

The tic marks along the x-axis in the plot of the horizontal orbits (second from the top) indicate parasitic crossing points in the event that there are 9, 5-bunch trains in each beam. Vertical electrostatic deflectors generate the half wave bump to separate the beams at the half way around the ring. Note that it is the square root of β_y and β_x that are plotted and β^*_y = 12mm. The horizontal emittance ε_x = 190nm. The horizontal emittance for the electron orbit is 10% less than for the positron orbit.

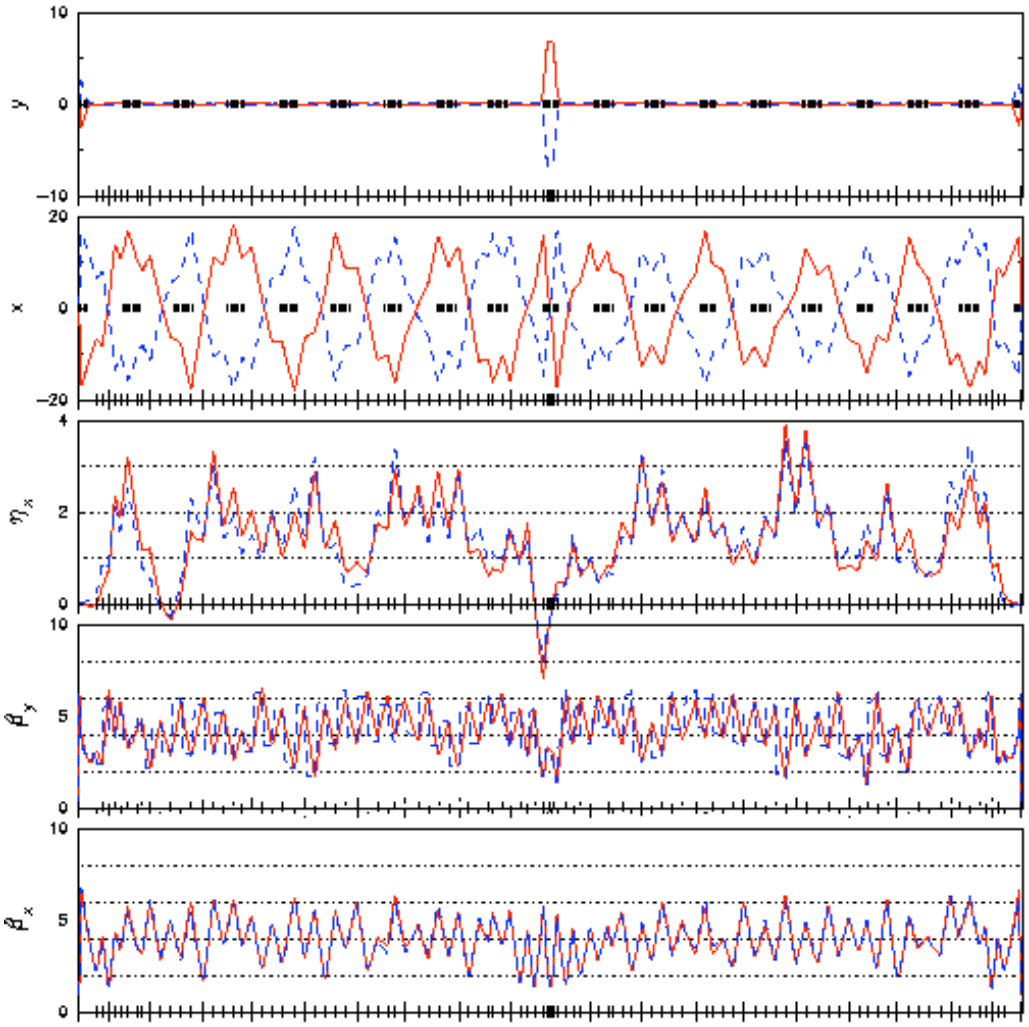

Figure 1. Electron and positron closed orbits and lattice functions for CESR-c 6 wiggler optics.

2.6.4 Lattice characteristics,

The design lattice is characterized in a variety of ways. A tune scan helps to identify particularly virulent resonances and also a promising working point. To scan the region of the tune plane indicated in Figure 2, we divide the region into a grid of about 900 pairs of horizontal and vertical tunes. At each point in the plane we follow the trajectory of a particle, with initial phase space coordinates displaced from the closed orbit, for 1000 turns. The contours in the plot correspond to the maximum vertical amplitude of the trajectory over the course of the 1000 turns. Synchrobetatron sidebands of the coupling resonance and the third integer are evident. (The synchrotron tune is ~0.1.) Details of the scan are sensitive to the initial displacement of the trajectory. Here $\Delta x_0=5\sigma_x$, $\Delta y_0=\sigma_y$, $\Delta E/E_0=4\sigma_e$,

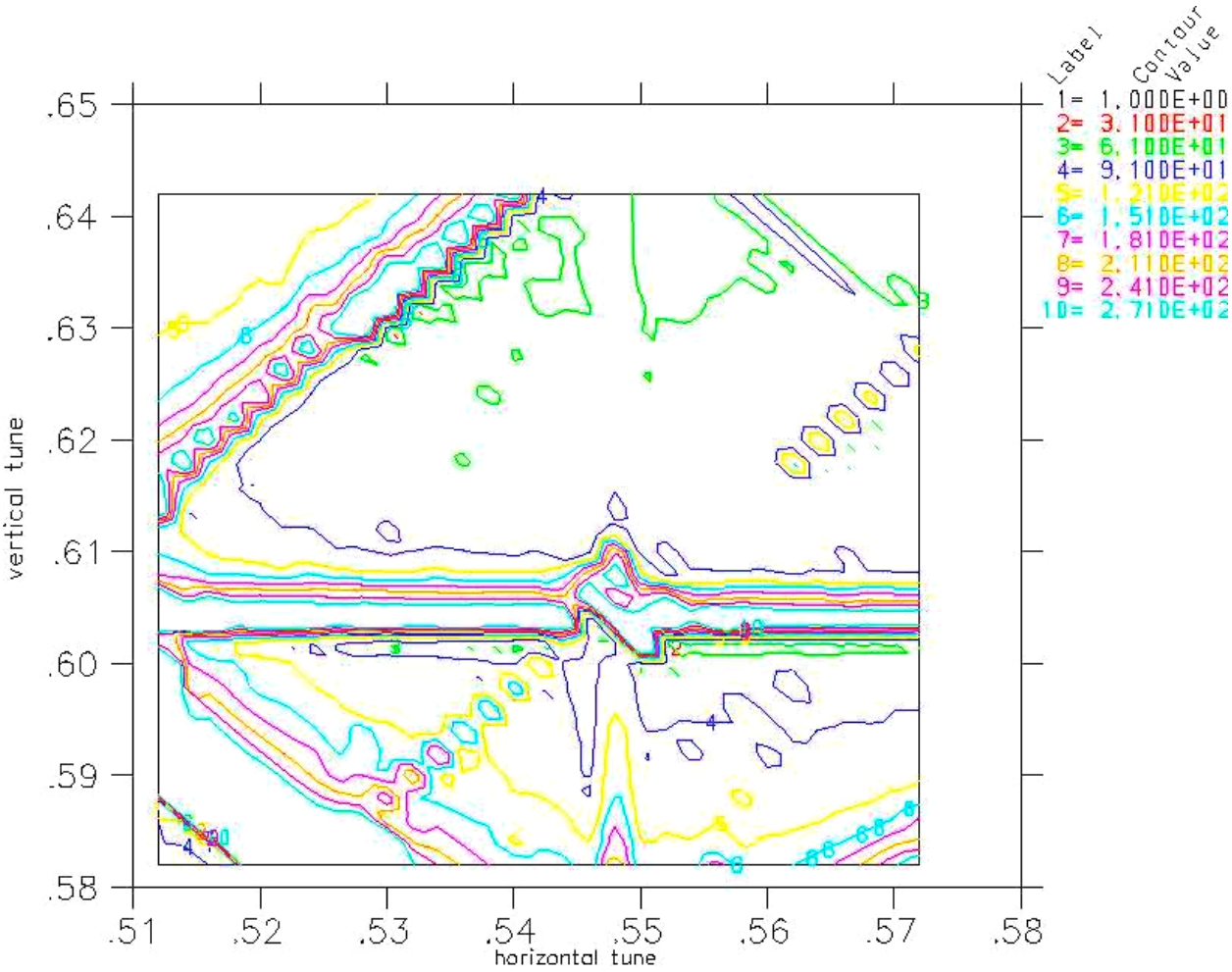

Figure 2: Contours of maximum vertical amplitude in 1000 turns for CESR-c 6 wiggler lattice.

2.6.5 Conclusions

The CESR-c optics are designed to satisfy a large number of criteria. The process is complicated by the ubiquitous nature of the "pretzel" separation scheme in which counter rotating beams are displaced from the axis of the guide field. Electrons and positrons will in general have significantly different optical functions, and this asymmetry in the optical functions is amplified by the lack of geometric symmetry in the lattice. Furthermore, the very strong damping wigglers have nonlinearities that cannot be simply compensated by multipole correctors and must be incorporated in the lattice design process. An iterative optimization with first quadrupoles and then sextupoles yields a good result.

2.6.6 References

[1] D.Rubin and D. "CESR Lattice Design," Proc. 2001 Part. Acc. Conf., p. 3517 (2001)

[2] D.Rice and D. "Parameters for Low Energy Operation of CESR," Proc. 2001 Part. Acc. Conf., p. 374 (2001)

[3] D.Rubin et al. "CESR Status and Performance," Proc. 2001 Part. Acc. Conf., p. 3520 (2001)

[4] D. Sagan, J. A. Crittenden, D. Rubin, “A Magnetic Field Model for Wigglers and Undulators,” Proc. 2003 Part. Acc. Conf. (2003)

[5] S. Temnykh and J. Welch, D.Rice, “The Long Range Beam-Beam Interaction at CESR – Experiments, Simulation and Phenomenology,” Proc. 1993 Part. Acc. Conf., p. 2007 (1993)

2.7 A Magnetic Field Model for Wigglers and Undulators

D. Sagan*, J. A. Crittenden, D. Rubin, E. Forest
Cornell University, Ithaca NY, USA
* dcs16@cornell.edu

2.7.1.1 *Analysis*

One of the major challenges in designing the damping rings for the next generation of linear colliders is how to model the many wigglers that will be needed for emittance control. A prerequisite for the study of particle dynamics is the ability to calculate transfer maps. This is difficult for wigglers since analytic formulas do not exist except in the most simplified cases. Wigglers can have strong nonlinear components [1,2], which can be a major limitation on the dynamic aperture, and impose stringent conditions on any analytic approximations. Recently, a field model has been developed at Cornell that can be used to accurately track particles through a wiggler[3]. The advantages of the model are that it can be used to track symplecticly and the model includes the end fields of the wiggler.

The field model is used with symplectic integration to do tracking. The symplectic integration algorithm was developed by Y. Wu et al [4]. The analysis starts with the Hamiltonian in the paraxial approximation

$$H = \frac{(p_x - a_x)^2}{2(1+\delta)} + \frac{(p_y - a_y)^2}{2(1+\delta)} - a_s,$$

where $p_{x,y} = P_{x,y}/P_0$ is the normalized transverse momentum, $\delta = \Delta E/P_0 c$ is the relative energy deviation, z is the longitudinal position relative to the reference particle, and $\mathbf{a}(x,y,s) = q\mathbf{A}/P_0 c$ is the normalized vector potential.

Wu has shown that by dividing this Hamiltonian in a certain way symplectic integration can be done. This procedure has been integrated into the PTC (Polymorphic Tracking Code) subroutine library of Etienne Forest [5] which in turn has been integrated into the Cornell BMAD particle simulation software library [6].

The BMAD library is written in Fortran90 and has been developed to supply a flexible framework that simplifies the task of writing custom programs to do particle simulations. The BMAD input format is very similar to the MAD input format so translating lattice files between the two formats is a fairly simple task. Besides most of the standard MAD elements, BMAD recognizes wigglers, combination solenoid/quadrupoles, and LINAC accelerating cavities. Features include: Twiss parameter calculations, tracking, generating and manipulating Taylor Maps, Wakefields, etc.

2.7.2 Field Model

As input to the symplectic integrator one must have an analytical formula for the magnetic field that can be integrated to obtain the vector potential (the need to be able to repeatedly differentiate the vector potential precludes the alternative of interpolation from a field table). The Cornell wiggler field model starts by writing the field $B_{fit}(x,y,s)$ as a sum of terms

$$B_{fit} = \sum_{n=1}^{N} B_n(x,y,s;C_n,k_{xn},k_{sn},\phi_{sn},f_n).$$

Each term B_n is parameterized by 5 quantities C, k_x, k_s, ϕ_s, and f. The index $f_n = 1,2,or\,3$ is used to designate which of 3 forms a B_n term can take. The first form ($f_n = 1$) is

$$\begin{aligned} B_x &= -C\frac{k_x}{k_y}\sin(k_x x)\sinh(k_y y)\cos(k_s s+\phi_s) \\ B_y &= C\cos(k_x x)\cosh(k_y y)\cos(k_s s+\phi_s) \\ B_s &= -C\frac{k_s}{k_y}\cos(k_x x)\sinh(k_y y)\sin(k_s s+\phi_s) \end{aligned} \qquad (1)$$

$$\text{with}\quad k_y^2 = k_x^2 + k_s^2$$

The second form ($f_n = 2$) is

$$\begin{aligned} B_x &= C\frac{k_x}{k_y}\sinh(k_x x)\sinh(k_y y)\cos(k_s s+\phi_s) \\ B_y &= C\cosh(k_x x)\cosh(k_y y)\cos(k_s s+\phi_s) \\ B_s &= -C\frac{k_s}{k_y}\cosh(k_x x)\sinh(k_y y)\sin(k_s s+\phi_s) \end{aligned} \qquad (2)$$

$$\text{with}\quad k_y^2 = k_s^2 - k_x^2$$

The third form ($f_n = 3$) is

$$\begin{aligned} B_x &= C\frac{k_x}{k_y}\sinh(k_x x)\sin(k_y y)\cos(k_s s+\phi_s) \\ B_y &= C\cosh(k_x x)\cos(k_y y)\cos(k_s s+\phi_s) \\ B_s &= -C\frac{k_s}{k_y}\cosh(k_x x)\sin(k_y y)\sin(k_s s+\phi_s) \end{aligned} \qquad (3)$$

$$\text{with}\quad k_y^2 = k_x^2 - k_s^2$$

k_y is considered to be a function of k_x and k_s. The relationship between them ensures that Maxwell's equations are satisfied.

Given a calculation or measurement of the field at a set of points $\mathbf{B}_{data}$, the problem is to find a set of N terms such that $\mathbf{B}_{fit}$ and $\mathbf{B}_{data}$ agree to some given precision set by how accurately one needs to be able to track through a wiggler. This is a standard problem in nonlinear optimization [7, 8]. The solution is to minimize a merit function M

$$M = \sum_{\text{data pts}} |B_{\text{fit}} - B_{\text{data}}|^2 + w_c \sum_{n=1}^{N} |C_n|$$

The second term in M is to help preclude solutions with degenerate terms that tend to cancel one another. The weight w_c should be set just large enough to prevent this but not so large as to unduly distort the fit.

2.7.3 CESR-c Wiggler Model

The wiggler magnets being installed in the Cornell CESR-c storage ring [9] have been modeled using the above procedure. Using the finite element modeling program OPERA-3D, a table of field versus position was generated. The validity of the field calculations was experimentally confirmed by measurements of tune as a function of beam position in a

wiggler [10]. Table data and fit curves of B_y as a function of s and x for the CESR-c 8-pole wiggler are shown in Figures 1 and 2. 82 terms were used for the fit. The peak field is about 2 Tesla and the RMS of the difference $|\mathbf{B}_{\text{data}} - \mathbf{B}_{\text{fit}}|$ was 9 Gauss which gives an RMS to peak field ratio of 0.05%.

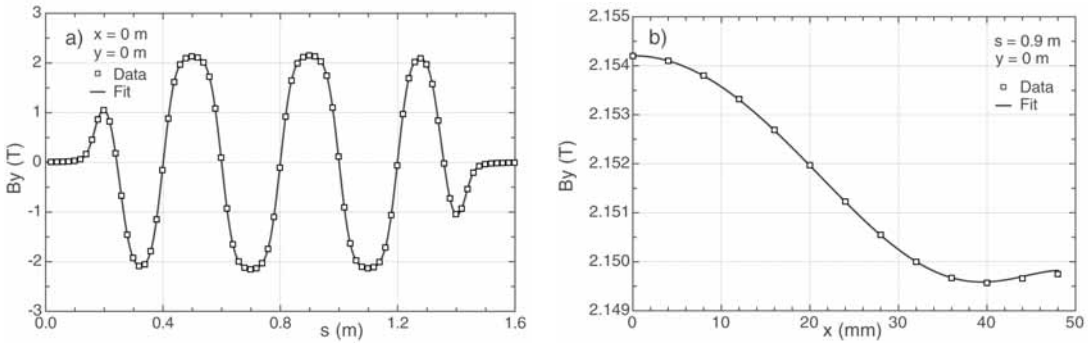

Figure 1: a) B_y as a function of s. b) B_y as a function of x. The data points are from a finite element modeling program. The curves are calculated from an 82 term fit.

Figures 2 and 3 show tracking simulation results for the CESR-c 8-pole wiggler. Figure 2 shows p_x at the end of the wiggler as a function of x at the start with a starting condition of $y = 20$ mm. Figure 3a shows p_y at the end as a function of y at the start with x_{start} set at 30 mm. The solid lines in Figures 2 and 3a are the results of using a Runge-Kutta (RK) integrator with adaptive step size control [7] and with the field values obtained from interpolating the table from OPERA-3D. The dashed lines are from symplectic integration (SI) using the fitted field and 250 integration steps. The dash-dotted lines are from a 7^{th} order Taylor map (TM) which is generated using symplectic integration with 250 integration steps.

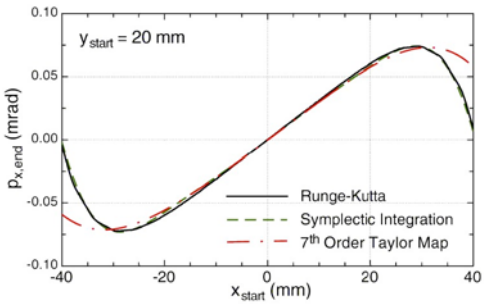

Figure 2: p_x at the end of the wiggler as a function of x at the start using 3 different tracking methods.

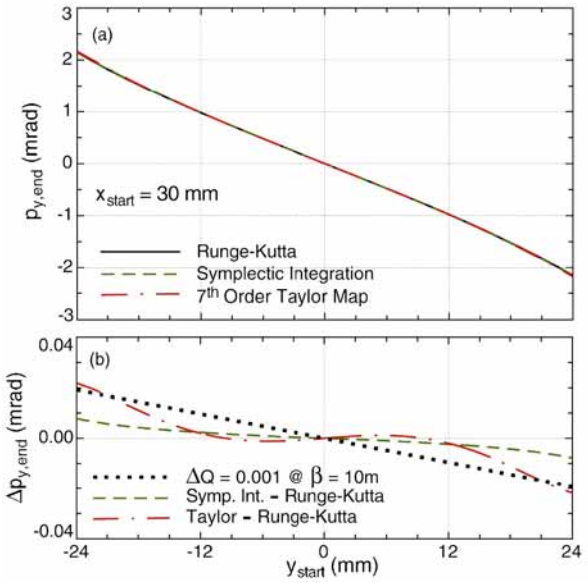

Figure 3: a) p_y at the end of the wiggler as a function of y at the start using 3 different tracking methods. b) Difference between RK tracking and the two other methods.

RK tracking, since it is derived directly from the equations of motion and the magnetic field table, is the gold standard with which to compare other tracking results. Figure 3b shows the difference between the SI and RK tracking as well as the difference between the TM and RK tracking. Additionally, for comparison, a line is shown whose slope represents a tune shift of $\Delta Q = 0.001$ assuming a β of 10 m. The SI tracking agrees well with the RK, better than 4 μrad in Figures 2 and 8 μrad in Figure 3. Slope differences of the curves are also small, representing tune shifts of less than 0.001 (at β = 10 m) everywhere in the figures. The advantage of the SI tracking is that it preserves the Poincare invariants, such as phase space density, while the RK does not. This is an important consideration in long term tracking where RK can give unphysical results.

The TM also show excellent agreement with the RK tracking except in Figure 2 when the magnitude of x is larger than 30 mm or so. In the domain where the TM agrees with the RK, the TM can be used for such purposes as lattice design and other analyses that are not sensitive to non-symplectic errors. The advantage of the TM is that it is fast. In the present instance the TM was over a factor of 30 faster than the other two methods. (This does not include the time to calculate the TM to begin with, but that only has to be done once). To overcome the non-symplecticity of the TM it can be partially inverted to form a symplectic generating function [11].

2.7.4 Conclusion

The wiggler model that we have developed is especially useful because it can accurately include end fields. This leads to efficient symplectic mapping which is needed in long term tracking, and avoids the non-physical violation of conserved quantities inherent when tracking is dependent upon interpolation of a field table. For applications where symplecticity is not a concern, a Taylor map, generated using the fit with symplectic integration can greatly reduce computation time.

For long periodic wigglers, the number of terms needed to fit the field may become large. In this case, a simple solution would be to divide the wiggler into 3 sections: the periodic center section and two end sections. Each section can be fitted separately. Since the center section is periodic, the number of terms needed to fit it is independent of its length. For the end sections it might be possible to cut down on the number of fit terms by making use of three additional forms that have an exponential s-dependence. These forms can be derived from (1), (2), and (3) using the substitution $k_s \rightarrow -ik_s$.

If pole misalignments need to be simulated, then planar symmetry cannot be assumed. In this case, (1), (2), and (3) can be modified, at some small increase in complexity, by using $k_x x + \phi_x$ in place of $k_x x$, and $k_y y + \phi_y$ in place of $k_y y$. With this, any arbitrary magnetic field profile can be modeled.

References

[1] P. Kuske, R. Gorgen, and J. Kuszynski,
"Investigation of Non-Linear Beam Dynamics with Apple II-Type Undulators at Bessy II,"
Proc. 2001 Part. Acc. Conf., pg. 1656 (2001).

[2] C. Milardi, D. Alesini, G. Benedetti, et al., "Effects of Nonlinear Terms in the Wiggler Magnets at DAϕNE,"
Proc. 2001 Part. Acc. Conf., pg. 1720 (2001).

[3] D. Sagan, J. A. Crittenden, D. Rubin, "A Magnetic Field Model for Wigglers and Undulators," Proc. 2003 Part. Acc. Conf. (2003)

[4] Y. Wu, E. Forest, D. S. Robin, H. Nishimura, A. Wolski, and V. N. Litvinenko,
"Symplectic Models for General Insertion Devices,"
Proc. 2001 Part. Acc. Conf., pg. 398 (2001).

[5] See: <http://bc1.lbl.gov/CBP_pages/educational/TPSA_DA/Introduction.html>.

[6] D. Sagan, and D. Rubin, "CESR Lattice Design," Proc. 2001 Part. Acc. Conf., pg. 3517 (2001)

[7] W. Press, B. Flannery, S. Teukolsky, and W. Wetterling, *Numerical Recipes in Fortran, the Art of Scientific Computing*, Second Edition, Cambridge University Press, New York, 1992.

[8] F. James, *MINUIT, Function Minimization and Error Analysis*, CERN program library writeup D506.

[9] J.A. Crittenden, A. Mikhailichenko, and A. Temnykh, "Design Considerations for the CESR-c Wiggler Magnets," Proc. 2003 Part. Acc. Conf. (2003).

[10] A. Temnykh, J. A. Crittenden, D. Rice and D. Rubin, "Beam-based Characterization of a New 7-Pole Super-conducting Wiggler at CESR," Proc. 2003 Part. Acc. Conf. (2003).

[11] E. Forest, *Beam Dynamics: A New Attitude and Framework*, Harwood Academic Publishers, Amsterdam (1998).

2.8 Beam Based Characterization of a New 7-pole Super-conducting Wiggler at CESR*.

A. B. Temnykh*, D.Rice and D. Rubin

Laboratory of Nuclear Studies
Cornell University, Ithaca NY 14953, USA
*abt6@cornell.edu

Abstract

The paper describes the beam based measurements of the magnetic field characteristics of the first 7-pole super-conducting wiggler recently installed in CESR. The results are compared with the model prediction and with the estimates based on magnetic field measurements. It also presents results of the beam resonance mapping which was done by a 2D scan of betatron tunes while recording vertical beam size. The scan clearly exposed resonances excited by the wiggler nonlinear magnetic field components. In conclusion, the ways to optimize the wiggler magnetic field in order to reduce destructive effects on beam dynamics are discussed.

2.8.1 Introduction

The CESR low energy upgrade project calls for 12 super-conducting wigglers installation to provide adequate radiation damping. The first 7-pole super-conducting wiggler [1] was built [2] and, after magnetic measurement [3], in the fall of 2002 was installed in CESR. A number of machine study periods were devoted to a beam based characterization of the wiggler magnetic field. Results of this characterization in comparison with the magnetic measurement and model prediction are described below.

2.8.2 Model calculation and Magnetic measurement result

The wiggler field integrals along straight lines and along wiggling beam trajectories are used for wiggler field characterization. Depending on the wiggler design, the difference between those integrals can be substantial. The straight line integrals calculated from model can be easily verified by a long flipping coil measurement [5]. The measurement of the field integrals along beam trajectory can be done by using modified vibrating wire technique [6] or with a beam after wiggler installation in the ring.

Magnetic measurement results for 2.1T and 1.9T wiggler peak fields in comparison with a model calculation are presented in the Table 1. Moments "*a*n" and "*b*n" are the coefficients of the polynomial fit of the horizontal and vertical field integral dependence on horizontal position: $I_x(x) = \sum_n an \times x^n$ and $I_y(x) = \sum_n bn \times x^n$. Columns "Straight line" and "Straight coil" refer to calculated and measured straight line integrals. Columns labeled with "Wiggling trajectory" and "Wiggling wire" are for integrals calculated and measured along wiggling trajectory of beam of 1.8GeV energy. The measurement technique is described in [3].

Table 1. Calculated and measured the wiggler integrated field characteristics.

an,bn [Gm/cm^n]	Model		Magnetic measurement	
	Straight line	Wiggling trajectory	Straight coil	Wiggling wire
Wiggler peak field ~ 2.1T				
a1	0.0	0.0	1.53+-0.01	N/A
b1	0.0	1.33	-0.19+-0.02	2.5+-0.15
b2	-0.29	-0.29	-0.28+-0.004	-0.51+-0.03
b3	0.0	-0.11	0.004+-0.002	-0.19+-0.02
Wiggler peak field ~ 1.9T				
a1	0.0	0.0	1.37+-0.01	N/A
b1	0.0	0.83	-0.21+-0.03	N/A
b2	-0.06	-0.18	-0.02+-0.001	N/A
b3	0.01	-0.10	0.007+-0.003	N/A

Because of the model symmetry, the skew and normal quadrupole moments *a1* and *b1* of straight line integrals are equal to zero. However the straight coil magnetic measurement revels non-zero but negligible normal quadrupole moment *b1*~0.2Gm/cm and significant for beam dynamics skew quadrupole component *a1* ~ 1.57-1.37Gm/cm. While the *b1* occurrence can be explained by a small error in pole geometry, the cause of relative large *a1* is not understood. The normal sextupole moment *b2* measured with straight coil is in good agreement with model calculation for both 2.1T and 1.9T wiggler fields. For 2.1T it is ~-0.28Gm/cm^2 and for 1.9T it is close to zero. The change in *b2* with a field level is due to specifics of the wiggler design. In the 7-pole design, the central pole is compensated by the two opposite polarity end poles. Because the magnetic field environment in the middle of the wiggler is different from the wiggler ends, the compensation can be provided in a limited range of excitation. Calculated and measured octupole moments *b3* are negligible.

Although the comparison between calculated and measured straight line integrals is the most convenient way to verify the model, the beam dynamics depends on the field integrals along ***wiggling beam trajectories***. In [4] it was noticed that interference between the beam trajectory wiggles and field variation across the single pole, $B_y(x)$, results in an additional integrated field: $\Delta I_y(x) \cong -(1/2)\cdot L\cdot x_p \cdot dB_y(x)/dx$; where x_p and L are the trajectory wiggling amplitude and the wiggler length. As $B_y(x)$ is a symmetric function, $dB_y(x)/dx$ and $\Delta I_y(x)$ are odd function of x. The latter generates the odd order moments (normal quadrupole *b1*, normal octupole *b3*) seen in column "Wiggling trajectory" of the Table 1. Magnetic measurement with a vibrating wire (column "Wiggling wire") confirmed existence of these moments but gave approximately two times bigger amplitudes. This inconsistency is likely to be a result of a not accurate calibration of the used vibrating wire technique.

2.8.3 Beam based characterization

2.8.3.1 *Wiggler generated coupling*

Beam based measurement of the local coupling around the ring indicated ~2.0Gm/cm skew quadrupole moment generated by the wiggler, which is in good agreement with a magnetic measurement result. This component was compensated with skew quadrupole magnet installed near the wiggler.

2.8.3.2 *Wiggler generated betatron tune variation*

Vertical and horizontal betatron tunes were measured as a function of horizontal beam position in the wiggler at several wiggler field levels. For the beam displacement a closed orbit bump was used. The result of the measurement at 2.1T and 1.9T fields in comparison with tune variation obtained from the model tracking are plotted in Figures 1 and 2. In all cases one can see a reasonable consistency between calculation and measurement.

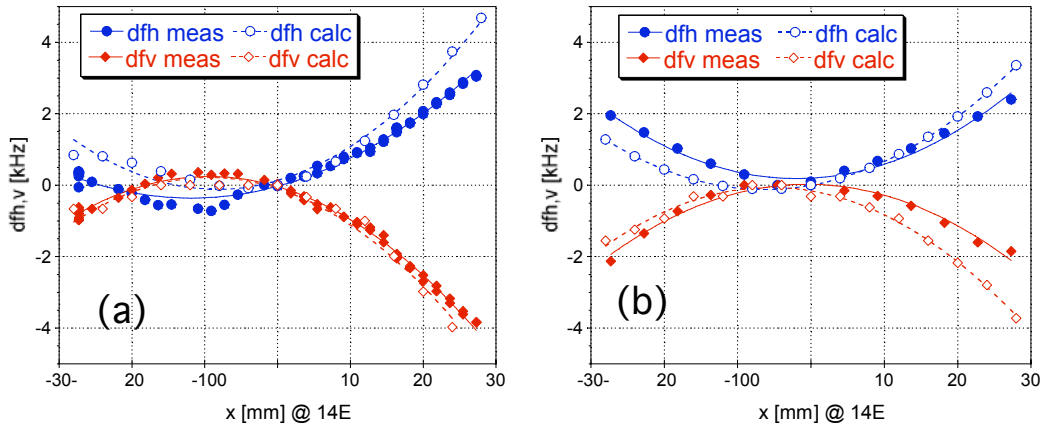

Figure 1. Measured and calculated betatron tune variation versus horizontal beam position in the wiggler at 2.1T (a) and 1.9T (b) wiggler peak field.

The sextupole and octupole moments calculated from the coefficients of the polynomial fit of the measured horizontal tune variation are given in Table 2. They are in good agreement with calculated, see column "Wiggling trajectory" in Table 1.

Table 2. The *b2* and *b3* moments calculated from the measured dependence of horizontal tune on horizontal beam position in the wiggler.

Moment	2.1T	1.9T
b2[Gm/cm^2]	-0.29+-0.01	-0.059+-0.011
b3[Gm/cm^3]	-0.082+-0.002	-0.10+-0.004

2.8.3.3 *Nonlinear resonances excitation and tune plane appearance*

The machine performance (luminosity, injection efficiency, beam life time and etc.) often critically depends on the appearance of the betatron tune plane. The tune scan, a measurement of beam characteristics as a function of the betatron tunes, exposing the tune

plane resonance structure facilitates the choice of the working point and the structure analysis may help to reveal the cause of magnetic field nonlinearities affecting machine performance.

To explore effect of the wiggler magnetic field on the nonlinear beam dynamics we made a series of tune scans with a vertical beam size measurement. Two examples are shown in Figures 2.

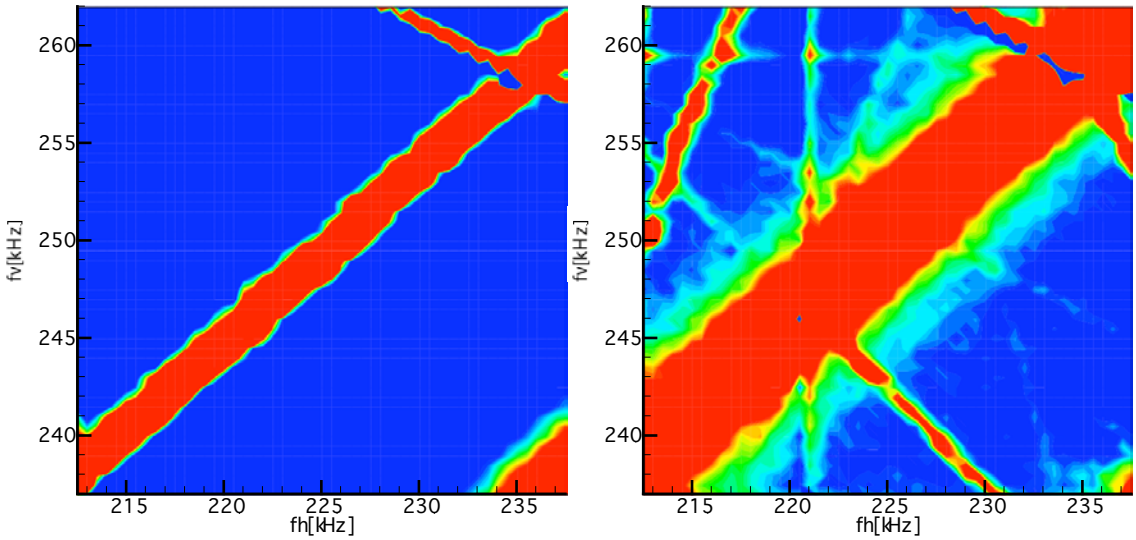

Figure 2. Vertical beam size versus betatron tune measured with CESRC-c wiggler turned OFF (left plot) and at 2.1T wiggler magnetic field (right plot).

Here is depicted the vertical beam size as a function of betatron tunes on a 40x40 grid measured with zero and 2.1T wiggler peak field and a flattened orbit. Both plots have the same vertical beam size scale. Vertical beam size was measured using synchrotron light monitor. To help identify resonances Figure 3 shows a resonance map corresponding to the experimental condition.

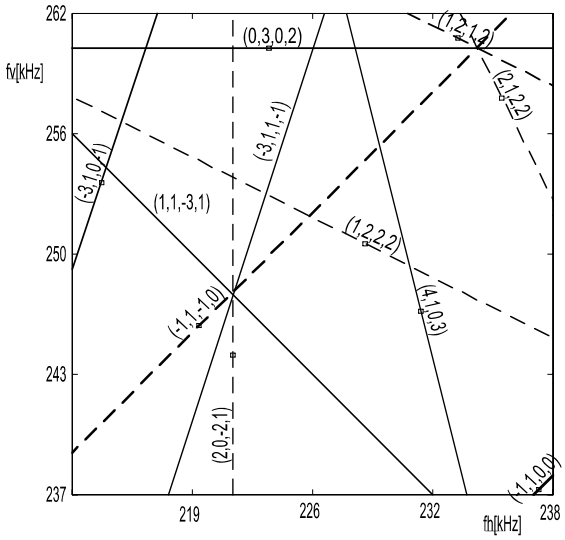

Figure 3. Resonance map for a scanned tune plane area. Shown are resonances seen in measurement. Labels (p, q, r, n) indicate $p f_h + q f_v + r f_s = nf_0$ resonance lines.}

On the map, only resonances seen in measurement are shown. The effect of the wiggler field on the beam dynamics can by clear observed by comparison of these two measurements. With wiggler field turned off, the scanned area is relatively clean. There are only 3 resonance lines: -fh+fv = 0, -fh+fh-fs=0, fh+2fv+fs=2f0. With 2.1T wiggler field one can see 8 additional "working" resonances: -3fh+fv=-f0, fh+fv-3fs=f0, 3fv=2f0, fh+2fv+2fs=2f0,

4fh+fv=3f0, 2fh+fv+2fs=2f0, 2fh-2fs=f0 and -3fh+fv+fs=-f0 covering much bigger area then the previous. Based on this observation one can conclude that in the given case the wiggler nonlinearity is a major player in a nonlinear beam dynamics.

A tracking simulation of the observed effect of the wiggler field on beam dynamics is progress.

2.8.4 Conclusion

The magnetic field of the first 7-pole super-conducting wiggler was characterized by the magnetic and beam based measurements. Reasonable agreement has been found between these measurements and the model calculations. Results of tune plane scanning suggest that the effect of the wiggler field nonlinearity on beam dynamics dominates over the effect from the rest of the ring and could compromise machine perfomance.

The part of the wiggler nonlinearity problem can be associated with the design specific. In symmetric 7-pole configuration the central pole is compensated by two opposite polarity end poles. But because of very different magnetic environment at the ends and in the middle of the magnet this compensation can not be fulfilled completely. The corroboration of the modeling of the CESR-c wigglers by the measurements presented above was an important step in the decision for the final 8-pole configuration of the wigglers. In 8-pole design each pole is compensated by the identical pole of opposite polarity. This provides better field nonlinearity compensation in a wider range of the wiggler field excitation.

References

[1] James Crittenden et al., *Design Considerations for CESR-c Wiggler Magnets*, to be published in PAC2003 proceedings.

[2] David Rice, Richard Gallagher et al., *Production and Testing Considerations for CESR-c Wiggler Magnets*, to be published in PAC2003 proceedings.

[3] A. Temnykh, *Vibrating Wire and Long Integrating Coil Based Magnetic Measurements of a 7-pole Super-Conducting Wiggler for CESR.*, to be published in PAC2003 proceedings.

[4] J. Safranek et al., *Nonlinear Dynamics in SPEAR Wigglers*, EPAC' 2000, p.295

[5] This measurement technique was developed by the ID group at ESRF. *Developpment de Banc de measures magnetiques pour undulateurs et wigglers*, D. Frachon Thesis, April 1992.

[6] A. Temnykh, *Some aspects of the use of Vibrating Wire Technique for a wiggler magnetic field measurement*, Preprint CBN 01-17, Cornell 2001.

2.9 Recent Developments for Injection into CESR

M.G. Billing, J.A. Crittenden, M.A. Palmer, LEPP, Cornell University
mgb@cesr10.lns.cornell.edu, critten@cesr10.lns.cornell.edu, map36@cornell.edu

2.9.1 Introduction to Injection into CESR

Since 1978 the Cornell Electron Storage Ring (CESR) facility has functioned as an electron-positron collider. During its operation CESR has employed several injection schemes, including the coalescing of positrons, injection with and without pretzeled orbits, topping-off mode, and injection with horizontal and vertical separation. A feature common to these injection methods has been the use of a full betatron wavelength bump at the injection point, which is pulsed with a half-sinusoidal amplitude variation and has a duration of 4 rotation periods (turns.) This bump typically places the stored beam centroid within 4 horizontal sigma of the injection septum's vacuum chamber wall to reduce the oscillation amplitude of the injected beam. The stored beam is left with no oscillation amplitude from the pulsed bump, while the injected beam oscillates with its amplitude equal to the full injected-beam-to-stored-beam displacement. A pinger magnet, which applies a constant deflection to the beam for one turn, is timed to decrease the injected beam's oscillation amplitude and to cause the stored beam to acquire an amplitude equal to the reduction of the injected beam's oscillation. This sharing of the injected beam's oscillation between the stored and injected beam reduces the required injection aperture.

With the introduction of horizontal pretzel separation of multibunch beams for collisions in CESR, the available aperture in the arcs for electron injection was substantially reduced by the aperture needed for the stored positron beam. To improve injection under these conditions, several important techniques were developed. The first was to operate with different tunes for the two beams to reduce the parasitic beam-beam coupling effects. This was accomplished with sextupole control knobs, making use of the differential horizontal displacements of the two beams in the sextupoles. Another technique was to operate on the coupling resonance, effectively reducing the horizontal eigenmode's emittance at the expense of the vertical eigenmode. Since there is a large shift in the coherent uncoupled tunes from the beam-beam interaction as the electron beam is filled to full current against the stored positrons, the coupling resonance width must be large enough to maintain the electron beam on resonance. In addition, off-energy injection is routinely employed to reduce the betatron motion of the injected electrons at the expense of increasing the synchrotron motion. Lastly bunch-by-bunch beam stabilizing feedback was added to damp coherent horizontal, longitudinal and vertical motion. The most demanding part of the injection process is the injection of electrons in the presence of the stored positron beam, since this requires adequate apertures for both stored beams and for the injected bunches of electrons

During the last year, CESR has begun the conversion from a beam energy of 5 GeV to operations at energies near the charm threshold (1.5 to 2.5 GeV.) In the initial studies of this new configuration from September 2002 through January 2003, only one of the new superconducting damping wigglers was installed. Despite the additional damping provided by two CHESS low field permanent magnet wigglers, the overall increased radiation damping time, as compared with 5 GeV operation, had a significant impact on injection. The most obvious effect is that the injection repetition rate, normally at 60 Hz, must be reduced to 7.5 Hz to allow for enough damping of the injected electrons before the next injection cycle.

In addition the multiple scattering of the injected beam in the thin window separating the vacuum of the transport line from CESR's vacuum causes an increase in the angular distribution by about a factor of 3. Also, the initial optics had some compromises that adversely affected injection. As a result of the increased machine studies time devoted to injection, some new tools have been developed to assist in the study of injection and in certifying the quality of new optics designs.

2.9.2 Analysis of Injection Transients

In 2002 the electronics for about 15 (of the 100 total) beam position monitors (BPM's) in CESR were upgraded to give higher position resolution and to allow for the single shot acquisition of 1000 turns of position and intensity data, even at the low injected beam currents. The increased resolution and the transient acquisition capability allow the collection of BPM data in a variety of injection conditions. Software has been developed for analyzing these transient measurements by projecting freely propagating uncoupled betatron and energy oscillations forward from the injection point in CESR. For the horizontal and vertical position data for each detector, the analysis begins by subtracting the average horizontal and vertical position, respectively, from the data. The remaining "transient" undergoes a least-squares fit for the parameters a_0, a_1, c_0, and c_1 which uses all the BPM's for N turns and has the following general form,

$$\chi^2 = \sum_d \sum_{n=n_0}^{n_0+N} \left\{ x_{dn} - \langle x_{dn} \rangle - \begin{pmatrix} 1 & 0 \end{pmatrix} T_{d0}\, T_{00}^m \begin{pmatrix} a_0(n_0) \\ a_1(n_0) \end{pmatrix} - \begin{pmatrix} \eta_d & 0 \end{pmatrix} E_{00}^m \begin{pmatrix} c_0(n_0) \\ c_1(n_0) \end{pmatrix} \right\}^2$$

with $m = n - n_0$, where the fit begins on the n_0–th turn after the injection transient, d is the detector index, x_{dn} is the position at detector d on the n-th turn and the angle brackets denote the average. In this equation, T_{00} is the 2-by-2 one turn betatron transport matrix at the injection point, T_{d0} is the transport matrix from the injection point to detector d. The dispersion at detector d is denoted as η_d and E_{00} is given by

$$E_{00} = \begin{pmatrix} \cos \mu_z & \sin \mu_z \\ -\sin \mu_z & \cos \mu_z \end{pmatrix}$$

where the total synchrotron oscillation phase advance is $\mu_z = 2 \pi Q_z$, with Q_z denoting the synchrotron tune. This equation represents the single-turn transport of the synchrotron oscillation and applies since the 15 detectors occupy a continuous region of the ring. The equation for χ^2 above is used in this form for the analysis of the horizontal BPM data, but the term involving c_0, and c_1 is excluded when fitting the vertical BPM data. In addition, the matrix T_{00} is written explicitly in terms of $\mu_x = 2 \pi Q_x$ or $\mu_y = 2 \pi Q_y$, where Q_x and Q_y are the betatron tunes. In a separate step, the tunes are varied to minimize the fit and, using these tunes, a_0, a_1, c_0, and c_1 are again calculated. These steps are repeated until a minimum χ^2 is reached.

For CESR, N is chosen to be 42 turns since this encompasses a few synchrotron oscillation periods. To assure that the beam motion propagates as a free betatron and synchrotron oscillation, the fit begins on turn 5 to be certain that all deflections from the pulsed bumps and pinger do not affect the fit. The results are presented into two different formats. One gives the best-fit values for the projection of the initial injection coordinates, x, x', y, y', δ, and δ' = Δz / (α_p C), where Δz is the change of path length, α_p is the momentum

compaction factor and C is the circumference of the ring. These results are also written in terms of one form of action-angle variables, A_x, θ_x, A_y, θ_y, A_z, and θ_z, which here are defined as

$$A_u = \sqrt{u^2 + (\alpha_u u + \beta_u u')^2} \qquad \theta_u = \tan^{-1}\left(\frac{\alpha_u u + \beta_u u'}{u}\right)$$

$$A_\delta = \sqrt{\delta^2 + (\delta')^2} \qquad \theta_\delta = \tan^{-1}\left(\frac{\delta'}{\delta}\right)$$

and where u refers to either x or y. In addition, the fitted values of μ_x, μ_y, and μ_z are described in terms of their oscillation frequencies. The second format presents a set of 9 plots which give the initial injection coordinates in action-angle variables and the three oscillation phase advances per turn as a function of the starting turn, n_0, for the fit, as n_0 is moved along in 7 turn steps. The projected injection angles from fit windows starting with later initial turns are corrected with the fitted values of μ_x, μ_y, and μ_z from windows starting with earlier turns. The successful correction of these tune changes will be visible as a constant projected θ_x, θ_y, or θ_z as the initial turn of the fit window is varied.

Table 1. Results from fits of the initial injection oscillation of a single bunch of electrons projected to the injection point. The spatial coordinates, x, x', y, y', δ, and δ', as well as the action-angle coordinates, A_x, θ_x, A_y, θ_y, A_z, and θ_z, are described in the text. f_x, f_y, and f_z are the fitted frequencies of the horizontal, vertical and longitudinal oscillations.

Horizontal			Vertical			Longitudinal		
x	0.51	mm	y	1.2	mm	δ	-4.4	x 10^{-3}
x'	0.34	mrad	y'	0.13	mrad	δ'	0.4	x 10^{-3}
A_x	7.6	mm	A_y	1.3	mm	A_z	4.5	x 10^{-3}
θ_x	1.50	rad	θ_y	0.57	rad	θ_z	2.65	rad
f_x	206.8	KHz	f_y	242.8	KHz	f_z	36.4	KHz

Results are given in Table 1 for the 42-turn fit to data beginning on turn 5 from one measurement of the oscillation of an injected electron bunch. These results imply a 7.6 mm horizontal injection oscillation as observed at the injection point while the vertical has a small oscillation amplitude. This bunch was injected into CESR 0.4% below the storage ring's energy. All three fitted oscillation frequencies are in good agreement with the injection optics working point. Figure 1 presents the plots of the fits from stepping the fit window along the injection transient. The horizontal fits show the initial 7.6 mm oscillation amplitude "damps" in about 400 turns, while over the same time, μ_x remains relatively constant (as is seen in relatively flat fits for both μ_x and θ_x.) This "damping" of the motion is not due radiation damping, which is approximately 34,000 turns, or feedback (as the injected bunch signal is below the system's noise threshold), but rather represents the decoherence of the bunch's motion. When the position signal decoheres sufficiently after turn 420, the fitting of μ_x and, hence, θ_x becomes poor. The longitudinal motion also indicates a decoherence of its motion with a charactreristic time constant of about 1200 turns. As observed in the plot of A_z vs. turns, there is no significant change in the bunch's synchrotron frequency over the data sample. The fits to the vertical position data appear to be good fits only for the first 200 turns, probably due at least in part to the very small initial amplitude. After turn 200, the fitting of the vertical frequency and the oscillation phase become unreliable. The apparent oscillation of the vertical amplitude within the first 200

turns is suggestive of some possible horizontal-to-vertical coupling of the motion, but no firm conclusion may be drawn from this analysis.

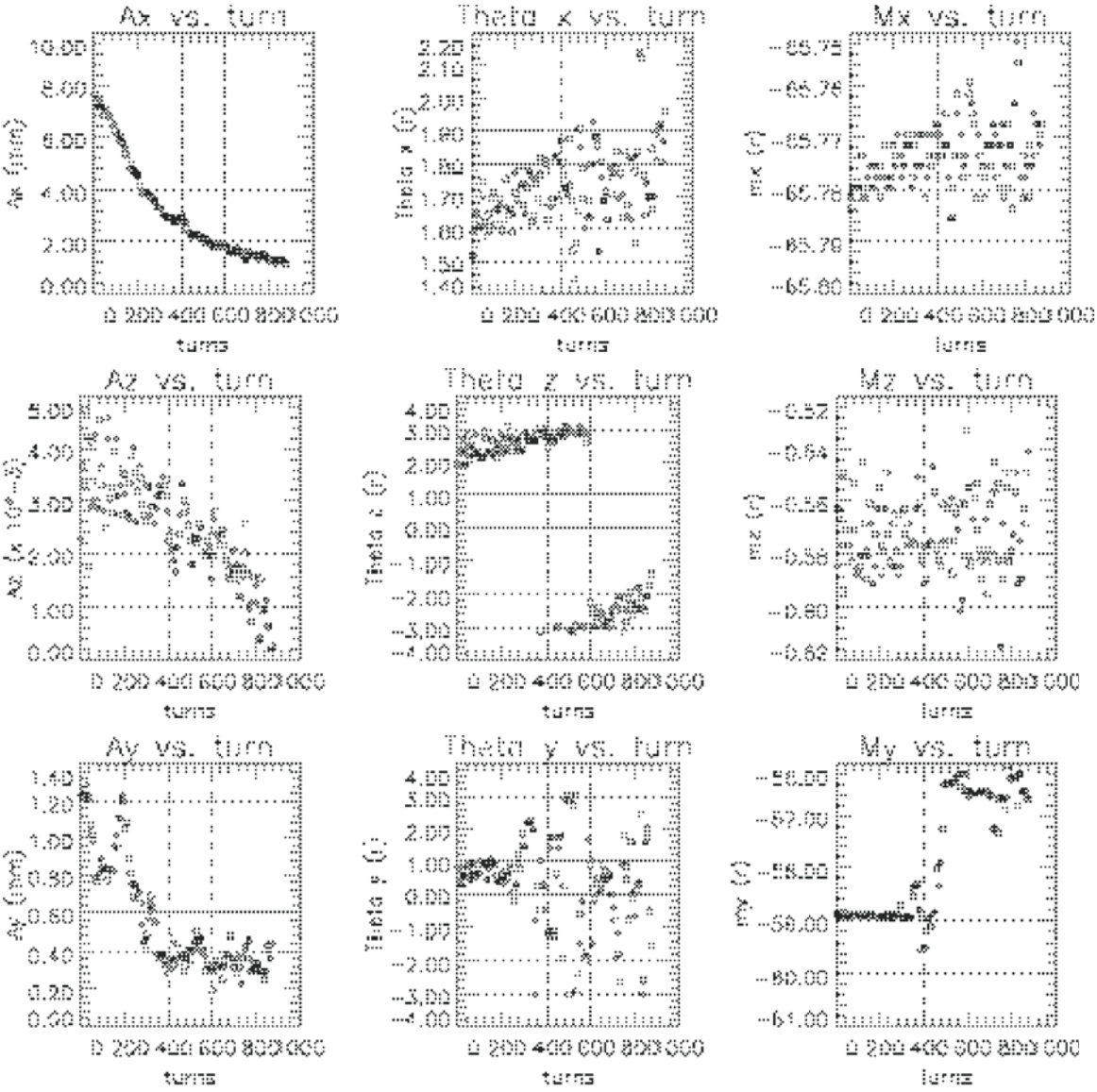

Figure 1. Plots of A_x, θ_x, A_y, θ_y, A_z, and θ_z vs. the initial turn number of the 42 turn fit window as the initial turn is changed. In the remaining plots, M_x, M_y, and M_z refer to μ_x, μ_y, and μ_z, respectively.

A number of sets of data for the injected or stored beams, containing injection transients under different conditions during January 2003 at 1.8 GeV have been acquired and analyzed. A summary of these results is presented in Table 2; the uncertainties represent a combination of statistical and estimated systematic errors. The total displacement of the injected beam relative to the stored beam at the septum magnet equals the sum of the amplitude for the injected beam from the pulsed bump, the amplitude for the stored beam from the pinger and the dispersion at the injection point (1.5 m) times the fractional energy error, giving 18 mm in reasonable good agreement with the expected displacement.

Table 2. Summary of the transient position measurements at 1.8 GeV beam energy and for injection conditions with different pulsed elements firing. The horizontal and vertical results represent the oscillation amplitudes, while the longitudinal is the fractional energy deviation amplitude. All results are projections to the injection point at the injection time for electrons.

Condition	Amplitude		
	Horizontal	Vertical	Longitudinal
Injected Electrons with Pulsed Bumper and Pinger Magnets	7.4 ± 0.7 mm	1.3 ± 0.1 mm	4.7 ± 0.2 x 10^{-3}
Stored Electrons with Pulsed Bumper Magnets	1.6 ± 0.3 mm	0.17 ± 0.02 mm	0.1 ± 0.1 x 10^{-3}
Stored Electrons with Pulsed Pinger Magnet	3.5 ± 0.3 mm	0.39 ± 0.05 mm	0.2 ± 0.1 x 10^{-3}

2.9.3 Characterization of Optics Designs

The ability to analyze the injection trajectories with reasonable accuracy suggests that this information may be applied to improving the modeling of injection of electrons against stored positrons. One facet of this conclusion is that it should be possible to make a more realistic computation of the physical space required by the injected and stored beams during the injection process. The physical space required for each beam is defined as the volume that contains the injection oscillations plus some number of sigma of the beam's size. One method to determine this injection volume for each beam would be via by tracking multiple particles representing the distribution of this beam, and then keeping track of space in which particles survive some large number of turns. This approach requires substantial computing time and a good representation of the particle distributions in the beams. Another, albeit approximate, method is considered here as a much less computationally intensive approach to studying the injection properties of a set of optics.

The new approach defines an envelope for each beam as the physical space occupied by the beam's centroid and is expected to be useful when the motion of the centroid is comparable to or larger than the size of the beam. This choice of a definition for the beam's envelope removes from the analysis any questions concerning the particle distribution immediately preceding the injection process. A further assumption is that as a beam oscillates, undergoing betatron or synchrotron motion, the damping of this motion occurs after a large number of oscillations such that the maximum amplitude of the oscillation will be achieved at every point around the storage ring. This additional assumption gives a limiting envelope for the beam and simplifies the calculation so that this envelope may be easily computed at each element in the storage ring. From this envelope and the known pretzel displaced equilibrium orbits of each beam, the clearance of the envelope from the physical aperture or the centroid of the other beam is then calculated. In the present implementation of the software this clearance is presented both in the units of length and in terms of the number beam-size sigma of stored beam.

At any location s in the ring, the analysis may be described as follows. (For simplicity only the x direction will be described here.) The calculation makes use of the local beta-

function β_x and dispersion η_x and, for the computation of the beam-size σ_x, the global properties of the stored beam's emittance ε_x and fractional energy spread σ_δ.

$$\sigma_x = \sqrt{\varepsilon_x \beta_x + \left[\eta_x \delta_E \right]^2}$$

At this same location the pretzel displacement of the orbit for the stored beam x_p and maximum displacement due to the pulsed bump x_{PB} are required. Any betatron injection oscillations will be described by their equivalent action (in the same units as the emittance), while energy oscillations will be characterized by their maximum fractional energy amplitude.

At s the envelope for the stored electrons x_{se} is then

$$x_{se} = \max\left\{ \left| x_{PB} \right| , \left| \sqrt{A_{se} \beta_x} \right| \right\} + \left| \eta_x \delta_{w,se} \right|$$

where A_{se} is the horizontal action from residual oscillations and $\delta_{w,se}$ is the energy oscillation amplitude, both produced by the pinger and any non-closure of the pulsed bumps for the stored electrons. Thus the wall clearance for the stored electrons $x_{c,\,se}$ is

$$x_{c,se} = A_{wall} - \left| x_p \right| - x_{se}$$

where the half aperture A_{wall} is reduced by the displacement of the pretzeled orbit and the stored electron envelope. A negative value implies scraping.

The action of the betatron injection oscillation of the injected bunch A_{ie} is

$$A_{ie} = \frac{1}{\beta_x (\mathrm{Inj})} \left\{ x(\mathrm{Inj}) - \left| x_p (\mathrm{Inj}) \right| - \left| \eta_x (\mathrm{Inj}) \delta_{ie} \right| - \sqrt{A_{Ping,ie} \beta_x (\mathrm{Inj})} - \left| x_{PB} (\mathrm{Inj}) \right| \right\}^2$$

where (Inj) designates the value is taken at the injection point, x(Inj) is the displacement of the injected beam from the storage ring axis, δ_{ie} is the fractional energy error of the injected beam and $A_{Ping,\,ie}$ is the action removed from the injected beam's oscillation by the pinger magnet. Thus the injected electron's envelope x_{ie} is

$$x_{ie} = \sqrt{A_{ie} \beta_x} + \left| \eta_x \delta_{ie} \right|$$

So that the injected beam's wall clearance is written as

$$x_{c,ie} = A_{wall} - \left| x_p \right| - x_{ie}$$

and the injected beam's clearance of the stored positrons $x_{c,ie+}$ is

$$x_{c,\,ie+} = 2\left| x_p \right| - x_{ie} - \sqrt{A_{se} \beta_x} - \left| \eta_x \delta_{se} \right|$$

where the last two terms give the positron beam's envelope. In writing this expression two assumptions have been made, the pretzel displacement is opposite in sign for the positron stored beam and the magnitudes of the oscillation transients are same for the stored positron and electron beams.

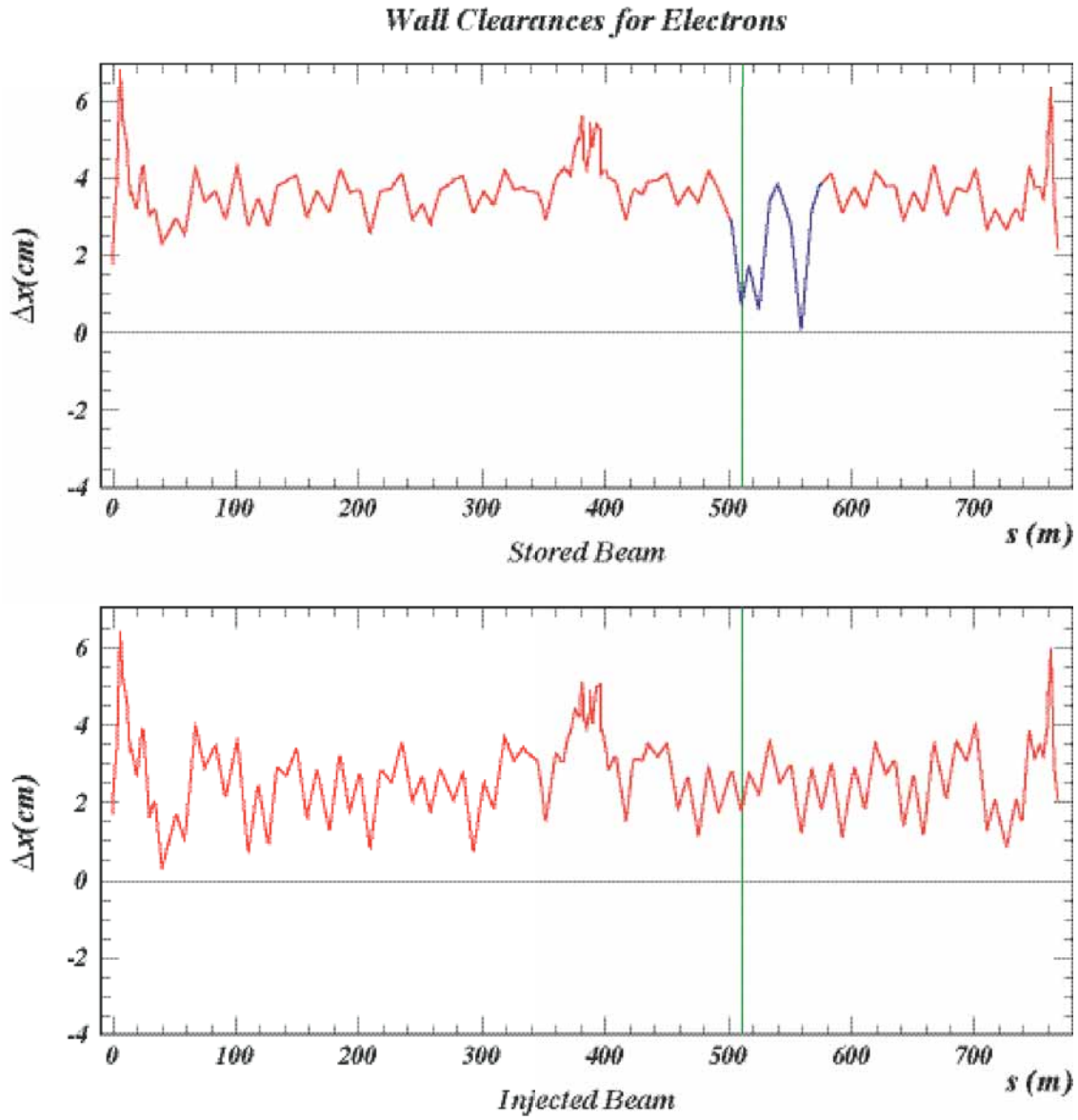

Figure 2. Wall clearances for the stored and injected electron beams around the entire storage ring. The section of the stored electron wall clearance plot, which is in blue, represents the reduced clearance due to the pulsed bump. The vertical green line marks the injection point.

The results of the analysis of the injection trajectories, which were described in the previous section, have been used as inputs for software that calculates the envelopes and clearances. For the calculations shown here, it has been assumed that the vertical size of the beam has been increased due to the full emittance coupling from the horizontal, which in turn reduces the horizontal emittance to half its uncoupled value. Figure 2 shows the wall clearances for the stored and injected electron beams in the 1.8 GeV optics used in January 2003. The wall clearance for the stored beam is at least 24 mm in the arc of CESR, except in the region of the pulsed bump, which is plotted in blue. The stored beam is permitted a much closer approach of the wall by the injection septum, since the pulsed bump only places the stored beam in proximity of the wall for one turn per injection cycle (7.5 to 60 Hz.) The wall clearance is at least 9 horizontal sigma around the ring except in the pulsed bump. Notice the pulsed bump clearance at 510 m (the injection point, where the clearance is 4 sigma,) is greater than at 520 and 560 m. These optics required a closed orbit bump placed with peaks near 520 and 560 m to improve the lifetime of the stored beam when the pulsed bump was triggered. This analysis predicts that the centroid of the injected will have the closest

approach to the wall at 40 m. This region also required a closed orbit bump to optimize injection.

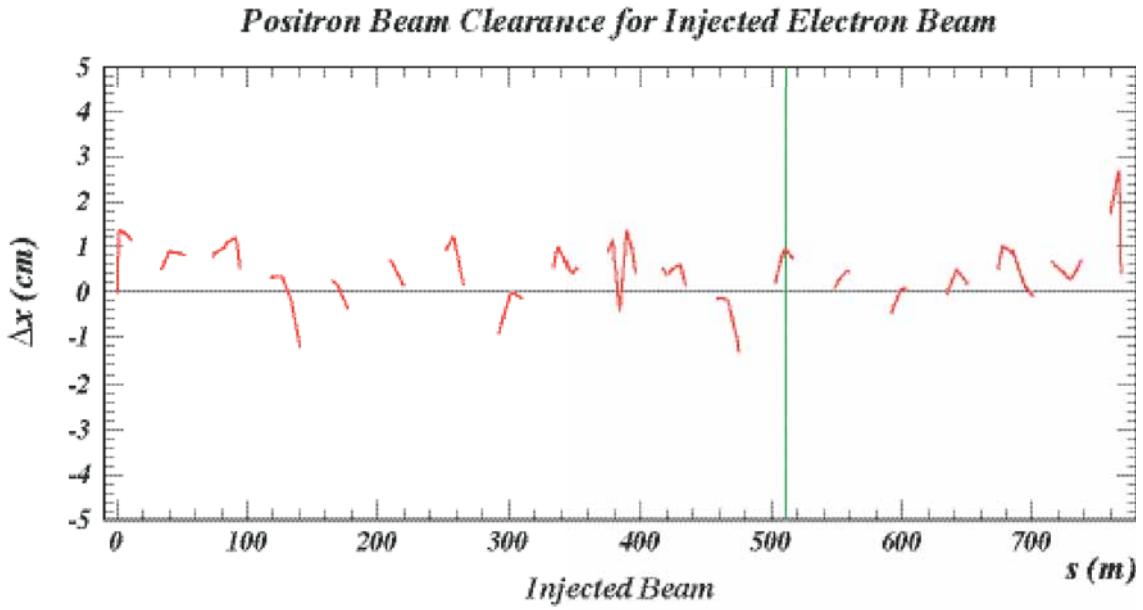

Figure 3. Clearance between the stored positron beam and the injected electrons. The plot shows only regions in the ring near the locations where the injected electrons encounter trains of positrons bunches.

The clearance of the injected electrons from the stored positron beam is shown in Figure 3. Here the results show that, although the injected beam clears the center of the stored positron beam most places, it will approach or pass through the center of the positron beam in a few locations. Although the accuracy of these predictions has not yet been confirmed, in practice it was quite difficult to produce good injection rates in these optics in January 2003.

2.9.4 Conclusions

The analysis of BPM data taken during injection transients appears to be a useful tool for the understanding of the injection process. In addition to helping to understand and evaluate injection into CESR, these tools are expected to give statistical information about the quality of the beam as it emerges after acceleration in the linear accelerator and synchrotron.

Even with the simplifying assumptions, the analysis method for evaluating optics for injection based on the envelope and clearance of the beam centroids should become quite useful after some experience observing conditions that have differing levels of success with injection. One must be careful to remember that although these assumptions are sufficient to predict successful injection, they are not absolutely necessary. In particular how close an injected electron bunch may pass by a stored positron bunch time after time before a significant number of electrons are lost is not known very well, nor is its dependence on the stored beam current.

2.10 Progress of the PEP-II B-Factory *

J. Seeman, M. Browne, Y. Cai, W. Colocho, F.-J. Decker, M. Donald, S. Ecklund, R. Erickson, A. Fisher, J. Fox, S. Heifets, R. Iverson, W. Kozanecki, P. Krejcik, A. Kulikov, A. Novokhatski, P. Schuh, H. Schwarz, M. Stanek, M. Sullivan, D. Teytelman, J. Turner, U. Wienands, Y. Yan, J. Yocky, SLAC, Stanford, CA 94309, USA;
M. Biagini, INFN, Frascati, Italy; M. Zisman, LBNL, Berkeley, CA 94720, USA

mailto: seeman@slac.stanford.edu

Abstract

PEP-II is an e^+e^- B-Factory Collider located at SLAC operating at the Upsilon 4S resonance. PEP-II has delivered, over the past five years, an integrated luminosity to the BaBar detector of over 139 fb^{-1} and has reached a luminosity of $6.58x10^{36}/cm^2/s$. Steady progress is being made in reaching higher luminosity. The goal over the next several years is to reach a luminosity of at least $2x10^{34}/cm^2/s$. The accelerator physics issues being addressed in PEP-II to reach this goal include the electron cloud instability, beam-beam effects, parasitic beam-beam effects, high RF beam loading, shorter bunches, lower betay*, interaction region operation, and coupling control. A view of the PEP-II tunnel is shown in Figure 1.

The present parameters of the PEP-II B-Factory are shown in Table 1 compared to the design. The present peak luminosity is 219% of design and the best integrated luminosity per month is 7.4 fb^{-1} that is 225% of design. The best luminosity per month is shown in Figure 2. The integrated luminosity over a month is shown in Figure 3 and the total integrated luminosity in shown in Figure 4.

The progress in luminosity has come from correcting the orbits, adding specific orbit bumps to correct coupling and dispersion issues, lowering the beta y* in the LER, and moving the fractional horizontal tunes in both rings to just above the half integer (<0.52).

* Supported by US DOE contracts DE-AC03-76SF00515 and DE-AC03-76SF00098.

Table 1: PEP-II June 2003 Parameters.

Parameter	**PEP-II Design**	**PEP-II Present**
Energy (GeV)	3.07x9	3.1x8.97
HER Vertical tune	23.64	23.57
HER Horizontal tune	24.62	24.516
LER Vertical tune	36.64	36.63
LER Horizontal tune	38.57	38.509
HER current (mA)	750	1175
LER current (mA)	2140	1550
Number of bunches	1658	1034
Ion gap (%)	5	2.6
HER RF klystron/cav	5/20	7/24
HER RF volts (MV)	14.0	11.5
LER RF klystron/cav.	2/4	3/6
LER RF volts (MV)	3.4	3.2
β_y* (mm)	15-25	12
β_x* (cm)	50	35
Emittance (x/y) (nm)	49/2	21 to 49/3
σ_z (mm)	11	12
Lum hourglass factor	0.9	0.84
Crossing angle(mrad)	0	<0.5
IP Horiz. size Σ (μm)	222	150
IP Vert. Size Σ (μm)	6.7	6.8
HER Horizontal ξ_x	0.03	0.071
HER Vertical ξ_y	0.03	0.054
LER Horizontal ξ_x	0.03	0.070
LER Vertical ξ_y	0.03	0.059
Lumin. ($x10^{33}/cm^2/s$)	3.00	6.58
Int. Lum/month (fb^{-1})	3.3	7.4
Integ. Lumin. (fb^{-1})	100 (for CP)	139

Figure 1 View of the PEP-II tunnel.

2.10.1 Run 3 Status

PEP-II has been providing colliding beams for the BaBar detector since May 1999 [1-8]. The present run started in November 2002 and ended in June 2003. There will be a two-month down this summer with beam starting again in September 2003. During the recent run, colliding beams occupied 70% of the time, 20% for repairs, and 10% for machine development and accelerator physics studies. About 87% of the data logged by BaBar was on the Upsilon 4S resonance and 13% off-resonance about 40 MeV lower. PEP-II has scanned the Upsilon 3S, shown in Figure 5. The highest luminosity in PEP-II is $6.58 \times 10^{33}/cm^2/s$ with the corresponding parameters listed in Table 1. The horizontal beam size of the LER is enlarged at this peak luminosity by about 20%. Also, the vertical beam size of the HER is enlarged by about 20% at the peak luminosity. Both increases are due to the beam-beam effect. 391 pb^{-1} has been delivered in 24 hours. The present delivered luminosity to BaBar is 139 fb^{-1}.

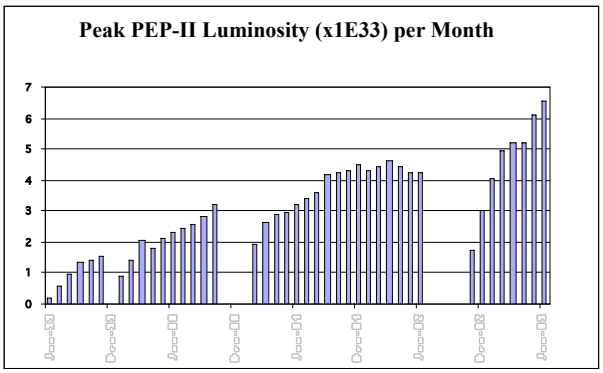

Figure 2 Peak luminosity each month since May 1999. The peak luminosity has reached $6.58 \times 10^{33}/cm^2/s$ in June 2003.

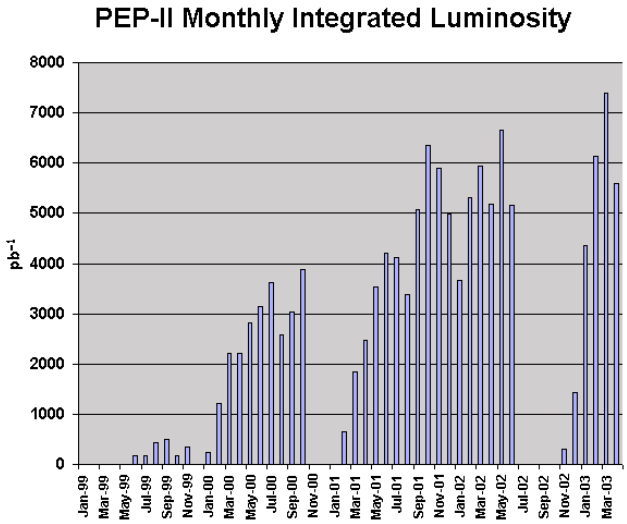

Figure 3 Integrated luminosity per month. In March 2003 PEP-II deliver 7.4 fb^{-1} and BaBar logged 7.2 fb^{-1}.

2.10.2 Beam-Beam interaction

At low currents, the luminosity increases as the product of the electron and positron bunch charges. At higher currents the LER-x and HER-y beam sizes enlarge due to beam-beam and, perhaps, electron cloud effects in LER, thus, reducing the luminosity increase with current. The HER and LER bunch charges are appropriately balanced to produce near equal beam-beam effects. If there is a miss-balance, flip-flop effects can occur. The horizontal tunes of both rings were recently moved to just above the half integer (~0.52) and an immediate increase of about 20% in luminosity occurred. In order to move the LER to the half integer, the horizontal beta beats in the LER had to be fixed. Moving close to the half integer makes the beta beats worse. A computer algorithm (MIA) was created and recently has been made to work. The beta beats in the LER are below 10%. The HER still needs additional work and will be worked on soon.

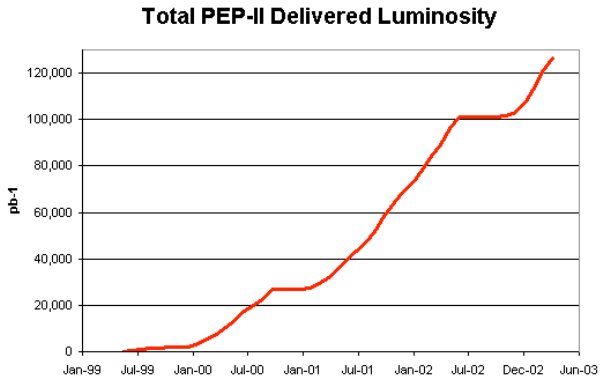

Figure 4 Total delivered integrated luminosity to BaBar by PEP-II is 139 fb^{-1} completed in June 2003.

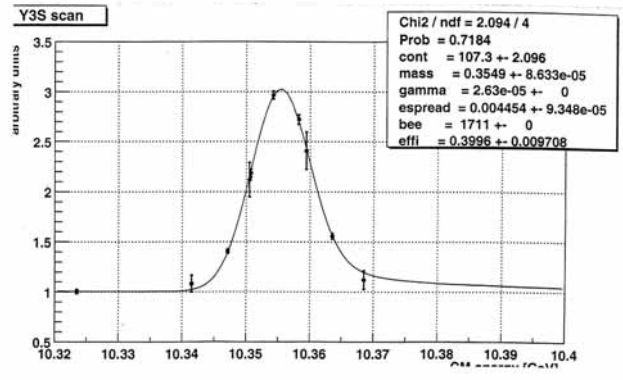

Figure 5 Energy scan of the Upsilon 3S resonance in November 2002.

Recently, PEP-II has been operated with bunches every three RF buckets but with mini-gaps after about 10 to 11 bunches to allow easy bunch number changes and to reduce small ECI effects. A plot of the bunch luminosity over the whole train is shown in Figure 6. There are no obvious signs of ECI over the train. With two bucket spacing, there are signs of electron cloud effects and parasitic beam-beam effects. To help reduce the ECI effects in the By-2 pattern, stronger solenoids will be added to the LER straight sections this coming summer. The parasitic crossing beam-beam effects are largest in the vertical plane where the vertical betas are much larger than the horizontal betas at the parasitic collisions displaced 63 cm from the IP on both sides. As the betay* is lowered the parasitic effects will become stronger. The exact limit of this effect is under study.

Beam-beam parameters from 0.054 to 0.071 are now routinely achieved in PEP-II that far exceed our design goal of 0.03.

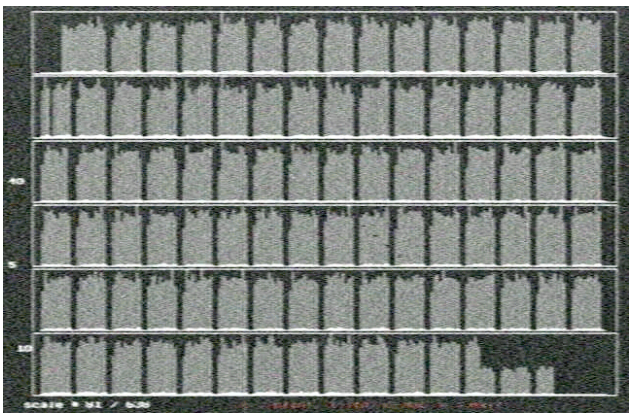

Figure 6 Bunch luminosity along the train with every 3th RF bucket filled and a 2.6% ion gap at the end of the train. There are mini-gaps of about 5 RF buckets.

2.10.3 Interaction Region Heating

At the interaction point of PEP-II there is a Be chamber surrounded by a precision silicon strip detector SVT of BaBar. The Be chamber is double-walled with water cooling between. At present, the water removes about 1 kW of HOM and I^2R heat load. This 60 cm long chamber is connected to the nearby B1 dipole magnet chamber with a two convolution bellows on each end. In the summer of 2002, the IR support tube was removed and extra cooling of air and water added, new temperature instrumentation was added to the Be chamber bellows, a new Q2

crotch chamber with lower HOM generation was installed, and new higher power Q2 bellows were installed. The increased power capability of a factor of four to five should allow a factor of about four increase in luminosity. During recent operation, the new cooling techniques have performed according to specification.

2.10.4 Future Plans

PEP-II has an upgrade plan that is leading towards a luminosity of greater than $2x10^{34}$ in FY2006. Combining the equations for luminosity and the vertical beam-beam parameter, one derives the traditional luminosity scaling

$$L = 2.17 \times 10^{34} (1 + r) \xi_y \left(\frac{EI}{\beta_y^*} \right) \ \text{cm}^{-2}\text{sec}^{-1} \qquad (1)$$

equation with r the y to x aspect ratio (~0.02), E the beam energy, I the beam current, and β_y* the vertical beta at the collision point. In order to get a factor of four above the present luminosity (to $2x10^{34}$), the currents will be raised about a factor of two, the tune shifts increased about 10% and β_y* reduced from 12 mm to about 7 mm. The number of RF stations in the LER will be increased from three to four in order in achieve about 3.6 A. A positron current of 2.43 A has already been successfully stored. The number of RF stations in the HER will be increased from seven to eight allowing a current of 1.6 A. The β_y* can be decreased to about 7 mm using the present IR quadrupole configuration but with extra permanent magnet quadrupole slices replacing some B1 dipole slices. Somewhat increased backgrounds are expected that are under study. The chromatic corrections will be more difficult but early tests indicate an acceptable dynamic aperture. To achieve near $4x10^{34}$ the β_y* must be lowered to about 5 mm and additional RF stations added to the HER and LER. In order to shorten the bunches, to reduce the hourglass effects, lower alpha lattices would be needed in the HER and LER or higher harmonic RF cavities to increase the effective RF voltage. The details of the $4x10^{34}$ upgrade will be evaluated in the next few months.

2.10.5 Acknowledments

We wish to thank the Operations Group for their help.

2.10.6 References

[1] J. Seeman *et al.,* “Status and Future Plans of the PEP-II B-Factory,” EPAC 2002, Paris, June 2002.
[2] Y. Cai *et al*, “Search of the Gold Orbit with a New Steering Algorithm,” PAC 2003, Portland.
[3] U. Wienands *et al.,* "Betatron-function measurement in lattices with 90° sections,” EPAC 2002, Paris.
[4] Y. Cai *et al*, “Build up of the Electron Cloud with Different Bunch Patterns in the Presence of a Solenoid Field,” PAC 2003, Portland.
[5] Y. Cai *et al,* “Tracking Simulations near the Half-Integer Tune at PEP-II,” PAC2003, Portland.
[6] F.-J. Decker *et al.*, “Bunch Pattern By-3 in PEP-II,” PAC2003, Portland.
[7] Y. Nosochkov *et al.*, “Lattice with a Smaller Momentum Compaction Factor for PEP-II HER,” PAC2003, Portland.
[8] P. McIntosh *et al.*, “An Over-Damped Cavity Longitudinal Kicker for the PEP-II LER,” PAC 2003, Portland.

2.11 Design Studies for a 10^{36} SuperB-Factory*

J. Seeman, S. Heifets, Y. Cai, F.-J. Decker, S. Ecklund, A. Fisher, J. Fox, S. Heifets,
Y. Nosochkov, A. Novokhatski, M. Sullivan, D. Teytelman, U. Wienands, Y. Yan
SLAC, Menlo Park, CA 94025, USA
M. Biagini, INFN, Frascati, Italy

mailto:seeman@slac.stanford.edu

Abstract

A Super B Factory, an asymmetric e^+e^- collider with a luminosity of 10^{36} $cm^{-2}s^{-1}$, can provide a sensitive probe of new physics in the flavor sector of the Standard Model. The success of PEP-II and KEKB in producing unprecented luminosity with unprecedently short commissioning time has taught us about the accelerator physics of asymmetric e^+e^- colliders in a new parameter regime. It appears to be possible to build on this success to advance the state of the accelerator art by building a collider at a luminosity approaching 10^{36} $cm^{-2}s^{-1}$. Such a collider would produce an integrated luminosity of 10,000 fb^{-1} (10 ab^{-1}) in a running year. Design studies are underway to arrive at a complete parameter set based on a collider in the PEP-II tunnel but with an upgraded RF system (perhaps a higher frequency) and an upgraded interaction region [1-6].

2.11.1 Design Constraints

The construction and operation of modern multi-bunch e^+e^- colliders have brought about many advances in accelerator physics in the area of high currents, complex interaction regions, high beam-beam tune shifts, high power RF systems, controlled beam instabilities, rapid injection rates, and reliable uptimes (~95%).

The present successful B-Factories have proven that several design concepts are valid. 1) Colliders with asymmetric energies can work. 2) Beam-beam energy tranparency conditions are weak. 3) Interaction regions with two energies can work. 4) IR backgrounds can be handled. 5) High current RF systems can be operated (2 amps x 1 amp). 6) Beam-beam parameters can reach 0.06 to 0.9. 7) Injection rates can be good and continuous injection is feasible. 8) The electron cloud effect (ECI) can be managed to a small effect. 9) Bunch-by-bunch feedbacks at the 4 nsec spacing work well.

In addition to the above lessons learned, new techniques can be employed [1,3]. A) The beam lifetimes will be low so continuous injection will be needed. B) Continuous injection will be used to push the beam-beam parameter to higher values than can be tolerated when long lifetimes are required. C) Much higher currents are needed and the vacuum chamber and feedbacks must be made to match. D) Bunch-by-bunch feedbacks will need to operate at the 1 nsec scale, down from the present 4 nsec time. E) Much shorter bunches will be needed; on the order of 2 mm. F) Higher-power vacuum chambers and HOM tolerant chambers will be needed. The use of expansion bellows will need to be minimized or a high-power design developed. G) Very low vertical beta functions at the interaction of about 1.5 to 2.5 mm will be needed. H) Special chromaticity corrections will be needed. I) Every technique to reduce the wall plug power will need to be used. For example, reducing the energy asymmetry to reduce synchrotron

* Supported by US DOE contract DE-AC03-76SF00515.

radiation, increase the vacuum chamber bores to reduce resistive wall effects,, and increasing the RF cavity bores to reduce HOM losses.

2.11.2 Parameters

The design of a 10^{36} $cm^{-2}s^{-1}$ e^+e^- collider combines a natural extension of the design of the present *B* Factories with a few new ideas and special circumstances to allow improved beam parameters to be achieved. The luminosity L in an e^+e^- collider that has a limited vertical tune shift ξ_y with flat beams (r=0.02) is given by the standard expression

$$L = 2.17\times10^{34}(1+r)n\xi_y\left(\frac{EI_b}{\beta_y^*}\right)\ \text{cm}^{-2}\text{sec}^{-1} \qquad (1)$$

where I_b is the bunch current (amperes), n is the number of bunches, E is the beam energy (GeV), and β_y* is the vertical beta function (cm) at the collision point. The luminosity gain of the Super *B* Factory comes from the increase of the beam currents by about a factor of eight, lowering β_y* about a factor of five, and increasing the beam-beam tune shifts about 25%. The resulting gain is about a factor of 50 over that of the present *B* Factories when they are upgraded to about $2x10^{34}$ $cm^{-2}s^{-1}$ over the next few years. In addition, due to continuous injection with the luminosity always near the maximum, the integrated luminosity per unit time of the Super *B* Factory is expected to increase another 20 to 30% over the present machines. The parameters of a representative 10^{36} $cm^{-2}s^{-1}$ e^+e^- collider are listed in Tables 1 and 2 for different RF frequencies. These parameters were chosen after balancing beam dynamics effects, technology limits, luminosity performance, and SLAC site AC power issues. The PEP-II tunnel is an excellent site for this collider. The SLAC power substation can provide 140 MW if needed.

The beam energies are 8 GeV for the high-energy ring and 3.5 GeV for the low-energy ring. Lowering the high-energy ring energy from 9 GeV reduces the synchrotron radiation load on the RF system. The e^+ and e^- may be exchanged if need be as either particle can be stored in either ring using the versatile SLAC injector. The linac can provide low emittance beams with 80 Hz of electrons and 20 Hz of positrons. The remaining 20 Hz will be used to generate positrons at the production target.

2.11.3 RF Frequency Selection

Two RF frequencies for the Super *B* Factory have been studied: 476 MHz as in the present PEP-II and 952 MHz. At the higher frequency, more bunches (about 6900) can be stored, thereby reducing single bunch effects and higher order mode losses at the high total current. Industry has the ability to make cw 952 MHz klystrons at the MW level needed for this accelerator. RF cavities at 952 MHz can be made with a similar design to the PEP-II style copper cavities, using improved HOM dampers and with additional storage cavities to help reduce longitudinal multi-bunch instabilities.

In the Super *B* Factory, the single bunch currents are a factor of two higher than those of PEP-II or KEKB; the total current is increased by a factor of eight, but there are four to eight times as many bunches. Furthermore, the bunch lengths are about five times shorter. These short high-charge bunches lead to increased single bunch effects; Higher-Order-Mode (HOM) losses and resistive wall losses that have to be minimized in each ring, see Figure 1. HOM losses in the RF cavities will be reduced by opening the beam channel through the RF cavities about 50%. The resistive wall losses of the short bunches in the vacuum chambers will be reduced by a factor of two by increasing the vacuum chamber radius.

Table 1 Super B Factory Parameters with 476 MHz RF.

Parameter	**LER**	**HER**
Energy (GeV)	3.5	8
RF frequency (MHz)	476	476
Vertical tune	72.64	56.57
Horizontal tune	74.52	58.52
Current (A)	11.0	4.8
Number of bunches	3450	3450
Ion gap (%)	1.2	1.2
HER RF klystron/cav	22/44	18/36
HER RF volts (MV)	29	24
β_y* (mm)	2.2	2.2
β_x* (cm)	15	15
Emittance (x/y) (nm)	27.5/0.4	27.5/0.4
σ_z (mm)	2.5	2.5
Lum hourglass factor	0.82	0.82
Crossing angle(mrad)	15	15
IP Horiz. size (μm)	64	64
IP Vert. size (μm)	0.9	0.9
Horizontal ξ_x	0.15	0.15
Vertical ξ_y	0.15	0.15
Lumin. ($x10^{34}/cm^2/s$)	50	50

2.11.4 Interaction Region

The interaction region is being designed to leave the same longitudinal free space as that presently used by *BABAR* but with superconducting quadrupole doublets as close to the interaction region as possible, as shown in Figure 2. A crossing angle is used to separate the two beams as they enter and leave the interaction point. The overall interaction region is shorter than for PEP-II, allowing a shorter detector if that is advantageous [6].

Recent work at Brookhaven National Laboratory on precision conductor placement of superconductors in large-bore low-field magnets has led to quadrupoles in successful use in the interaction regions for the HERA collider in Germany [7]. A minor redesign of these magnets will work well for the Super *B* Factory.

The beams must have a crossing angle at the collision point to avoid parasitic crossing effects; the anticipated crossing angle is +/- 12 to 17 mrad. Short bunches are also needed to avoid the geometrical hour-glass effects that could reduce the luminosity during collisions. The short Super *B* Factory bunches are made by providing extra over-voltage in the RF system and by a high phase-advance quadrupole lattice in each ring.

The low beta functions at the collision point will make the ring chromaticity high. Correcting the chromaticity is the task of sextupole magnets, but sextupoles reduce the dynamic aperture of the storage ring. Due to the naturally reduced lifetimes of the beams, the dynamic

aperture and the resulting vacuum system do not have to be designed for lifetimes of hours, only for one hour, thus, reducing costs.

The increases in the beam-beam parameters from the present 0.06 to 0.09 range to 0.15 will be achieved by operating just above but very close to the half-integer horizontal tune where standard, but strong, dynamic beta effects occur. Also, pushing the transverse tunes closer to specific resonances allows a higher tune shift and more luminosity but with shorter beam lifetimes. Both techniques have been successfully demonstrated at the present *B* Factories.

Table 2 Super B Factory Parameters with 952 MHz RF

Parameter	**LER**	**HER**
Energy (GeV)	3.5	8
RF frequency (MHz)	952	952
Vertical tune	72.64	56.57
Horizontal tune	74.52	58.52
Current (A)	15.5	6.8
Number of bunches	6900	6900
Ion gap (%)	1.2	1.2
HER RF klystron/cav	32/64	25/50
HER RF volts (MV)	43	33
β_y* (mm)	1.5	1.5
β_x* (cm)	15	15
Emittance (x/y) (nm)	19.5/0.19	19.5/0.19
σ_z (mm)	1.75	1.75
Lum hourglass factor	0.8	0.8
Crossing angle(mrad)	15	15
IP Horiz. size (μm)	54	54
IP Vert. size (μm)	0.5	0.5
Horizontal ξ_x	0.15	0.15
Vertical ξ_y	0.15	0.15
Lumin. ($x10^{34}/cm^2/s$)	100	100

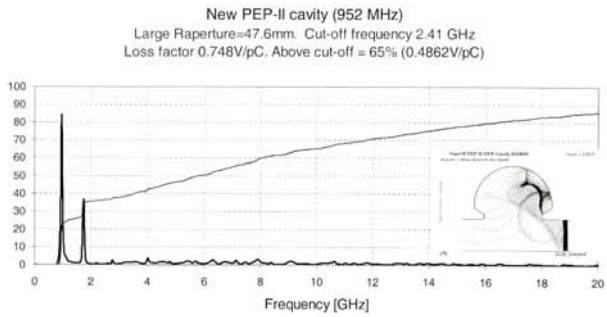

Figure 1 HOM calculation for a 952 MHz PEP-II style RF cavity with an increased bore.

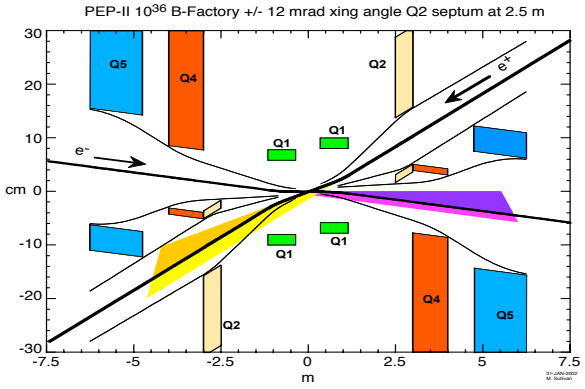

Figure 2 Interaction region for a Super B-Factory. Note the first quadrupole is at 30 cm from the interaction point. This first quadrupole will have a quadrupole, x and y dipole, solenoidal, and skew quadrupole windings.

2.11.5 Power Scaling

The power required by a collider is the sum of a site base plus RF sources. With a Super B-Factory, there will be an overall base level due to the SLAC campus (~15 MW), the linac running for PEP-II at 30 Hz (~8MW), The PEP-II magnets (~7 MW), the linac running for LCLS (~10 MW), and SPEAR (~5 MW) for a total of about 40 MW.

The total RF power is the sum of the cavity wall losses, beam synchrotron radiation, beam resistive wall losses, beam higher order mode losses (HOM), and AC distribution inefficiencies. The AC transformers and high voltage power supplies are about 90% efficient. The RF klystrons are about 65% efficient. For beam stability control, the klystrons do not run at full power which reduces their efficiency to about 50%. The RF power losses to the cavity walls are 70 to 100 kW depending on the voltage. The synchrotron radiation losses are minimized by reducing the energy asymmetry of the B-Factory to 3.5 x 8 GeV and by adding dipoles to the low-energy ring to reduce the effective bending radius. The vacuum chamber bores are enlarged to reduce the resistive wall losses that go inversely with the chamber size. The HOM losses are reduced by going to a higher RF frequency with more bunches but same total current.

The total power of a Super-B Factory at the SLAC site as a function of luminosity is shown in Figure 3. If the site power is limited to 120 MW that is within the range of the incoming power lines, then a luminosity of about 5×10^{35} luminosity is possible at 476 MHz and 1×10^{36} at 952 MHz.

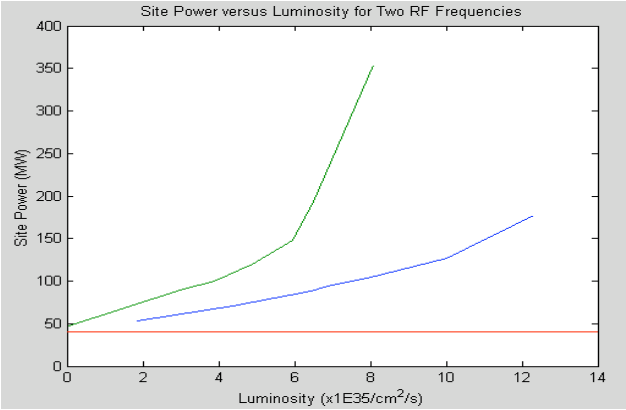

Figure 3 Site power scaling for two RF frequencies The upper curve is for 476 MHz and the lower curve 952 MHz. The power above the 40 MW horizontal line is from the overall PEP-II RF system. The currents increase with the luminosity and, thus, increase the power usage.

2.11.6 References

[1] J. Seeman, "Initial Parameters for a $10^{36}/cm^2/s$ Luminosity e^+e^- B-Factory,", SLAC-PUB-8787, March 2001.
[2] J. Seeman, "Higher Luminosity B-Factories," PAC 2001, Chicago, p. 305.
[3] J. Seeman, "Prospects on Future Higher Luminosity e+e- Colliders," ICFA e+e- Factories Workshop, Ithaca, New York, October 2002.
[4] P. Burchat et al, "Physics at a 10^{36} e+e- B-Factory," Snowmass, July 2001.
[5] S. Henderson et al., "Lepton Colliders Working Group Report," Snowmass, July 2001.
[6] M. Sullivan, "Interaction Region Upgrades of e+e- B-Factories," PAC, Portland, May 2003.
[7] B. Parker et al., "Superconducting Magnets for use inside the HERA ep Interaction Regions," PAC 1999, New York, p. 308.

2.12 Experiences at KEKB

Y. Funakoshi for the KEKB commissioning group
mailto: yoshihiro.funakoshi@kek.jp

KEK
1-1 Oho, Tsukuba, Ibaraki, 305-0801, Japan

2.12.1 Introduction

The KEKB B-Factory is an electron-positron double ring collider located at KEK. Its peak luminosity surpassed $1x10^{34}/cm^2/s$ on May 9 2003 for the first time in the history of collider machines. This is also the design peak luminosity of KEKB. In this paper, we briefly review the history of KEKB and examine its design concepts with an emphasis of beam dynamics issues at this opportunity. What we aim at here is to clarify what have been realized at KEKB, what have not yet and what were different from expectations in the design phase. These works also seem worthwhile when we consider future machines with yet higher luminosity.

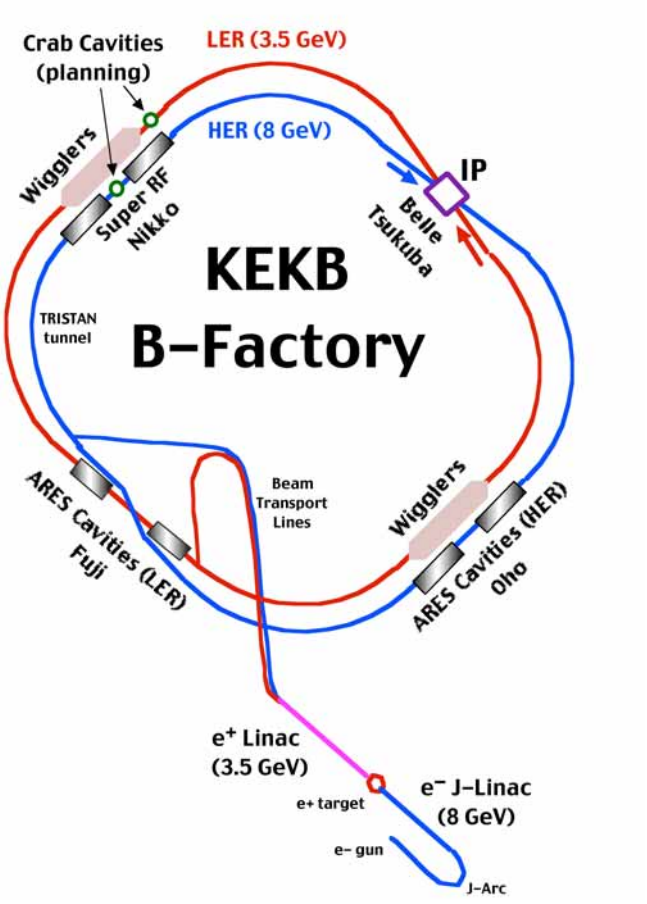

Figure1:Schematic view of the KEKB accelerator

2.12.2 Design concepts of KEKB

In this section, we very briefly summarize design concepts of KEKB [1][2].

2.12.2.1 *Machine parameters*

In Table 1, machine parameters of KEKB are summarized. The design values of KEKB are shown in parentheses. Also shown in the table are achieved values at the record peak luminosity on May 13 2003. This table tells us some basic features of KEKB. First of all, KEKB is an energy asymmetric collider. Although it is operated on the Y(4s) resonance like CESR-B, the energies of the two beams are different. This asymmetry comes from a physics motivation. The second feature is an extremely high design luminosity, which also comes from a physics requirement. To realize this luminosity, we chose the following design parameters;

(1) Very low β_y^*: 1cm for both beams
(2) Very high beam currents: 1.1A for electrons and 2.6 A for positrons
(3) Relatively high beam-beam parameters: 0.052 in the vertical plane.

2.12.2.2 *Energy transparency*

As is seen in Table 1, we assumed so-called energy transparency conditions in order to balance the beam-beam effects between the two beams. We assumed that the beta functions at IP, the beam-beam parameters, the radiation damping time, the emittances, the synchrotron tune and the (fractional part of) betatron tunes are the same for the two beams. As a result of these, the design beam currents are inversely proportional to the beam energy.

2.12.2.3 *IR Design*

We introduced a horizontal crossing angle of +/-11mrad. There are two motivations for this. One is to avoid harmful effects of parasitic collisions. The other is to simplify the IR design. With this scheme, no separation bending magnets for separating two beams around IP are needed. This contributes to avoid possible problems of detector beam background from synchrotron radiation emitted from the separation bending magnets. To investigate effects of the synchro-betatron coupling from the crossing angle which strictly limited performance of DORIS, a large amount of beam-beam simulations were done. The conclusion was that (contrary to the case of the vertical crossing at DORIS) there is no deleterious effect of the horizontal crossing angle provided that we avoid some small region of the syncro-betatron resonance. As for the final focus quadrupoles, we adopted superconducting magnets. In the LER (Low Energy Ring), we adopted a local chromaticity correction scheme. With this scheme, the chromaticity created by the IR quadrupoles is corrected within the straight section including the IP. We also introduced compensation solenoid magnets for the purpose of compensating the detector solenoid. By using them, an integral of the solenoid field along the longitudinal direction around IP can be set to zero. This scheme contributed to reduce strength of skew quadruples drastically.

Table 1: Machine parameters of KEKB on May 13 2003. The design values are also shown in parentheses.

	LER	HER	
Circumference	3016.3		m
Beam energy	3.5 (3.5)	8.0 (8.0)	GeV
Horizontal Emittance	18 (18)	24 (18)	nm
Beam current	1377 (2600)	1050 (1100)	mA
Number of bunches	1284 (~5000)		
Bunch current	1.07 (0.52)	0. 818 (0.22)	mA
Bunch spacing	2.4 (0.6)		m
Bunch trains	1		
Total RF voltage Vc	8.0	13.0	MV
Synchrotron tune ν_s	-0.0249	-0.0207	
Bunch length	5~8@8.0 (~4@10)	6~7@13.0 (~4@18)	mm@MV
Betatron tune ν_x /ν_y	45.507/43.546 (45.52/44.08)	44.512/41.580 (44.52/42.08)	
beta's at IP β_x /β_y	59/0.58 (33/1)	58/0.7 (33/1)	cm
Momentum Compaction	3.39×10^{-4} (1×10^{-4}~2×10^{-4})	3.43×10^{-4} (1×10^{-4}~2×10^{-4})	
Estimated vertical beam size at IP σ_y	2.2	2.2	μm
beam-beam parameters ξ_x /ξ_y	0.096/0.069 (0.039/0.052)	0.065/0.052 (0.039/0.052)	
Beam lifetime	127@1377	256@ 1050	min.@mA
Luminosity (Belle CsI)	1.0567 (1)		$10^{34}/cm^2/sec$
Luminosity records per day / 7days/ month	579/3876/12760		/pb

2.12.2.4 *Lattice design*

In the modern machines like KEKB, the lattice design is of much more importance than the past machines. Goals of the lattice design at KEKB were to keep enough dynamic aperture in both transverse and longitudinal directions, to give short bunch length in order to reduce the hourglass effect and to keep enough tunability in the

momentum compaction factor and the emittance. To keep enough (transverse) dynamic aperture, we adopted the non-interleaved sextupole scheme. In this scheme, each pair of sextupole magnets having the same strength are connected with $-I'$ transformer. This means that non-linearity of the sextupole magnets is cancelled out within each pair of sextuples for on-momentum particles. For wider longitudinal dynamic aperture, all of the sextuple pairs are separated and are independently excited. A new lattice called "2.5 π lattice" was devised. In this scheme, five of 90-degree FODO cells are combined and make a unit cell. The number of bending magnets is decreased from ten to four. With this 2.5 π cell lattice, a very flexible change of the emittance and the momentum compaction factors is realized by controlling dispersion functions. As is seen in Table 1, the design emittance and the momentum compaction are relatively small. The small value of the momentum compaction factor is favorable to the short bunch length. If needed, the momentum compaction factor and the emittance can be changed in a very wide range. For example, the momentum compaction factor can be set negative with the same absolute value as the design value.

2.12.2.5 *High beam current issues*

The design beam currents of 2.6A and 1.1A are unusually high values even compared with those of existing SOR machines. What we conceived the most severe obstacle for these high currents was a coupled bunch instability from the fundamental modes of RF cavities. To overcome this problem, we developed two different types of RF cavities. One is a cavity system called ARES. In this system, a large energy storage cavity is attached to an accelerating cavity and RF power is fed through this storage cavity. Owing to this large energy storage, the R/Q value of the system can be reduced drastically, which contributes to suppression of the instability. This ARES system is used both in LER and HER. The other system we developed is a superconducting RF system. The high field gradient and a high Q value of the system can also suppress the instability against a heavy beam loading. This SCC system is used in HER in which we need a high RF voltage. Both of ARES and the SCC system have a damped structure with HOM absorbers for the purpose of suppressing the coupled bunch instability from HOMs. The other possibly harmful (coupled bunch) instabilities we considered were the fast ion instability in HER and the electron cloud instability in LER. To stabilize these instabilities, a (transverse) bunch-by-bunch feedback system was developed. Damping time of about 1 msec was expected with the system. In addition to the development of the feedback system, we chose the design value of the vacuum pressure as 10^{-9} Torr for suppression of the fast ion instability. As for the electron cloud instability, we did not adopt the ante-chamber. We kept a backup plan to install solenoid magnets around the LER ring in case the instability should be unexpectedly severe. As for the single bunch instability, we considered that the microwave instability could be the most serious. To avoid this possible problem, we planed to fill all the RF buckets with beams except for some beam gap which is needed to keep sufficient rise time of abort kicker magnets and also to suppress the ion trapping effect. The design value of the beam gap is 10% of the ring. With this beam filling scheme, the bunch currents of the beams are relatively small and the design emittances were chosen to fit these bunch currents. The bunch current of LER thus chosen is about 1/5 of the estimated threshold intensity for the microwave instability.

2.12.2.6 *Beam-Beam effect*

Some basic concepts related to the beam-beam effect at KEKB are already mentioned above. In the design, every RF bucket except for the 10% beam gap is filled with the beams. A horizontal crossing angle of +/- 11 mrad could be effective to avoid the effects of parasitic collision. We considered that the short bunch length (say half of β_y^*) is effective to raise the beam-beam limit. The radiation damping time of LER is shortened to be equal to that of HER (4000 turns in the transverse direction) by installing wiggler magnets as is shown in Fig. 1. A large amount of tune surveys by using a strong-weak technique were done for the best tune values. The simulations showed that the vertical beam-beam parameter of 0.052 is possible with the design tune values.

2.12.3 Brief history of KEKB

In this section, we briefly review the history of the KEKB commissioning. We will mainly describe what were difficulties for increasing the luminosity and how the commissioning team has been overcoming the problems.

Fig. 2 shows the history of the KEKB luminosity. The top row shows the peak luminosity. The second row shows the daily integrated luminosity. The third row shows the peak beam currents of a day. The bottom row shows the history of an accumulated luminosity by the Belle detector. In the figure also shown are some notable changes or events.

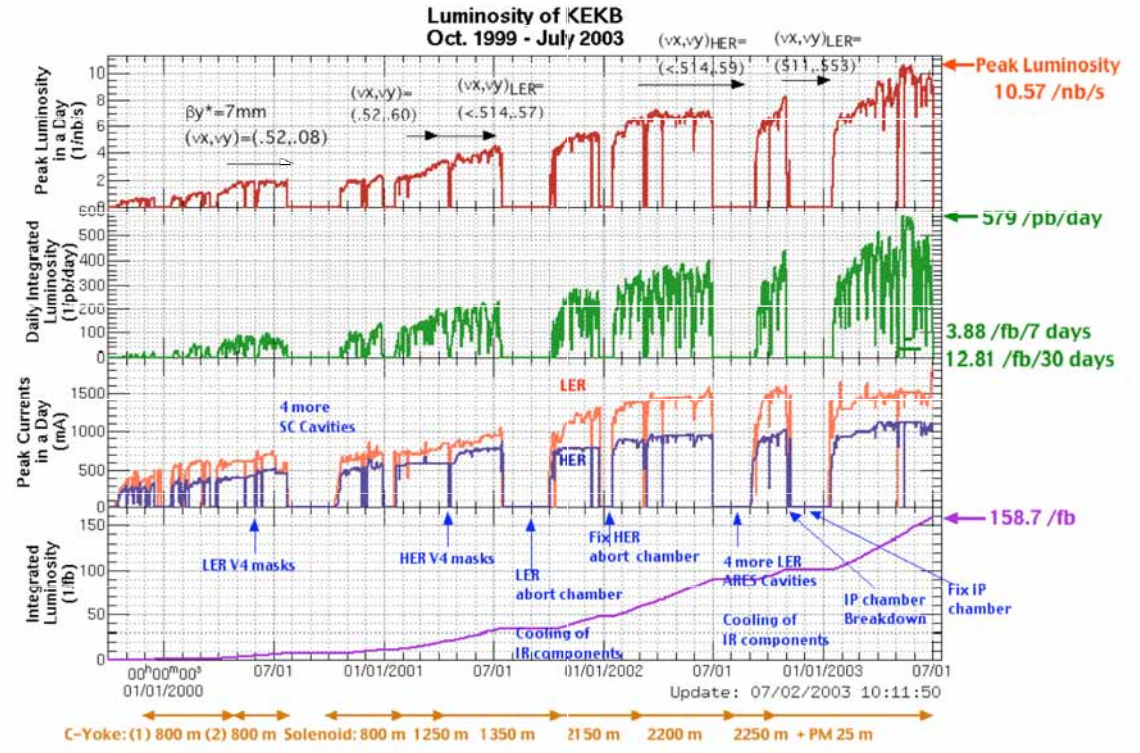

Figure 2: History of KEKB

As is seen in Fig. 2, β_y^* of both beams were successfully squeezed to 7mm at the very early stage of its history. This value is even smaller than the design one. After the success of squeezing β_y^* to thus small value, the KEKB luminosity increased slowly but steadily as is seen in the figure. There are three important points in the increase of the luminosity. One is the increase of the beam currents. The second is suppression of the single beam blowup in LER due to the electron cloud instability. The last point is choice of the betatron tunes which was effective to increase the beam-beam parameters.

2.12.3.1 *High Beam current issues [2]*

In the history of the KEKB, the beam currents have been limited from many reasons including the detector beam background. Among those, the most serious limitation has come from tolerance of several hardware components to the high beam currents. We have solved those hardware problems mainly by replacing hardware components in question with the new ones and/or by reinforcing cooling power for components having heating problems. Hardware components which had problems include movable masks for protecting the Belle detector from the beam background, vacuum chambers at the beam abort sections, bellows and vacuum components near the IP. In October 2002, we experienced a breakdown of the IP chamber. It took a few months to recover from this accident. Although a heat-cycle related to the high beam currents was suspected for the cause of the breakdown, our present view is that the breakdown was induced not by a heat-cycle but by some corrosion related to impurities in the cooling system of the chamber. As for the fast ion instability in HER, it is suppressed by the feedback system in a usual vacuum condition. Only in some bad vacuum condition such as after a vacuum leakage or vacuum works, the instability limits the total beam current. The coupled bunch instability from the electron cloud instability can be suppressed by the feedback system and the solenoid magnets mentioned below at the present level of the beam current. However, the single beam blowup in LER due to the electron cloud, which is essentially a single bunch effect and was not expected in the design phase, has been very serious as is described below.

2.12.3.2 *Single beam blowup from the electron cloud instability*

A beam size enlargement depending on the beam current in the LER has given one of the most serious luminosity restrictions to the KEKB. The source of the blowup is believed to be the electron cloud formed by photoelectrons and secondary electrons. Here, we summarize basic characteristics of the blowup [3].

1) LER single beam (beam size) blowup
2) Observed only in the vertical direction
3) Observed only in the multibunch case
4) No dipole oscillation with a high chromaticity
5) The blowup has a threshold current that is determined by the charge density (bunch current / bunch spacing).
6) Almost no tune dependence
7) The vertical tune increases along the train and almost saturates at about 20th bunch.

The mechanism of this blowup has been studied theoretically. F. Zimmermann and K. Ohmi. They showed by simulations that the blowup can be explained by a single bunch head-tail instability induced by an electron cloud [4]. Photoelectrons and secondary electrons form the electron cloud. A single-bunch like nature of the instability has been confirmed in a test bunch experiment [5]. Although we tried to detect the head-tail motion by using a streak camera system, we have not yet obtained a conclusive observation [6].

To suppress this instability, solenoid coils have been wound around the LER ring. Works for solenoid winding were done several times. In Fig. 2, the history of the solenoid winding is also shown. In the bottom of the figure, cumulative length of the solenoid magnets is shown. At present, 2250m of the LER ring is covered with the solenoid coils and 25m is with permanent solenoid magnets. More than 90% of the field free region of the ring is covered with solenoid field. A typical length of the solenoid coils is about 50cm, although there is some variety in length. A typical field strength is around 50 Gauss at the centre of each solenoid when excited with a current of 5 A. With these solenoid magnets, the single beam blowup is suppressed at the present level of the beam current. However, it is expected that the blowup will appear again with a higher beam current. We are now planning to install more solenoids and to increase field strength of existing solenoids. Effectiveness of the solenoids on the luminosity was also tested in March 2001. The experiment showed that the solenoid magnets are very effective to raise the luminosity. In this experiment, the luminosity with all solenoids on was about twice as high as that with all solenoids off.

2.12.3.3 *Beam-Beam effects [7]*

The beam-beam parameters calculated from the luminosity are listed in Table 1. In the calculation, we assumed that the vertical beam sizes of the two beams are equal. It is also assumed that there is no beam-beam blowup in the horizontal direction, since we do not observe serious beam size blowup in the horizontal direction. The hourglass effect from a finite bunch length and the effects from a finite crossing angle are also considered. As for the bunch length, 7mm is assumed. The vertical beam-beam parameters surpassed the design value of 0.052. The horizontal beam-beam parameters are very high. As is shown in Table 1, the working points of KEKB are close to the half integer resonance. Particularly the horizontal tunes are very near to the resonance. In this situation, an important effect is that the beta function and the emittance are affected by the beam-beam force (dynamic-beta and dynamic-emittance). As a result of these changes, the horizontal beam size at the IP decreases to some extent and the horizontal beam-beam parameter decreases. In the KEKB, there is a tendency that the horizontal tune closer to the half integer resonance brings a higher luminosity. This tendency seems to be explained by the dynamic-beta and dynamic-emittance effects. These effects also explain why we can reach extremely high beam-beam parameters in the usual sense in the horizontal direction shown in Table 1. The history of tune change at KEKB is shown in Fig. 2. In the design, the vertical tune is above the integer resonance. At present, both the horizontal and vertical tunes are above the half integer resonance. This change was done in February 2001 based on the beam-beam simulation [8] and actually brought some increase of the luminosity as is shown in Fig. 2. This change also brought more stable beam operation through less orbit drift in the vertical direction.

In addition to tune surveys, an enormous amount of efforts have been devoted to suppress the beam-beam blowup and to raise the luminosity. In every day's machine tuning, we make repeatedly scans of several parameters related to the beam collision for searching better collision conditions by using tuning knobs. We developed several kinds of tuning knobs that manipulate waist points of both beams, dispersions at IP, x-y coupling parameters at IP, RF phase of one beam and target values for the IP orbit feedback system and others. This kind of tuning in KEKB seems much more difficult than in conventional machines. This difficulty comes mainly from the point that KEKB is an asymmetric (double-ring) collider. We experienced that a balance between the two beams is very important in the collision tuning. For example, in some situation the luminosity increases by intentionally enlarging the vertical beam size of the stronger beam. We developed this kind of tuning knob [2]. In another situation, the luminosity and the beam lifetime is improved by changing the β_x^* of one beam slightly. Also we experienced that the luminosity is sensitive to the x-y coupling parameters at IP.

Another issue related to the beam-beam effect is so-called a bunch spacing problem. To explain this problem, let us consider the following specific luminosity per bunch

$$L_{spec} = \frac{L}{n_{bunch} I^+_{bunch} I^-_{bunch}}.$$

Here, L, n_{bunch} , I^+_{bunch} and I^-_{bunch} denotes a usual luminosity, the number of bunches per beam, the positron bunch current and the electron bunch current, respectively. If the beam sizes of the two beams were determined only by the beam-beam effects, the specific luminosity per bunch would not depend on bunch spacing. Our observations are that the shorter bunch spacing is, the lower specific luminosity per bunch we have. As is shown in Table 1, present bunch spacing at KEKB is about four times longer than the design to mitigate this bunch spacing problem. These observations indicate that blowup mechanisms other than the beam-beam effects exit. The single beam blowup of LER from the electron cloud is the first candidate for this. However, even below the threshold of this blowup, the specific luminosity per bunch depends on bunch spacing. Another candidate is an effect of the parasitic collisions. However, in a dedicated machine study on this subject, we could not find any indication that the effects of the parasitic collision affected the specific luminosity. Although we have not understood completely the mechanism of this extra blowup depending on bunch spacing, our present hypothesis is that some synergistic effect of the beam-beam and the electron cloud may be responsible. This hypothesis is supported by an experience that installing solenoid magnets decreased the bunch spacing dependence of the specific luminosity.

2.12.4 Experiences in KEKB and future prospects

In this section, we briefly summarize experiences in KEKB and mention some future prospects.

2.12.4.1 *Machine parameters*

Main design parameters of KEKB have been achieved including the peak luminosity. One big difference from the design is that the LER beam current is still rather low compared with the design. Another difference is that the bunch spacing is nearly four times longer than the design.

2.12.4.2 *Energy transparency*

As is seen in Table 1, the present KEKB parameters break the energy transparency conditions heavily. An origin of this break is asymmetry of the design beam currents, which is a consequence of the energy transparency conditions. The design beam current of LER is much higher than of HER. Even at the present KEKB, the LER beam current is about 70% of the design at maximum. This current limitation comes mainly from the hardware problems. In this situation, the luminosity can be increased with a higher HER current by intentionally breaking the energy transparency conditions. The other origin of this break is a charge asymmetry. The electron cloud instability, which is induced only in the positron ring, is much severer than the fast ion instability in the electron ring. When the blowup due to the electron cloud was serious, the luminosity did not increase with increasing the LER beam currents. Even in the situation at present that the single beam blowup is suppressed by the solenoid magnets, it is believed that the electron cloud has some influence on the beam-beam interaction.

2.12.4.3 *IR Design*

Almost all of the design concepts have been successfully realized. The vertical beta functions at IP are smaller than the design. With the small β_y^* achieved, we can keep enough dynamic aperture in both transverse and longitudinal directions. The horizontal crossing angle also seems successful. We have observed no serious effects from the synchro-betatron resonance. With the crossing angle, the vertical beam-beam parameters of both beams reached the design value.

2.12.4.4 *Lattice design*

The lattice design has been also successful. The chromaticity correction scheme including the non-interleaved sextupole scheme gives enough dynamic aperture even with the smaller β_y^* than the design. The momentum compaction factor is relatively small that is consistent with the short bunch length. The measured bunch length in Table 1, which depends on the bunch current, is somewhat longer than was expected. This bunch lengthening comes from the potential-well distortion whose effects are large with using higher bunch currents than the design. As for the tunability of the lattice, the present emittances and the momentum compaction factors are not far from the design values and we have not changed these values since December 2000. However, recently we started an investigation on a lattice with negative values of the momentum compaction factors. The motivation of this lattice is to get a shorter bunch length and to reduce effects of the hourglass effect. So far the new lattice seems very promising [9].

2.12.4.5 *High beam current issues*

HER is operated routinely with the design beam current of 1.1A in usual physics operation. The record peak beam current of LER is 1.86A, which is about 70% of the design. Under these high beam currents, both of ARES and SCC systems work very well. The longitudinal coupled bunch instability from the fundamental mode is suppressed by these systems, although we need additional –1 mode and 0 mode dampers to overcome the instability completely. No beam instabilities originated from HOMs of the RF cavities have been observed at KEKB. At KEKB, the longitudinal

feedback system for suppressing the coupled bunch instability is not needed. On the other hand, bunch-by-bunch feedback systems in the transverse directions are vital at KEKB. Without such systems, the beam currents would be limited to below 100mA. The feedback system whose damping time is less than 1msec stabilizes the instabilities except for some exceptional situations. One of such exceptions is the fast ion instability in a bad vacuum condition. Another exceptional situation is a case that some broken vacuum component such as bellows creates unexpectedly high impedance. We experienced such situations several times. The coupled bunch instability from the electron cloud is not serious if we use solenoid magnets.

At present the HER beam current is limited by RF power. We will install two more ARES cavities in HER in the summer shutdown this year. The main beam current limitation of LER is hardware problems. We are still struggling with these problems. Our experience is that storage of high beam currents are achievable only in step-by-step by fixing such hardware troubles. The operation with high bunch currents for mitigating the bunch spacing problem makes the hardware problems serious. Therefore, reducing bunch spacing is one of the challenges of the KEKB operation in future.

The single beam blowup in LER was not expected in the design phase of KEKB. This is still one of the major performance limiting issues at KEKB. The dust trapping effects on which we had much discussion in the design phase has been less serious than was expected.

2.12.4.6 *Beam-Beam effect*

In the design phase of KEKB, the beam-beam simulations played an important role. Based on the simulations, we introduced the horizontal crossing angle. The design tunes were also determined from the simulations. Although we used the strong-weak method for the simulations due to limited computer power in the design phase, results at KEKB show that accuracy of the predictions from the simulation was not so bad. Recently, new beam-beam simulations showed further possibility of getting higher luminosity [10]. If we combine the horizontal betatron tunes very close to the half-integer like the present KEKB with the head-on collision, we can get about two times higher vertical beam-beam parameters. Considering these new results of the simulations, we have now a plan to install crab cavity systems in both rings in 2005 for realizing the head-on collision.

Our experience on the tuning of the beam-beam effects is that improvements in the tuning of the beam-beam effects are made only in step-by-step. It makes the tuning very difficult that we have to optimize lots of optics parameters and they are usually rather sensitive to the beam-beam blowup. We found that the tuning on parameters of the liner optics including x-y coupling at IP is important for suppressing the beam-beam blowup. In usual beam operation, we frequently (typically every 2 weeks) make optics corrections where we correct global beta functions, x-y coupling parameters and dispersions. The optics corrections were also important in the sense that we had to narrow the stop-band when we moved the horizontal tunes closer to the half-integer resonance. Difficulties in such tunings at KEKB partially come from its feature of an asymmetric double ring collider. Since we can not rely on the energy transparency conditions, with a different combination of the beam currents we have to find a different set of the parameters to optimize the beam-beam interaction for the two beams.

2.12.4.7 *Future prospects*

We have a major upgrade plan of KEKB called "SuperKEKB". Based on the experiences of KEKB, we will aim at a peak luminosity of $1x10^{35} \sim 5x10^{35}$ cm^2/sec in SuperKEKB. Details of SuperKEKB are discussed in anther article in this Newsletter [11]. Although the SuperKEKB project has not been approved yet, we hope that the physics experiments with the SuperKEKB machine will start in 2007 in the earliest case.

Before starting the SuperKEKB project, we will continuously upgrade KEKB performance. Considering the experiences at KEKB so far, it is not easy to predict a precise path of performance improvements. We confine ourselves here to listing up items that may be effective to improve KEKB performance. We will introduce the crab cavity scheme in 2005. Contrary to the original scheme, we will install one crab cavity for each ring from the viewpoint of cost reduction. This means that the crabbing motion is not localized near IP but leaked around the rings. This might induce additional problems such as the synchro-betatron resonance.

We will install two more ARES cavities in HER in this year. The HER beam current will be increased by about 10% with these cavities. The LER beam current will also be increased by solving hardware problems. To avoid the HOM related troubles, it is desirable to reduce the bunch currents by increasing the number of bunches. For this purpose, installing more solenoids and reinforcing their field strength may be effective. These may be, of course, effective to prevent the single beam blowup with the higher LER beam current. We will try to shorten the bunch length to reduce the hourglass effects by adopting the lattice bringing the negative momentum compaction. There remains some room to improve the luminosity with some fine tunings such as optimizations of the tunes, the emittances, β_x^*s and so on. In very near future, we will try to use so-called a "continuous injection scheme" in usual physic operation. With this scheme, the beam currents are almost kept at their peak values and the physics experiment continue during the beam injection. It is expected that the integrated luminosity will be increased by about 20% with this scheme.

References

1. KEKB B-Factory Design Report, KEK Report 95-7, June 1995.
2. K. Akai et al., "Commissioning of KEKB", Nucl. Instrum. Meth. A499: 191-227, 2003.
3. H. Fukuma et al., "STUDY OF VERTICAL BEAM BLOWUP IN KEKB LOW ENERGY RING", HEACC 2001, Tsukuba, March 2001.
4. K. Ohmi and F. Zimmermann, CERN-SL-2000-015 (AP), May 2000.
5. H. Fukuma et al., "OBSERVATION OF VERTICAL BEAM BLOW-UP IN KEKB LOW ENERGY RING", in Proceedings of EPAC 2000, pp 1122-1124, Vienna, June 2000.
6. H. Ikeda, private communications.
7. Y. Funakoshi et al., "Beam-beam effects observed at the KEKB", Factories 2001, Ithaca, October 2001.
8. Y. Wu, "A NEW WORKING POINT FOR THE KEKB", HEACC 2001, Tsukuba, March 2001.
9. H. Koiso, private communications.
10. K. Ohmi, in this Newsletter.
11. Y. Ohnishi, in this Newsletter.

2.13 Accelerator Design of Super B Factory at KEK

Y. Ohnishi
mail to: yukiyoshi.onishi@kek.jp
High Energy Accelerator Research Organization (KEK)
Tsukuba, 305-0801, Japan

2.13.1 Introduction

The KEKB asymmetric B factory project [1] has achieved remarkable performance with a peak luminosity of 10^{34} $cm^{-2}s^{-1}$. A total integrated luminosity of more than 150 fb^{-1} has been collected for three years since 1999 and makes one of measurements of CP violation possible, especially the first CP quark mixing phase, ϕ_1, in the neutral B meson. The KEKB asymmetric B factory project will be continued until an integrated luminosity of 300 fb^{-1} is accumulated so far. With this successful operation of the Belle detector and the KEKB collider, the physics focus is expected to move to a precise measurement of the unitarity of the CKM matrix and a search for *New Physics* induced by Supersymmetry (SUSY) beyond the Standard Model. In order to accomplish this physics target, the KEKB collider should be upgraded to obtain the luminosity of 10^{35}-10^{36} $cm^{-2}s^{-1}$ [2].

The super B factory, the target luminosity of 10^{35}-10^{36} $cm^{-2}s^{-1}$, is considered at SLAC and KEK. The target luminosity of the super B factory at SLAC, the SuperBaBar and the SuperPEP-II [3], is definitely 10^{36} $cm^{-2}s^{-1}$ to compete with hadron colliders, such as LHCb and BTeV. On the other hand, the target luminosity of the SuperBelle and the SuperKEKB is 1-6x10^{35} $cm^{-2}s^{-1}$ at the present design work. This target luminosity is estimated by beam-beam simulations and depends on whether the effective head-on collision with crab cavities is employed or not [4]. For the physics at this luminosity range, there are many critical channels with missing neutrinos or with gammas having definite advantage in an e^+e^- collider. In fact, some of those modes are difficult for the hadron collider experiments. Consequently, the e^+e^- asymmetric B factory at 1-6x10^{35} $cm^{-2}s^{-1}$, the SuperKEKB project, is a natural extension of the KEKB project in the field of High Energy Physics.

In order to achieve the unprecedented luminosity of 1-6x10^{35} $cm^{-2}s^{-1}$, which is from ten-times to sixty-times as large as the present luminosity, the beam current of the low energy ring (LER) should be increased up to approximately 10 A. A higher beam current implies much difficulties of the design for vacuum system and RF system. It will become a fight against a large power loss of the higher order mode (HOM) and of the large synchrotron radiation. A substantial upgrade in injector linac also becomes necessary because of the shorter beam lifetime and the injection of the large beam current. Beam instruments, such as beam position monitors, tune measure for the pilot bunch, synchrotron radiation interferometers to measure beam size is inevitable to optimize the luminosity and should work at the large beam currents. Bunch-by-bunch feedback system has to be improved to cure multi-bunch beam instabilities. The effects of photoelectron cloud [5] that is one of the present limitations for the beam current in the LER will have to be overcome by that time. Thus, we plan to upgrade the KEKB collider to SuperKEKB around the year 2007.

2.13.2 Machine parameters

Luminosity is defined as the interaction rate per unit cross section :

$$L = \frac{N_e N_{\bar{e}} f}{4\pi\sigma_x^*\sigma_y^*} R_L \ , \tag{1}$$

where e stands for e^- or e^+, N is the number of particles, f is the collision frequency, R_L is the luminosity reduction factor, σ_x^* and σ_y^* are the horizontal and vertical beam size at I.P, respectively. Alternative expression of the luminosity can be written by

$$L = \frac{\gamma_e}{2er_e}\left(1+\frac{\sigma_y^*}{\sigma_x^*}\right)\left(\frac{I_e\xi_{ye}}{\beta_y^*}\right)\left(\frac{R_L}{R_{\xi y}}\right), \tag{2}$$

where beam-beam parameters :

$$\xi_{x,ye} = \frac{r_e}{2\pi\gamma_e}\frac{N_{\bar{e}}\beta_{x,ye}^*}{\sigma_{x,y}^*\left(\sigma_x^*+\sigma_y^*\right)} R_{\xi x,y} \ , \tag{3}$$

with assuming that the transparency conditions as :

$\gamma_e I_e = \gamma_{\bar{e}} I_{\bar{e}}$, $\varepsilon_e = \varepsilon_{\bar{e}}$, and so on.

In the above expressions, r_e is a classical electron radius, I_e is the beam current, β_y^* is the vertical beta function at I.P, R_ξ is the reduction factor for the beam-beam tune shift, γ is the Lorentz factor, and ε is the emittance. The beam energy of the high energy ring (HER) is 8 GeV and 3.5 GeV for the LER. The transparency condition is not satisfied at the present KEKB, since the beam current of theHER is increased to maximize the luminosity. We consider that the luminosity is degraded by the vertical beam size blow-up due to the photoelectron clouds. Therefore, we try to reduce the effects with solenoid coils and ante-chambers adopted in the arc section. The beam energy exchange, an electron is injected to the LER instead of the HER and a positron is injected to the HER instead of the LER, is also considered simultaneously to reduce the effect of the photoelectron cloud and to have an advantage for the beam top-up or injection from scratch. In general, intensity of the injected beam of the positron is smaller than that of the electron. The luminosity formula (Eq.(2)) tells us that the luminosity is proportional to the beam current, beam-beam parameter, and inverse of the beta function at I.P. We consider the flat beam at the present design. The other parameters except for the ratio of the reduction factors are constant. Therefore, small vertical beta function at I.P, large beam-beam parameters, and large beam currents are necessary to obtain higher luminosity. In order to achieve the primary target of the luminosity, 10^{35} $cm^{-2}s^{-1}$, we propose that β_y^* is 3 mm, the bunch length, σ_z, is also 3 mm to reduce the hour-glass effect, and the beam current is 9.4 A for the LER and 4.1 A for the HER. The number of bunches is 5018 results from 2% abort gap since we adopt the same RF frequency as that of KEKB, 509 MHz. The beam-beam parameter is assumed to be 0.05 in the case of the finite horizontal crossing angle of 30 mrad without crab cavities. The final focusing quadrupole magnets, QCS, would be moved toward the I.P to squeeze β_y^*. The special quadrupole magnets, QC1 and QC2, in the vicinity of the I.P would be rearranged and/or would be replaced with superconducting magnets. The loss in the luminosity comes from a geometrical effect for Gaussian beams significantly if the bunch length is larger than β_y^*. Another luminosity reduction factor comes from the finite crossing angle. The ratio of the reduction factors, R_L/R_ξ, can be estimated to be 0.80 for the horizontal beta function at I.P, β_x^*=30 cm and 0.82 for β_x^*=15 cm in the

case of 30 mrad crossing angle analytically. The choice of β_x^* affects the luminosity and dynamic aperture as well as the detector backgrounds.

Recently, we have studied the effect of finite crossing angle [6] at large beam-beam parameters [4]. The KEKB has achieved the beam-beam parameter of 0.05 with the crossing angle of 22 mrad. The beam-beam performance seems to be less dependent on the finite crossing angle up to 0.05. However, we need larger beam-beam parameters when we expect that the luminosity of several times larger than 10^{35} $cm^{-2}s^{-1}$ as the target luminosity. The beam-beam effects are investigated using weak-strong and strong-strong beam-beam simulations. The beam-beam parameter is increased up to 0.25 linearly for the head-on collision, while it is saturated at around 0.08 for the finite crossing angle. Beam-beam halo also limits the beam-beam parameter. We find that the head-on collision is better than the finite crossing angle concerning with the beam-beam halo from the weak-strong simulations. The finite crossing angle induces the z-dependent dispersion at I.P. However, there are many benefits that the finite crossing angle makes IR design rather simple and avoids undesired collisions due to multi-bunch operation. We introduce the crab cavities [7] to cancel the z-dependent dispersion. When the effective head-on collision with crab crossing is realized, the beam-beam parameter is expected to be 0.2-0.3 approximately. The main parameters are listed in the following:

	LER	HER
Energy (GeV)	3.5	8
Beam current (A)	9.4	4.1
Number of bunches	5018	
Horizontal emittance (nm)	18 - 33	
Vertical emittance (nm)	0.18 - 2.1	
Bunch length (mm)	3	
Horizontal beta at I.P (cm)	15 - 30	
Vertical beta at I.P (mm)	3	
Crossing angle (mrad)	0 (crab crossing) - 30	
Beam-beam parameter	0.05 - 0.26	
Luminosity ($cm^{-2}s^{-1}$)	1 - $6x10^{35}$	

2.13.3 R&D and outlook

The issues arise from the intense synchrotron radiation (SR) due to the large beam current. In order to cure the heating from SR and/or the effect of the photoelectron cloud, an ante-chamber will be used in the arc section [8]. The ante-chamber consists of a beam channel and an SR channel. The SR goes through the SR channel and hits the sidewall at far side of the ante-chamber. The maximum power density at the sidewall is expected to be 40 W/mm^2 for the LER. A photon stop scheme will not be utilized due to the high concentrated power from SR.

The SR from the positron beam hits the chamber wall and the photoelectron cloud emitted from the wall drifts toward the positron beam without the SR channels. However, with the ante-chamber, photoelectrons created inside the SR channel do not

drift toward the positron beam in the beam channel. We consider a saw-tooth surface at the sidewall for the SR channel. The saw-tooth surface is also effective to reduce the reflection of SR. For the straight section, we prepare the external magnetic field provided by the solenoid coils and the permanent magnet built in the chamber from the beginning to put them into the quadrupole magnets, etc.

Copper is the most provable candidate for the chamber materials concerning with the high thermal strength, the high electrical conductivity, and the rather low photoelectron yield. A proto-type ante-chamber made of copper has been installed in the LER at the KEKB in 2001. There is no severe problem found during the operation of 1.5 A beam current. The number of photoelectrons in the beam channel was found to be decreased by about 1/7 of the single beam chamber. With applying the solenoid field of 50 G, it was found that the photoelectrons were further reduced by 50%. The second proto-type ante-chamber that is almost finalized design for the SuperKEKB is under manufacturing at BINP (Russia) and will be installed to the LER at the KEKB in this summer. We will measure the thermal properties and yield of the photoelectron cloud in the beam channel to make sure our design of the ante-chamber.

The HOM heating of bellows chambers that connect the beam chambers and adjust them will become a serious problem. Number of the bellows can be reduced by connecting the adjacent chambers directly with welding in situ. However, the bellows are necessary to absorb errors of alignment or manufacturing. Recently, a new RF-shield structure for the bellows chambers has been proposed [8]. The RF-shield is a comb-type instead of a finger-type. The structure is that a tooth has a width of 1 mm and a radial thickness of 10 mm, and that about 100 teeth are placed at the inner surface of the beam chamber. A gap between each nested tooth is about 0.5 mm. The thermal strength of the shield is much higher than the finger-type. The loss factor of the new RF-shield is also smaller than the finger-type. The R&D for the new bellows with the comb-type of the RF-shield has just started and will be tested in the next KEKB operation after summer shutdown.

We consider that two types of rf cavities, Accelerator Resonantly coupled with Energy Storage (ARES) [9] and single-cell superconducting cavities (SCC) [10], which are successfully operated at the KEKB. We expect that the RF system based on that of the KEKB can be utilized at the SuperKEKB. The RF system is that ARES for the LER and a combination of ARES and SCC for the HER. However, the following improvements are needed. The HOM dampers should be improved to absorb a large amount of the HOM power, about 100 kW generated in a cavity. The number of RF stations should be increased by a factor of 2. To reduce the loaded-Q values of the accelerating mode, steep tapers outside the cavity should be eliminated to make loss factors small.

In a storage ring, the resonant frequency of the cavities should be detuned toward the lower side in order to compensate for the reactive component of the beam loading. The detuning frequency is given by :

$$\Delta f = \frac{I \sin\phi_s}{2V_c}\left(\frac{R}{Q}\right) f = \frac{P_b \tan\phi_s}{4\pi U} , \qquad (4)$$

where I is the beam current, ϕ_s is the synchrotron phase, V_c is the cavity voltage, f is the RF frequency, P_b is the power to the beam, and U is the stored energy in the cavity. In the KEKB and the SuperKEKB, the detuning frequency, Δf, is reduced by increasing the stored energy, U, in ARES or by increasing the accelerating voltage, V_c, in SCC. In fact, the detuning frequency is reduced by a factor of ten than that of the conventional

normal conducting cavity in the KEKB. However, in the case of the SuperKEKB, the detuning frequency becomes close to the revolution frequency. The growth rate of the –1 mode will be much larger than the KEKB. Thus, the impedance should be reduced and a powerful feedback system with comb filters is inevitable, although ARES and/or SCC cavities are used.

The crab cavity would be an important component in the SuperKEKB. The crab cavity must be a HOM-damped structure since the crab cavity is operated in a dipole mode, such as the TM110 mode, which induces the lower frequency parasitic mode. We consider two types of the crab cavities. A superconducting crab cavity, Type-I, has been proposed in 1992 for the B factory. A coaxial beam pipe damper with a notch filter attached to an extremely polarized cell (squashed cell) is employed. This crab cavity is designed for the beam current of 1-2 A. It is difficult to operate it at 10 A because the HOM power of more than 200 kW must be absorbed by HOM dampers and it will be impossible. The R&D efforts have been continued at KEK [11] and will be installed in the KEKB in 2005 to confirm the feasibility of the crab crossing. Recently, a new crab cavity, Type-II, applicable for much higher beam current has been proposed [12]. This crab cavity is equipped with several waveguide HOM dampers. All parasitic modes except for the TM010 can be sufficiently damped at the beam current of 10 A. The highest HOM impedance is reduced by a factor of ten compared with Type-I. In order to avoid the instability driven by TM010, the frequency should be controlled to stay at the middle of adjacent revolution harmonic frequencies. We consider that a frequency monitor and two independent tuners. The coupling impedance at the driven frequency is further reduced by a feedback system with parallel comb filters. The required feedback gain is expected to be less than 20 dB that is comparable to the existing –1 mode damper at the KEKB.

The lattice design of the SuperKEKB is based on that of the KEKB. The emittance can be controlled from 18 nm to 33 nm via the dispersion at noninterleaved 2.5 π cells at the arc section, with wigglers for the LER occasionally. The half of wigglers in the KEKB will be replaced with the RF cavities in the LER for the SuperKEKB. Since the lattice has large flexibility, a optics of the negative momentum compaction can be applicable. In fact, the negative momentum compaction has been tested at the KEKB and the shorter bunch length is observed by a streak camera etc. The negative momentum compaction is one of the candidates for the SuperKEKB.

We use the local bumps at a pair of sextupole magnets which are connected with –I approximately for the optics corrections at the KEKB. In the case of the SuperKEKB, the height of the local bumps will be limited because the synchrotron light might hit the wall of the beam channel instead of the SR channel due to the bump orbit. Therefore, we consider sextupole magnet mover to make the same effect as the bump orbit. There are sextupole magnet movers in the KEKB, but the tolerance is very small about 0.5 mm due to the interference between the magnet and the beam chamber. However, we will test the sextupole magnet movers in the next KEKB operation.

The injector linac must be upgraded for beam injection to a high luminosity machine. We have found the luminosity degraded by the beam size blow-up due to the photoelectron cloud in the positron ring at the KEKB. Thus, the exchange of the beam energy between electrons and positrons may reduce the effects. Another advantage is the injection time. Before making the decision, we have to confirm that the electron beam is stable in the LER concerning with ion effects. Once we decide the energy exchange, the beam energy of the electrons becomes 3.5 GeV and the beam energy of

the positrons becomes 8 GeV. In order to exchange the beam energy, an energy upgrade of the positron beam is needed. We consider that the C-band accelerating scheme instead of the S-band for the energy upgrade [13]. A test stand for the RF conditioning and high power test of the C-band components has been constructed since last year. The C-band accelerating unit will be installed to the KEKB injector linac this summer and will be operated at the next KEKB operation.

Apart from the energy exchange, a continuous injection is useful to increase the integrated luminosity. In this scheme, the lost beam particles are continuously provided by the injection while the detector takes a physics data. We have also tested the continuous injection in the both of LER and HER. There was no serious problem during taking the data vetoed with 2 msec. The simultaneous injection of electrons and positrons is also considered for the SuperKEKB.

2.13.4 Miscellaneous

The SuperKEKB of the luminosity 1-6x10^{35} cm-^{2}s^{-1} is not trivial for either the accelerator design or construction. The budget is also unclear. We estimate the cost for the SuperKEKB project is approximately 380 million dollars in total that includes the upgrade of the Belle detector and a dedicated injector linac for the photon factories (PF/PF-AR). We also consider a strategy of minor upgrade to increase the luminosity year by year if the major upgrade will not be possible. There are various projects such as a large hadron facility (J-PARC), the next linear collider, experiments of the neutrino physics, and the B factory in Japan. So far, manpower as well as money will be an important issue for the future projects. However, we hope to propose the upgrade of the KEKB to the SuperKEKB for the super B factory as the next project of the High Energy Physics in Japan.

References

1. KEKB Design Report, KEK Report 95-7.
2. “Expression of Interest in A High Luminosity Upgrade of the KEKB Collider and the Belle Detector”, January 2002. http;//kcgsrv1.kek.jp/SuperKEKB/Documents.html.
3. D. G. Hitlin, Proceeding of 3th Workshop of the High Luminosity B Factories, Shonan Village, Japan, August 2002.
4. K. Ohmi, Proceedings of PAC 2003, Portland, USA, May 2003.
5. F. Zimmermann, CERN SL-2000-017(AP). K. Ohmi and F. Zimmermann, Phys. Rev. Let. 85 (2000) 3821.
6. K. Oide and K. Yokoya, Phy. Rev. A40, (1989) 315.
7. K. Akai et al., Proceedings of B factories, SLAC-400 (1992) 181.
8. Y. Suetsugu et al., Proceedings of PAC 2003, Portland, USA, May 2003.
9. Y. Yamazaki nad T. Kageyama, Part Accel. 44 (1994) 44.
10. T. Furuya et al., Proceedings of $e^{+}e^{-}$ factories ‘99, Tsukuba, Japan, September 1999.
11. K. Hosoyama et al., Proceedings of APAC ’98, Tsukuba, Japan, March 1998.
12. K. Akai, Proceedings of PAC 2003, Portland, USA, May 2003.
13. T. Kamitani et al., Proceedings of PAC 2003, Portland, USA, May 2003.

2.14 Challenge toward very high luminosity at super KEKB

K. Ohmi, M. Tawada
mailto: ohmi@post.kek.jp
KEK, Oho Tsukuba, Ibaraki, 305-0801, Japan

2.14.1 Introduction

High luminosity B factories, PEP-II and KEKB have been operated successfully in SLAC and KEK, respectively. They have next plans toward higher luminosity of 10^{35} to 10^{36} $cm^{-2}s^{-1}$[1,2]. Very high beam-beam parameter >0.1 is required to get the high luminosity, otherwise very high operating current or very small beta function at the collision point are required. We have studied beam-beam effects for very high beam-beam parameter in e^+e^- circular collider. The status of our studies is presented in this leter.

The luminosity is approximately given for collision between two flat beams as

$$L = \frac{\gamma_{\pm} I_{\pm} \xi_y}{2 e r_e \beta_y}. \tag{1}$$

For given relativistic factor (γ), our freedom is choice of the total current (I_{+-}), vertical beta function at interaction point, IP (β_y) and the beam-beam parameter (ξ_y), where the transparency condition $I_+\gamma_+=I_-\gamma_-$ is kept for two colliding beams. The total current and beta function at IP are connected with hardware and optics design. It is a beam dynamics issue how large the beam-beam parameter can be achieved. If I= 10 A for the energy E=3.5 GeV and β_y=3 mm are chosen, the luminosity 10^{35}-10^{36} $cm^{-2}s^{-1}$ is achieved by ξ_y =0.04-0.4, respectively. The maximum ξ_y, which is called the beam-beam limit, is believed to be about 0.05-0.1 depending on the radiation damping time. From this point, the luminosity 10^{35} $cm^{-2}s^{-1}$ is possible to be achieved, but 10^{36} $cm^{-2}s^{-1}$ is impossible.

The beam-beam limit can be caused by various reasons. The lattice map affects the beam-beam performance. Its linear part consists of Twiss parameters and dispersion functions at IP. Crossing angle is equivalent to a kind of dispersion function at IP. Nonlinear map, chromaticity and amplitude dependent tune shift, also affect the beam-beam limit. There may be some engineering problems.

We take notice of the ideal beam-beam limit, which is irrelevant to above source. Probably it is determined by the beam-beam parameter, tune, bunch length, damping time and some other basic parameters.

We set up parameters of super KEKB as is shown in Table 1. The beam-beam parameter and luminosity are set 0.2 and 5×10^{35} $cm^{-2}s^{-1}$, respectively. Computer simulations of the beam-beam effects based on the weak-strong and the strong-strong model have been performed whether the parameters can be realized. We show the present results in following sections.

Table 1 Tentative parameter list of super KEKB.

	HER	LER
I (A)	4.4	10
N_b	5000	5000
N_e	$5.5x10^{10}$	$1.26x10^{11}$
ε_x / ε_y (nm)	18/0.18	18/0.18
σ_z (mm)	3	3
β_x / β_y (cm)	30/0.3	30/0.3
ξ_x / ξ_y	0.2/0.2	
L ($cm^{-2}s^{-1}$)	$1x10^{32}x5000$	

2.14.2 Weak-strong simulation

In the weak-strong simulation, one beam is represented by a rigid Gaussian distribution located at IP, and another beam is represented by macro-particles. The beam-beam effect is investigated by tracking of the macro-particles. The bunch length is taken into account by longitudinal slicing and the synchro-beam mapping [3]. The weak-strong simulation is very rapid to be executed; therefore it is useful to scan various parameters. Figure 1 shows the result for tune scan of super KEKB. The luminosity is more than $1x10^{32}$ $cm^{-2}s^{-1}$ in the area near half integer line in the horizontal tune as is drawn by white area in the figure. We think this tune area is the best [4] for the luminosity, though tuning of optics, especially beta beating, is difficult. CESR [5] and KEKB have been operated with this tune area. The luminosity of PEPII increased due to change the operating point to this area in 2003. Tune area near (0.51,0.08) may be also good from the view of the beam-beam effect, but control of the closed orbit is sensitive due to the vertical tune close to an integer.

Figure 1 Luminosity in the transverse tune space. White and black areas are more than $L=1x10^{32}$ $cm^{-2}s^{-1}$ and less than 10^{31} $cm^{-2}s^{-1}$.

Figure 2 shows the beam-beam parameter and luminosity depending on the beam current obtained by the simulation. The figure is obtained for ε_x =33 nm, therefore the luminosity is slightly lower than the design for the current, I=2 mA. We have to note the beam-beam parameter is not saturated until more than 0.2. The luminosity for finite crossing angle, which is also plotted in the figure, is saturated at <0.1. The crossing angle is equivalent to a dispersion function $\zeta=x/\Delta z$, therefore the beam-beam limit is appear to be <0.1.

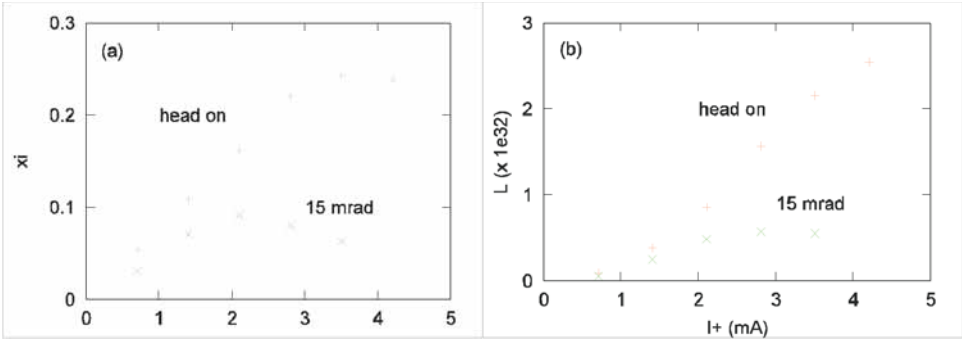

Figure 2 Beam-beam parameter and luminosity for increasing beam current obtained by the weak-strong simulation. The emittance, ε_x =33 nm, is used in this simulation.

2.14.3 Strong-strong simulation with Gaussian approximation

The beam-beam limit in the weak-strong simulation, which was quite high >0.2, should be checked by strong-strong simulations whether the high value can be achieved actually. In the strong-strong simulation, we have two options. One is soft Gaussian approximation, and another is particle in cell (PIC) method. Both of two beams are represented by enormous number of macro-particles in the strong-strong simulations. Macro-particles in one beam interact with the other beam, which is approximated to be a Gaussian in the first method. The parameters of the Gaussian distribution are determined by first and second order moment of the beam distribution. Bunch length is also taken into account by longitudinal slicing and the synchro-beam mapping.

Figure 3 shows evolution of the luminosity for the parameter in Table 1. Convergence for the number of macro-particles and slices was examined and was no problem as is shown in the figure. The input horizontal emittance is somewhat larger than the design. The dynamic beta and emittance squeeze the horizontal beam size due to the tune close to a half integer, with the result that the beam size roughly equal to the designed one. By the way the simulation using the design emittance showed a smaller horizontal size which gave vertical size enlargement.

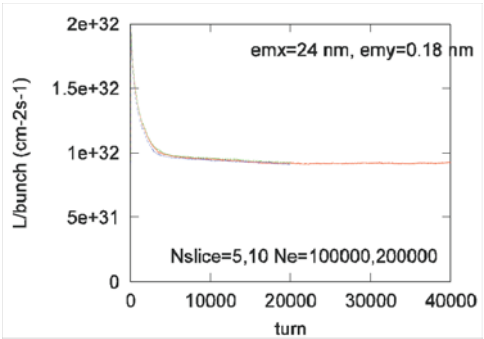

Figure 3 Evolution of luminosity. The emittance, ε_x =24 nm, is used to compensate the dynamical beta and emittance effects.

The strong-strong simulation with Gaussian approximation gave the results which is consistent with those of the weak-strong simulation, though the detailed control of the horizontal emittance, namely the beam-beam parameter 0.2 can be achieved as long as in the weak-strong and Gaussian strong-strong simulation.

2.14.4 Strong-strong simulation with particle in cell method

In the PIC method macro-particles are mapped on a grid space and electric potential on the grid point is given by solving Poisson equation. In the PIC method, the synchro-beam mapping is obtained by the potential interpolated between the longitudinal slice. Figure 4 shows the beam-beam parameter and luminosity depending on the beam current obtained by the simulation. The figure is obtained for ε_x =33 nm. We observe the beam-beam limit around 0.1 in this simulation, which is not consistent with the results of the weak-strong and Gaussian strong-strong simulations. This means that only the PIC strong-strong model can express a real beam-beam limit, or has something of numerical problem to give a fake beam-beam limit.

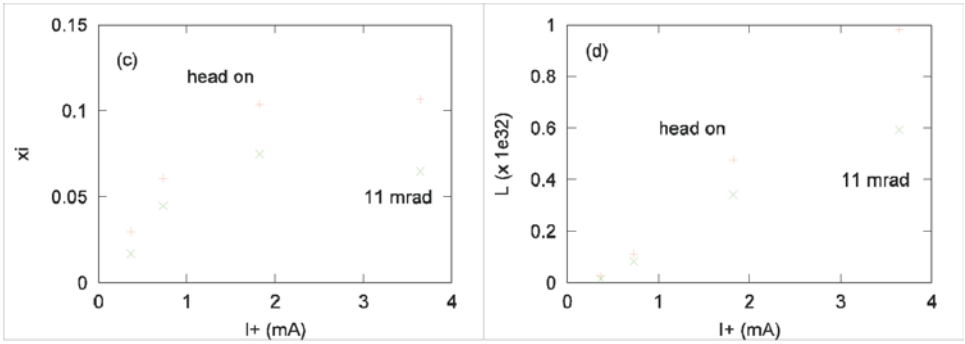

Figure 4 Beam-beam parameter and luminosity for increasing beam current obtained by the strong-strong simulation with PIC method. The emittance, ε_x =33 nm, is used in this simulation.

We do not have answer which simulation is reliable. There may be a hint in two dimensional (x-y) model of the strong-strong simulation. Beam-beam limit is caused by an enhancement of coherent dipole motion of π mode in the PIC method [6], while is not caused in Gaussian strong-strong simulation. Figure 5 shows σ and π mode spectra obtained by the two simulations. In the Gaussian strong-strong simulation, π mode spectrum was never enhanced to σ mode one. We are not sure that the results in two dimensional simulation is true for three dimensional simulation. In our three dimensional simulation, clear signal of the coherent mode is not observed. Therefore we can not conclude whether the coherent motion is essential for the beam-beam limit now.

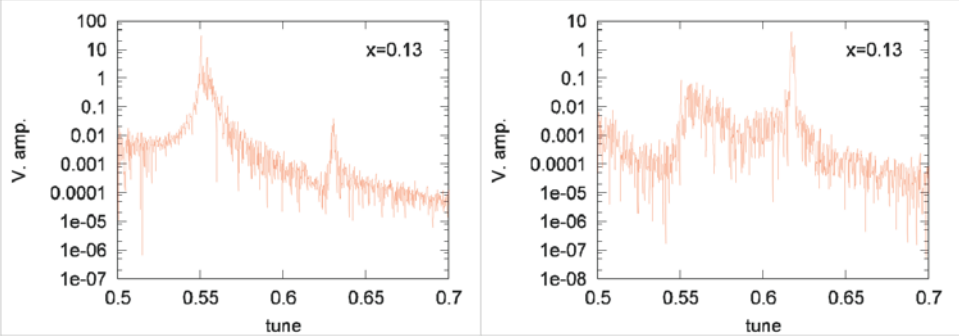

Figure 5 Tune spectra of vertical coherent dipole motion for ξ_y =0.13. Spectra given by Gaussian and PIC models are depicted in left and right pictures, respectively.

2.14.5 Summary and discussion

We have studied the beam-beam effect of collision of two flat beams to achieve high luminosity, 10^{35} to 10^{36} $cm^{-2}s^{-1}$. Luminosity has been estimated by three types of simulations, weak-strong, strong-strong with Gaussian approximation, and strong-strong with PIC method. The weak-strong and Gaussian strong-strong simulations gave a high beam-beam limit over 0.2, with the result that the luminosity $5x10^{35}$ $cm^{-2}s^{-1}$ showed to be achieved for our tentative design parameter. The strong-strong simulation with PIC method gave lower beam-beam limit around 0.1. The reason why they showed discrepant results has not been understood yet. The discrepancy may be essential information for mechanism of the beam-beam limit. We need more studies to understand the reason which causes the discrepancy.

We are also studying other options, four beam or compensation, and round beam, toward higher luminosity and higher beam-beam parameter. In four beam or compensation scheme, coherent motion becomes serious [7]. This fact is due to that the strength of linear force for a displacement between beams is kept for the neutralization, while nonlinear force, which helps Landau damping, does not exist. In our trial [8], we have not found a reliable operating point yet. In round beam, luminosity is twice of Eq.(1), because the tune shift (ξ_r) is a half of that of the flat beam. The beam-beam parameter is achieved to be 0.2 in the strong-strong simulation with the PIC method [9]. Beta function at IP should be lower than $2\beta_y$ to gain the high beam-beam parameter. There is no prospect to realize a lattice with the beta function yet.

The authors thank for many fruitful discussions with Y. Funakoshi, Ji Qiang, K.Oide and A. Valishev.

References

[1] "Expression of Interest in a High Luminosity Upgrade of the KEKB Collider and the Belle Detector", January 2002. http://kcgsrv1.kek.jp/SuperKEKB/Documents.html.
[2] J. Seeman, Proceedings of PAC2001, 305 (2001).
[3] K. Hirata, H. Moshammer and F. Ruggiero, Particle Accelerators, **40**, 205 (1993).
[4] KEKB design report, KEK Report 95-7 (1995).
Y. Z. Wu et al., KEK Report 2001-5 (2001).

[5] Rogers, Proceeding of PAC01, 336 (2001).
[6] K. Ohmi, Phys. Rev. E **59**, 7287 (2000).
[7] B. Podobedov, R. H. Siemann, Phys. Rev. E **52**, 3066 (1995).
L. Jin and J. Shi, Proceeding of beam-beam workshop 2003.
[8] Y. Ohnishi and K.Ohmi, Proceeding of Beam-beam Workshop 2003.
[9] A. Valishev, E. Perevedentsev, K. Ohmi, Proceeding of PAC03.

2.15 Experiments on electron cloud effects in lepton storage rings

H. Fukuma
mail to: hitoshi.fukuma@kek.jp

High Energy Accelerator Research Organization (KEK)

Tsukuba, Ibaraki 305-0801, Japan

2.15.1 Introduction

Electron cloud effects are observed in both hadron and lepton machines. In this report we summarize the electron cloud experiments in lepton storage rings because this issue of Beam Dynamics Newsletter covers high luminosity e^+ e^- colliders. For readers who are interested in the experiments on proton machines Ref.1 is a good reference.

Most experiments so far performed on the electron cloud have been focused on 1) the measurement of the electron cloud, 2) transverse coupled-bunch instability and 3) beam size blow-up.

2.15.2 Measurement of electron cloud

Electron yield and energy spectrum of cloud electrons have been measured at several storage rings [2,3,4]. All measurements in Refs. 2, 3 and 4 used a retarding field analyzer (RFA) that was developed at APS [2]. Among them the most detailed measurement was done at APS. As vacuum chambers at APS are made of Al which has a relatively high secondary electron yield coefficient it was expected that the electron cloud effects would be enhanced. Amplification of the electron yield was observed for a bunch spacing of 7 rf buckets. The data can best be explained by beam-induced multipacting (BIM). To explain the sharp peak at the 7 rf bucket spacing a general form of BIM condition where the drifting of secondary electrons with production energy was taken into account was suggested. A buildup and saturation of the electron cloud over a bunch train was observed. The electron cloud reached saturation at a level of about 1% of the average beam density near the BIM resonance. Longitudinal variations of the electron yield at saturation level suggests the importance of the geometrical details of the vacuum chamber in simulations. The effect of surface conditioning of a vacuum chamber by the beam was observed. Interestingly the BIM resonance was observed with electron beams though the amplification of the electron cloud was more modest than that for positron beams.

At BEPC [3], where the vacuum chamber is made of Al as at the APS, there was no saturation of the electron yield over a bunch train up to 40 bunches long and no BIM was observed. The leakage field of a dipole magnet which was very near to the RFA may influence the measurement as noted in Ref. 3.

Anomalous vacuum pressure rise is also an indication of the presence of an electron cloud. It was observed at the APS [2], PEP-II positron ring [5] and KEKB positron ring [6]. At APS vacuum pressure rise was dependent on fill pattern in both positron and electron beam. At PEP-II and KEKB the vacuum pressure increased nonlinearly with the beam current. The rate of pressure rise, expressed as dP/dI, where P and I are the

pressure and the beam current respectively, was dependent on fill pattern. It is explained by BIM. A solenoid field of several tens of Gauss applied over a vacuum chamber was effective to reduce the pressure rise at KEKB and PEP-II.

At KEKB a tune shift was observed along the train [7], from which the electron cloud density can be estimated[8]. The tune shift increases along the train and then saturates. A simple calculation using the measured tune shift suggested an electron density of 6×10^{11} m^{-3} at the saturation level which was consistent with a simulation [9]. When solenoid magnets which were installed to remove the electron cloud were turned on, the horizontal tune shift was reduced by half. On the other hand the vertical tune shift was reduced by only 20% with the solenoid field. The reason for the asymmetric effect of the solenoid magnets is not clear.

2.15.3 Transverse coupled-bunch instability

A coupled-bunch instability caused by an electron cloud in a positron storage ring was first observed at the PF at KEK [10, 11]. The instability occurred in the vertical plane. The following observations led to the proposition that the instability was caused by an electron cloud: 1) the broad distribution of the betatron sidebands suggested that the range of wake force was as short as about 7 rf buckets, which was considered to be due to the large mobility of cloud electrons; 2) the observed broad distribution of the betatron sidebands in positron storage was not seen in electron storage; 3) the sideband distribution changed when data were taken at different beam current; and 4) clearing electrodes reduced the vertical beam size by about 15%.

In BEPC [12] a vertical coupled-bunch instability that can be explained by electron clouds was found in the positron beam after the observation at the PF. A broad distribution of the betatron sidebands was observed in positron storage. It was not seen in the electron beam. The instability was strongly dependent on the bunch spacing, i.e., longer bunch spacing suppressed the instability. A flexible lattice and the ability to ramp energy enabled the measurement of the emittance and energy dependence of the threshold current of the instability. The threshold current increased when the emittance decreased. The instability got weaker when the energy increased. A simulation did not show such a dependence of the instability. The change of the threshold current may be explained by the change of the damping time due to Landau damping that come from nonlinear fields in the ring lattice. The instability was also suppressed by increasing the chromaticity. Landau damping was again considered to be a main reason for the effect.

At the APS [2] a horizontal coupled bunch instability was observed for positron beams near the BIM resonance. The instability has not appeared with electron beams .

At CESR [13] an anomalous growth of the horizontal coupled bunch instability was observed for both positron and electron operations. The instability was present only when the distributed ion pumps (DIPs) were powered. The instability is explained by photoelectrons trapped in the vacuum chamber by the bending magnet field and a quadrupole electrostatic field of a DIP.

At the KEKB LER [14] a coupled bunch instability was observed in both horizontal and vertical planes. The mode spectrum and the growth rate of the instability changed with activation of the solenoid magnets, which strongly suggests that the instability is caused by the electron cloud. The shape of the mode spectrum was almost the same in horizontal and vertical planes. A simulation explains the mode spectrum if the electron cloud is produced uniformly in the vacuum chamber. Measured horizontal and vertical

growth rates were roughly consistent with the simulation. The instability is suppressed by a bunch-by-bunch feedback system and not an issue for stable operation.

2.15.4 Beam size blow-up

A beam size blow-up was observed in the positron rings of two B-factories. The blow-up is explained by a single bunch head-tail instability caused by the electron cloud [15]. Multi-bunch operation is necessary to produce the electron cloud. The blow-up is one of the big issues limiting the luminosity.

At PEP-II [16, 17, 18] horizontal and vertical beam size blow-ups were observed by a measurement of the beam size. The threshold beam current of the blow-up is almost the same in both planes. Due to the blow-up the bunch-by-bunch luminosity decreased along the train. Various fill patterns were tried to minimize the blow-up. Beam size measurement by a gated camera showed that a mini-gap of three bunches between trains reduced the blow-up for the next train. In a "by-2-by-4" pattern which has colliding bunches alternating with 2 and 4 rf bucket spacing, the bunches that were 2 rf buckets apart had a lower luminosity than those separated by 4 rf spacing. Solenoid magnets were very effective to reduce the blow-up. The slope of the beam size as a function of the beam current was reduced when the solenoid magnets powered on. The typical solenoid field strength was 30 Gauss. The threshold current of the blow-up seemed not to change much when powering on the solenoid magnets. The solenoids even in arc sections, where large quantities of electrons are not expected because the vacuum chambers have antechambers and are made of TiN-coated Al, were effective in improving the luminosity.

In KEKB [19, 20, 21, 22] the beam size blow-up has been observed only in the vertical plane. A measurement by a gated camera showed that the vertical beam size increased along the train. A high chromaticty of about 10 was effective to reduce the blow-up though its effect on the instability seems larger than predicted by the transverse mode coupling theory [23]. Unlike PEP-II a clear variation of the bunch-by-bunch luminosity was not observed along the train. Solenoid magnets with a field strength of about 45 Gauss were effective to reduce the blow-up. The threshold current of the blow-up changed due to the solenoid field. The luminosity also changed with the addition of the solenoid field. The blow-up is not observed in daily operation with 4 rf bucket spacing after installing solenoid magnets over 75% of the circumference of the ring. However a recent measurement with 3.5 rf bucket spacing, where a fill pattern of 7 bunches with 4 rf bucket spacing followed by 7 bunches with 3 rf bucket spacing was repeated, showed a blow-up starting at 1300mA.

2.15.5 Summary

The effects of the electron cloud manifest themselves in several lepton storage rings as beam-induced multipacting, coupled-bunch instability, beam size blow-up and tune shift along the train. The beam-induced multipacting is reduced by installing solenoid magnets at PEP-II and KEKB. The coupled-bunch instability is well suppressed by the bunch-by-bunch feedback system and the solenoid magnets at KEKB.

The beam blow-up has a large impact on the luminosity of B-factories. The blow-up at KEKB and PEP-II seems have different characteristics: 1) while the blow-up is observed in only the vertical plane at KEKB, it is seen in both the horizontal and

vertical planes at PEP-II; 2) while the bunch-by-bunch luminosity is sensitive to the fill pattern at PEP-II, the variation of the bunch-by-bunch luminosity along the train is not clear at KEKB; and, 3) while the threshold current changed when turning on solenoid magnets at KEKB, it was almost unchanged at PEP-II. Though the blow-up is reduced by the solenoid magnets at both KEKB and PEP-II, it is still an important impediment to increasing the luminosity at bunch spacings less than 4 rf buckets.

Some interesting questions remain to be solved: 1) a trapping of the electrons inside the magnets is proposed [24] but not confirmed by experiments; 2) the head-tail motion which is considered as a source of the blow-up is not clearly observed yet; and 3) a predicted combined phenomenon of the electron cloud and the beam-beam effect [25] is not fully studied.

The author apologizes those who performed experiments or measurements which were not mentioned in this report due to a lack of his knowledge.

2.15.6 Acknowledgments

The author thanks J. W. Flanagan for careful reading of the manuscript.

2.15.7 References

1. Proceedings of Mini-Workshop on Electron-Cloud Simulations for Proton and Positron Beams", CERN, Geneva, Switzerland, 2002 (CERN-2002-001) edited by G. Rumolo and F. Zimmermann.
2. K. C. Harkay and R. A. Rosenberg, "Properties of the electron cloud in a high-energy positron and electron storage ring", Phys. Rev. ST Accel. Beams 6, 34402 (2003).
3. Z. Y. Guo et al., "EXPERIMENT TO MEASURE THE ELECTRON CLOUD AT BEPC", Proceedings of the 2001 Particle Accelerator Conference, Chicago, p. 676.
4. Y. Ohnishi et al., "DETECTION OF PHOTOELECTRON CLOUD IN POSITRON RING AT KEKB", Proceedings of the 18th International Conference On High Energy Accelerators, 2001, Tsukuba.
5. A. Kulikov et al., "PEP-II LER Nonlinear Vacuum Pressure Increase With Current", Proceedings of International Workshop on Performance Improvement of Electron-Positron Collider Particle Factories, 1999, Tsukuba, p. 83 (KEK Proceedings 99-24).
6. Y. Suetsugu, "OBSERVATION AND SIMULATION OF THE NONLINEAR DEPENDENCE OF VACUUM PRESSURES ON THE POSITRON BEAM CURRENT AT THE KEKB", Proceedings of the 2001 Particle Accelerator Conference, Chicago, p. 2183.
7. T. Ieiri et al., "Bunch-by-bunch measurements of the betatron tune and the synchronous phase and their applications to beam dynamics at KEKB", Phys. Rev. ST Accel. Beams 5, 094402 (2002).
8. K. Ohmi, S. Heifets and F. Zimmermann, "STUDY OF COHERENT TUNE SHIFT CAUSED BY ELECTRON CLOUD IN POSITRON STORAGE RINGS", Proceedings of Second Asian Particle Accelerator Conference (APAC'01), September 2001, Beijing, China, p.445.

9. F. Zimmermann., " Electron Cloud at the KEKB Low-Energy Ring : Simulations of Central Cloud Density, Bunch Filling Patterns, Magnetic Fields, and Lost Electrons ", CERN-SL-Note-2000-017 AP, 2001.
10. M. Izawa et al., "The Vertical Instability in a Positron Bunched Beam", Phys. Rev. Lett. 74, 5044(1995).
11. K. Ohmi, " Beam-Photoelectron Interactions in Positron Storage Rings ", Phys. Rev. Lett. 75, 1526(1995).
12. Z. Y. Guo et al., "Experimental studies on the photoelectron instability in the Beijing Electro Positron Collider", Phys. Rev. ST Accel. Beams 5, 124403 (2003).
13. T. Holmquist and J. T. Rogers, "A Trapped Photoelectron Instability in Electron and Positron Storage Rings", Phys. Rev. Lett. 79, 3186(1997).
14. S. Win et al., "STUDY OF COUPLED BUNCH INSTABILITY CAUSED BY ELECTRON CLOUD IN KEKB POSITRON RING", Proceedings of the 8th European Particle Accelerator Conference2001 Particle Accelerator Conference, 2002, Paris, p. 1592.
15. K. Ohmi and F. Zimmermann, "Head-Tail instability Caused by Electron Clouds in Positron Storage Rings", Phys. Rev. Lett. 85, 3821(2000).
16. A. Kulikov et al., "THE ELECTRON CLOUD INSTABILITY AT PEP-II", Proceedings of the 2001 Particle Accelerator Conference, Chicago, p. 1903.
17. F-J. Decker et al., "INCLEASING THE NUMBER OF BUNCHES IN PEP-II", Proceedings of the 8th European Particle Accelerator Conference, 2002, Paris, p. 392.
18. R.L. Holtzapple, "MEASUREMENT OF TRANSVERSE BUNCH SIZE BLOW-UP DUE TO THE ELECTRON CLOUD INSTABILITY AT PEP-II", SLAC-PUB-9222.
19. H. Fukuma et al., "OBSERVATION OF VERTICAL BEAM BLOW-UP IN KEKB LOW ENERGY RING", Proceedings of the 7th European Particle Accelerator Conference, 2000, Vienna, p. 1122.
20. H. Fukuma et al., "STUDY OF VERTICAL BEAM BLOWUP IN KEKB LOW ENERGY RING", Proceedings of the 18th International Conference On High Energy Accelerators, 2001, Tsukuba.
21. H. Fukuma et al., "Status of Solenoid System to Suppress the Electron Cloud Effects at the KEKB", Proceedings of the 20th ICFA Advanced Beam Dynamics Workshop on High Intensity and High Brightness Hadron Beams", 2002, FNAL, Batavia, Illinois, USA, 2002 (AIP Conference Proceedings 642), p.357.
22. J. W. Flanagan et al., "HIGH-SPEED GATED CAMERA OBSERVATIONS OF TRANSVERSE BEAM SIZE ALONG BUNCH TRAIN AT THE KEKB B-FACTORY", Proceedings of the 7th European Particle Accelerator Conference, 2000, Vienna, p. 1119.
23. K. Ohmi, F. Zimmermann and E. Perevedentsev, " Wake-field and fast head-tail instability caused by an electron cloud ", Phys. Rev. E 65, 016502 (2002).
24. L. F. Wang et al., " Photoelectron trapping in quadrupole and sextupole magnetic fields ", Phys. Rev. E 66, 036502 (2002).
25. K. Ohmi and A. W. Chao, " Combined phenomena of beam-beam and beam-electron cloud interactions in circular $e+e^-$ colliders ", Phys. Rev. ST Accel. Beams 5, 101001 (2002).

2.16 Review of theoretical investigations on electron cloud

Frank Zimmermann, CERN
mailto:frank.zimmermann@cern.ch

2.16.1 Introduction

Inside an accelerator beam pipe electrons are generated via ionization of the residual gas, and from the vacuum-chamber wall via photoemission due to synchrotron radiation or via secondary emission due to electron or ion impact. These electrons can collectively or coherently interact with the beam and, thereby, degrade the performance of accelerators operating with intense positively charged beams. Examples of accelerators presently observing an electron cloud comprise the positron rings of the two B factories at SLAC [1] and KEK [2], the Relativistic Heavy Ion Collider (RHIC) at BNL [3], and the Los Alamos Proton Storage Ring [4,5]. Electrons are also expected to possibly pose limitations for many future projects, such as the Large Hadron Collider (LHC) [6], under construction at CERN, the Spallation Neutron Source (SNS) at Oakridge [7], and the positron damping rings of future linear colliders [8,9]. Important theoretical studies concern the build up of the electron cloud, the single bunch instabilities, the multi-bunch instability, and the incoherent effects. Most of these phenomena can be addressed by simulation codes.

In the following, I attempt to summarize the history of electron-cloud observations and their interpretation, the analytical models and the simulations of various electron-cloud effects, the achieved level of understanding, the ongoing research activities and several open questions. Since the electron dynamics is similar for proton and positron rings, I will consider studies for both cases.

2.16.2 History

As early as 1967, instabilities driven by a cloud of electrons were seen at two Novosibirsk proton storage rings [10,11], where unusual transverse instabilities occurred both for bunched and unbunched beams. The interpretation that these instabilities were driven by electrons was first put forward by Budker and co-workers, who considered a model of coupled oscillations between the electrons and beam centroid as in Ref. [12]. Soon thereafter B. Chirikov studied the possible stabilization or destabilization of such 2-stream instabilities by Landau damping [13]. The instability in Novosibirsk was overcome by two different means [11]: (1) a further increase of the beam current, and (2) the installation of a transverse feedback system.

The deleterious effect of electrons gathered more prominence at the CERN Intersecting Storage Rings (ISR). Here, at the start of the 1970s, electrons created by gas ionization accumulated in the static attractive potential of the high-current coasting beams. Beyond a certain level of neutralization, the ISR beams became unstable. A theory of this instability was developed by Hereward [14], and, including Landau

damping effects, by E. Keil and B. Zotter [15]. The ISR problem was cured by installing a large number of clearing electrodes, which extracted the electrons from the beam potential. In 1977 when an aluminium test chamber was installed in the ISR a different type of instability occurred with a bunched proton beam. Above a threshold current, a rapid fast pressure increase was observed, triggered by a shift in the horizontal beam orbit towards the centre of the chamber [16]. A characteristic feature of aluminium is its high secondary emission yield. O. Grobner explained the pressure-rise threshold in the ISR by 'beam-induced multipacting', a resonance condition where secondary electrons emitted from the surface are accelerated in the field of a passing bunch such that they hit the opposite side of the chamber, producing new secondaries, just at the moment when the next bunch arrives. For a round beam pipe of radius *b*, the resonance condition reads $N_b L_{sep} r_0/b^2=1$ [16], where the other symbols denote the bunch population, the bunch spacing in meter, and the classical electron radius. However, as we know now, the electron build for a bunched beam can also occur very far from this resonance condition, for example, when electrons either interact with several passing bunches or, in the opposite limit, when low-energetic secondaries survive during an extended gap [17].

At the end of the 1980s, after switching operation from electron to positron beams, the KEK Photon Factory observed a wide-band coupled-bunch instability, which had not been seen earlier with electrons [18]. The instability and its pattern could be explained by a short-range wake, which was attributed to photoelectrons [18,19]. The first computer code, PEI, simulating the electron-cloud generation and the ensuing wake-field was written by K. Ohmi in this context [19].

In preparing for the KEK B factory, the electron cloud formed by photoelectrons was studied at the TRISTAN accumulation ring and at BEBC by an IHEP-KEK collaboration [20]. In parallel, since 1995 a simulation campaign for the PEP-II B factory was begun at LBNL by M. Furman and G. Lambertson [21]. One of the consequences of this study was the decision to coat the PEP-II vacuum chamber by Titanium Nitride, so as to lower the secondary emission yield. The program POSINST has been in use and continually refined since this time.

In 1997 simulations with yet another code, ECLOUD, predicted a strong effect for the LHC [22], the first proton ring with significant synchrotron radiation and a critical photon energy well above the photoemission threshold. The concerns here do not only pertain to the beam instabilities, but also to the heat load deposited by the electrons which impinge inside the cold magnets [23,24,25]. About two years afterwards the electron cloud was indeed observed with the LHC-type beam in the LHC injectors SPS [26] and, a little later, in the PS [27]. It manifested itself by its perturbing effect on the beam diagnostics (feedback pick ups, beam position monitors, secondary emission grids), by a pressure rise of about 4 or 5 orders in magnitude, and by both single- and multi-bunch instabilities. Since then a plethora of unique diagnostics was developed and many experiments were performed at CERN, both in the laboratory and also with an actual beam in the CERN SPS. The measurements at the SPS addressed the beam stability [28] as well as the properties and dependence of the electron-cloud build up on various parameters, like the beam sizes, beam intensity and chamber geometry [29].

Partly in response to the potential danger from the electron cloud, the LHC vacuum chamber is being prepared in a variety of ways. Namely, (1) a sawtooth pattern is impressed on the horizontal outward side of the beam screen mounted in the cold parts of the machine, reducing the photon reflectivity inside the strong dipole magnets [30]; (2) the pumping slots at the top and bottom of the vacuum chamber are shielded so as to prevent a direct impact of electrons onto the cold bore (at 1.9 K) of the magnet [31]; (3) the warm sections (about 20% of the LHC circumference) are coated with a newly developed getter material TiVZr [32], whose maximum secondary emission yield is low (between 1.1 and 1.4); (4) the commissioning program is tailored so as to maintain a continuous electron flux onto the surface of the chamber, sufficiently low that the heat load stays within the tolerance [33]. The reduction of the secondary emission yield as a function of the deposited electron dose has been measured and demonstrated both in the laboratory [34] and in the SPS for a warm surface [29]. The mechanism of this surface conditioning by the impinging electrons is not well understood, and further studies at cryogenic or liquid-helium temperatures are presently under way at CERN.

2.16.3 Electron-Cloud Build Up

Simulating the build up of the electron cloud, as done in the programs PEI, POSINST, ECLOUD, and the newer 3-dimensional PIC code CLOUDLAND [35], relies on accurate models of the primary electrons and of the secondary emission process. For example, the secondary emission probability depends on the energy of the incident electron, on its angle of incidence, and on the history of the surface (e.g., [21]). It may also be different for cold or warm temperatures and in a magnetic field. The energy distribution of the primary and secondary electrons is also an important factor, which critically determines the survival time of electrons between bunches. Several measurements aimed at characterizing these variables and dependencies were performed by N. Hilleret and colleagues at CERN, R. Kirby and co-workers at SLAC, also by T. Toyama and co-workers in KEK, and lately by R. Cimino and I. Collins, the latter two also at CERN. At low incident energies, there is a large nonzero probability that an electron hitting the surface will be reflected and does not enter into the metal. The latest measurements by Cimino/Collins suggest that this probability increases to one in the limit of vanishing energy, which appears consistent with a quantum-mechanical calculation, as first pointed out by M. Blaskiewicz of BNL. The inclusion of this elastic component has a large impact on the simulation results, e.g., it can increase the simulated heat load for the LHC by a factor 5 or more.

Often the cloud often is not uniform. Inside dipole magnets, it may build up in the form of 1, 2 or 3 vertical strips of high density, depending on the beam intensity [22,29,36]. The regions of high density correspond to electron impact energies for which the secondary emission yield is maximum. Their location depends on the surface properties, the electron dynamics, and on the beam parameters.

Detailed comparisons of the simulated and measured electron-cloud build up and its spatial or time structure were made for a beam consisting of closely spaced bunches at the KEKB positron ring [37] and in the CERN SPS [38], and for a long proton

bunch at the Los Alamos PSR [39]. In particular, the simulations demonstrated that a weak solenoid field (a few Gauss) or an electric field of about 100 kV/m [40] (e.g., clearing electrode) significantly suppress the cloud build up, consistent with observations.

The mechanism of electron build up for a bunch train is different from that for a single long bunch. In the case of a bunch train the electrons are amplified by the multi-bunch multipacting process, described above, which is also known as 'multibunch passage multipacting' [7]. Simulated and measured build up times along a bunch train were found to be in excellent agreement both for KEKB and the SPS. Usually it takes 10-20 bunches for an electron cloud to build up to the saturation level, where losses due to electron space-charge forces and the influx of newly generated electrons balance each other. In the case of a single long bunch the electrons can reach saturation during a single bunch passage. In this case the electrons amplify at the trailing half of the bunch, where the beam potential steadily decreases. Electrons can leave the beam potential, hit the wall, and create secondaries, which are accelerated by the present part of the beam, again acquire a net energy due to the decrease of the instantaneous beam current, and are lost to the wall as well. This process can repeat for about 20 times during one bunch passage. If the energy gain of the electrons is high enough, their number increases at each passage across the beam. This amplification process has been called 'trailing edge multipactoring' [41]. Extensive simulations of this process where performed for the Los Alamos PSR by M. Furman and M. Pivi, who, also for this case, obtained a good agreement of the simulated electron flux and electron energy spectrum with measurements. However, the trailing-edge multipactoring process is extremely sensitive to the detailed shape of the longitudinal bunch profile, which determines the energy gain and thus the amplification of electrons. This sensitivity was confirmed, for example, in a recent study for Los Alamos [42]. The trailing-edge multipactoring effect is also relevant for a possible future luminosity upgrade of the LHC, which could be based on long superbunches [43].

A novel approach for computing the electron-cloud formation was recently developed by A. Novokhatsky and J. Seeman [44] as an alternative to the multi-particle simulations. It is based on a numerical solution of the linearized Vlasov equation. So far this new scheme has only been implemented for a simplified geometry with a round chamber and no magnetic field. Comparisons with the more traditional simulations or with experiments have not yet been performed.

For positron beams and the LHC the distribution of the photoemission around the ring and azimuthally across the chamber are important, as is the energy spectrum of the photoelectrons. In particular, the reflectivity of the primary photons can have a dramatic effect on the simulation results. One distinguishes forward scattering, diffuse scattering, and backward scattering, all of which can be parametrized based on measurements, e.g., [45].

Modelling fine details of the vacuum chamber and the beam fields are necessary to make accurate quantitative predictions. An interesting work on this topic was performed this year by K. Harkay and her students at the ALS [46]. Other detailed

experimental studies and comparisons with simulations were conducted since many years at BEPC in Peking using a variety of programs, in preparation for the BEPC-II upgrade [47].

2.16.4 Instabilities

A blow up of the positron-beam vertical beam size was observed in the KEK B factory since 1999. It has been interpreted as a head-tail instability driven by an electron cloud [48,49]. In 2002, at KEKB the head-tail motion could directly be detected by a streak camera (J. Flanagan, H. Ikeda, et al.). Similar single-bunch instabilities induced by an electron cloud were also observed, e.g., using wideband pick ups, with the LHC proton beam in the CERN SPS since about 2000. The codes PEHTS by K. Ohmi and HEADTAIL by G. Rumolo and F. Zimmermann model the interaction of a single bunch on successive turns with an electron cloud that is supposed to be (re-)generated by preceding bunches. These codes also provide a simulated shape of the short-range wake field by displacing a bunch slice and computing the resulting force on the following parts of the bunch. Similarly, the long-range bunch-to-bunch wake can be obtained from the build-up simulations (e.g., in the codes PEI, POSINST or ECLOUD) by displacing one of the bunches. Recent studies by Daniel Schulte at CERN have revealed that the long-range wake varies greatly along the length of a bunch, indicating that these wakes may strongly drive higher-order coupled head-tail modes.

Several simple two or multi-particle models have been employed to estimate the threshold of the electron-cloud instability, which appears akin to a transverse mode coupling (TMCI) or strong head-tail instability. It is important to note, however, that the wake of the electron cloud differs from an ordinary wake in that it violates both linearity and time invariance. One of these factors, the time dependence, can be taken into account by extending the usual concept of wake and impedance to an additional dimension and employing two-dimensional Fourier transforms. This extension was worked out in full beauty by E. Perevedentsev, who also derived the transverse mode coupling threshold for such a generalized wake [50].

The interplay of the electron-cloud wake with a conventional impedance or with space charge forces has been studied by various authors, in particular by G. Rumolo [51]. These additional forces are easily implemented in simulation codes. G. Rumolo found a strong synergy using the HEADTAIL code. Describing the combined action of impedance and electron cloud by a two-particle model and a simplified matrix formalism, K. Cornelis has shown that the TMCI threshold in a flat chamber is (much) higher than that in a round chamber and that the main effect of the electron cloud is to make the flat chamber look like a round chamber [52].

Nonuniformity of the electron cloud, e.g., if it consists of 2 or 3 vertical strips, introduces additional nonlinearities, which can alter the beam dynamics. At locations with nonzero dispersion it could also be a source of synchro-betatron coupling.

For modelling the electron-dynamics and the beam instability correctly, both magnetic and electric boundary conditions and image currents are important. Recently, electric boundaries, in particular, the electron-image forces, were shown to make a large impact in simulations of a quasi-continuous beam-electron interaction [53].

In the case of a proton collider like the LHC, with little radiation damping, a potential long-term emittance growth below the TMCI threshold is a further concern. The usual instability simulations consider lumped interactions between a bunch and the electron cloud, which are located at a few discrete positions around the ring. These simulations always show a nonzero emittance growth [54,55], but the value of this emittance growth strongly depends on the choice and the number of the beam-electron interaction points [55]. Some simplistic plasma-type simulations have also revealed a similar emittance dilution [56]. Studies by E. Benedetto showed that systematic or random assignments of the intermediate betatron phases from turn to turn also give different results, indicating the possibility that the emittance growth is a purely numerical artifact [55]. This issue may soon be clarified by T. Katsouleas and A. Ghalam at the University of Southern California and their co-workers, who are performing detailed simulations of the continuous beam-plasma interaction using the 3-dimensional plasma code QUICKPIC [53].

Plasma treatments using a delta-f method for solving the Vlasov equation of a coasting beam interacting with an electron cloud were incorporated by the Princeton group, R. Davidsson and H. Qin, in the BEST code and applied to the Los Alamos PSR. Likewise T.-S. Wang (Los Alamos) and M. Blaskiewicz (BNL) have studied and simulated the instabilities in the Los Alamos PSR [57,58]; the latter also investigated the SNS, and the AGS booster [59.60]. A satisfactory level of understanding was achieved, though a few critical points (for example the near independence of the instability threshold on the bunch length in the PSR) still remain to be understood [58].

At both B factories the combined action of beam-beam interaction and electron cloud appears to be stronger than the sum of the two single effects. Several few-particle models were developed, both in weak-strong [50] and in strong-strong approximation [61], to illuminate this issue. Also multi-particle simulations were performed [61]. The results were not completely consistent with each other and neither with observations (e.g., concerning the effect of chromaticity). More studies of this interplay are needed.

An unsolved mystery also is why in almost all cases the single bunch instabilities driven by electrons are observed in the vertical plane (for example at KEKB or the CERN SPS), whereas the blow up at PEP-II predominantly happens in the horizontal plane.

2.16.5 Other Issues

In addition to coherent instabilities, a further possible source of emittance growth are incoherent effects, for example the incoherent tune shift and resonances driven by the highly nonlinear electron force, which emerges because the electrons are strongly

attracted by the nonlinear field of a bunch during its passage. The local density at the transverse beam center can increase by a factor of 20—50 along the length of a passing bunch [62]. This 'electron pinch' leads to a tune shift increase along the bunch, which may also excite synchro-betatron resonances [62]. Preliminary analytical estimates of the tune shift and synchro-betatron excitation were presented in [62,63]. Transverse nonlinear resonance excitation by the pinched electron cloud were recently unveiled [54] by a frequency-map analysis a la Laskar [64], using a frozen-field approximation.

A single high-energetic ion lost to the wall can liberate up to 10^7 electrons. This provides another rich source of electrons, which is of relevance for the heavy-ion beams in RHIC and in the LHC, as well as for proton collimators, e.g., at the LHC or the SNS. Studies of the possible existence of an electron cloud at the LHC proton collimators have been launched at CERN by A. Ferrari et al.[65], and first results of FLUKA simulations are available which can be used as input for other codes such as the KEK-EGS version and ECLOUD. The dependence of the electron multiplication on the collimator geometry and gap size is also under closer investigation. Electrons generated by beam loss from collimators have also been a study item for the SNS project [66].

The interaction of microwaves, e.g., injected either intentionally or in the form of wake fields created for example at the collimators, with the electron cloud is another open issue, which was put forward by F. Caspers, A. Chao, and S. Heifets. Preliminary evidence at PEP-II by F.-J. Decker [67] and at the CERN SPS by F. Caspers [68] suggests that there could be a large effect.

Finally, according to simulations an electron cloud can in principle also be formed in electron storage rings, and might lead to a multi-bunch wake field there as well [69]. This has not yet clearly been demonstrated in practice. Circumstantial evidence from the APS was reported by K. Harkay and co-workers [70].

2.16.6 Epilogue

There have been many other original studies of electron clouds and their effects, for example many beautiful experimental studies at the Los Alamos PSR by R. Macek and his colleagues [71] or at the APS by K. Harkay [72] and many further intriguing simulations, e.g., by K. Ohmi at KEK, G. Rumolo now at GSI, and S. Heifets at SLAC. The latter has, in particular, argued that for much higher bunch charges and short bunch spacings the number of electrons will be limited and that the electrons will be confined to the vicinity of the wall [73].

I apologize to those colleagues whose work I inadvertently omitted from this brief review. A comprehensive and rather complete overview of the present state of the art can be found in the proceedings of ECLOUD'02 [74]. A few more recent observations and some newer developments were presented at the PAC 2003 [75].

2.16.7 Outlook

In the near future two dedicated electron-cloud workshops are planned.

The first workshop, on 'Beam Induced Pressure Rise in Rings', (13th ICFA Beam Dynamics Mini-Workshop), will be held at BNL, December 9-12, 2003. It focuses on the mechanisms of beam-related pressure rise, in particular the pressure rise limiting the performance of RHIC, and it specifically addresses the electron cloud as one dominant mechanism. More informations can be found on the workshop web site *http://www.c-ad.bnl.gov/icfa*. The organizer and contact is S.Y. Zhang [76].

The second workshop, ECLOUD'04, will completely be devoted to electron-cloud simulations and analysis. It will be held as an ICFA workshop as well, and it is tentatively scheduled for April 2003 near Berkeley in California. The organizer and contact of ECLOUD'04 is Miguel Furman at LBNL [77].

References

[1] F.-J. Decker, Electron Cloud Effects at PEP-II, presented at ECLOUD'02, Geneva 15-18 April, 2002.
[2] H. Fukuma, Electron Cloud Effects at KEKB, Proceedings of ECLOUD'02, Geneva 15-18 April, 2002, CERN-2002-001 (2002).
[3] S.Y. Zhang, et al., RHIC Pressure Rise and Electron Cloud, Proceedings PAC 2003, Portland (2003).
[4] D. Neuffer et al., Observations of a Fast Transverse Instability in the PSR, NIM A 321, pp. 1—12 (1992).
[5] R. Macek, Studies of the Electron Cloud at the LANL PSR, presented at International Workshop on Two-Stream Instabilities, KEK, Tsukuba, 11-14 September (2001).
[6] F. Zimmermann, Electron Cloud in the LHC, Proceedings of ECLOUD'02, Geneva 15-18 April, 2002, CERN-2002-001 (2002).
[7] J. Wei and R. Macek, Electron-Cloud Effects in High-Inetsnity Proton Accelerators, Proceedings of ECLOUD'02, Geneva 15-18 April, 2002, CERN-2002-001 (2002).
[8] J. Jowett, et al., Damping Rings for CLIC, Proceedings PAC 2001, Chicago (2001).
[9] M. Pivi et al., Recent Electron Cloud Simulation Results for the Main Damping Rings of the NLC and the TESLA Linear Colliders.
[10] G. Budker, G. Dimov, V. Dudnikov, Experiments on Producing Intensive Proton Beams by Means of the Method of Charge-Exchange Injection, Soviet Atomic Energy 22, 5 (1967).
[11] V. Dudnikov, some Features of Transverse Instability of Partly Compensated Proton Beams, Proceedings PAC 2001, Chicago (2001).
[12] G.I. Budker, At. Energ. 1, 5 (1956).
[13] G.V. Chirikov, Stability of a Partially Compensated Electron Beam, Sov. Atomic Energy 19 (1965).
[14] H.G. Hereward, Coherent Instability Due to Electrons in a Coasting Proton Beam, CERN 71-15 ISR Division (1971).

[15] E. Keil and B. Zotter, Landau Damping of Coupled Electron-Proton Oscillations, CERN-ISR-TH/71-58 (1971).
[16] O. Grobner, Bunch Induced Multipacting, 10^{th} Int. Conference on High Energy Accelerators, Protvino, July (1977).
[17] F. Zimmermann, The Electron Cloud Instability – Summary of Measurement and Understanding, Proc. PAC 2001, Chicago (2001).
[18] M. Izawa et al., PRL 74, 5044 (1995).
[19] K. Ohmi, PRL 75, 1526 (1995).
[20] Z.Y. Guo et al., The Experimental Study on Beam-Photoelectron Instability in BEPC, Proc. PAC 97, Vancouver (1997).
[21] M. Furman and G. Lambertson, The Electron-Cloud Instability in the Arcs of the PEP-II Positron Ring, Proc. MBI97, KEK97-17, p.170 (1997).
[22] F. Zimmermann, LHC Project Report 95 (1997).
[23] O.S. Bruning, LHC Project Report 158 (1997).
[24] M. Furman, LHC Project Report 180 (1998).
[25] F. Zimmermann, Proc. Chamonix X & XI, CERN-SL-2000-001 DI (2000) and CERN-SL-2001-003 DI (2001).
[26] G. Arduini et al., Electron Cloud Effects in the CERN SPS and LHC, Proc. EPAC 2000, Vienna (2000).
[27] R. Cappi et al., PRST-AB 5, 094401 (2002).
[28] G. Arduini et al., Transverse Behaviour of the LHC Proton Beam in the SPS: An Update, Proc. PAC 2001, Chicago (2001).
[29] J.M. Jimenez et al., Electron Cloud with LHC-Type Beams in the SPS: A Review of Three Years of Measurements, LHC-Project-Report 632 (2003).
[30] I. Collins, private communication (1999).
[31] Presentations by the CERN AC Vacuum Group in the LHC Insertion Region Review, June 2003.
[32] C. Scheuerlein et al., The Secondary Emission Yield of TiZr and TiZrV Nonevaporable Getter Thin Film Coatings, CERN-EST-2000-007-SM (2000).
[33] F. Ruggiero, Parameters for First Physics and for 10^{33}, Proc. Chamonix XII, CERN-AB-2003-008 ADM (2003).
[34] V. Baglin et al., The Secondary Emission Yield of Technical Materials and Its Variation with Surface Treatments, Proc. EPAC 2000, Vienna (2000).
[35] L.F. Wang et al., Numerical Study of the Photoelectron Cloud in KEK Low Energy Ring with a Three-Dimensional Particle in Cell Method, PRST-AB, 5, 124402 (2002).
[36] J.M. Jimenez et al., Electron Cloud Studies and Analyses at SPS for LHC-Type Beams, Proc. PAC2003, Portland (2003).
[37] H. Fukuma, Electron Cloud Effects at KEKB, Proceedings of ECLOUD'02, Geneva 15-18 April, 2002, CERN-2002-001 (2002).
[38] F. Zimmermann, Electron Cloud – Operational Limitations and Simulations, Proceedings of Chamonix XII, CERN-AB-2003-008 ADM (2003).
[39] M. Pivi, M.A. Furman, Electron-Cloud Updated Simulation Results for the PSR, and Recent Results for the SNS, Proceedings of ECLOUD'02, Geneva 15-18 April, 2002, CERN-2002-001; see also PRST-AB 6, 034201 (2003).
[40] F. Zimmermann, Beam Sizes in Collision and Electgron-Cloud Suppression by Clearing Electrodes for KEKB, CERN-SL-Note-2001-022 (2001).
[41] V. Danilov et al., Proc. Workshop on Instabilities of High-Intensity Hadron Beams in Rings, Upton NY, June 1999, AIP Conf. Proc. 496, p. 315 (1999).

[42] M. Pivi, M. Furman, Mitigation of the Electron Cloud Effect in the PSR and SNS Proton Storage Rings by Tailoring the Bunch Profile, PAC 2003, Portland (2003).
[43] F. Ruggiero et al., Beam-Beam Interaction, Electron Cloud, and Intrabeam Scattering for Proton Super-Bunches, PAC 2003, Portland (2003).
[44] A. Novokhatsky, J. Seeman, Simulation Study of Electron Multipacting in Straight Sections of PEP-II, PAC2003, Portland (2003).
[45] V. Baglin et al., Photoelectron Yield and Photon Reflectivity from Candidate LHC Vacuum Chamber Materials with Implications to the Vacuum Chamber Design, EPAC'98, Stockholm (1998).
[46] K. Harkay, Studies of a Generalized Beam-Induced Multipacting Resonance Condition, PAC 2003, Portland (2003).
[47] J. Xing, The Simulation Study on ECI for BEPC and Its Upgrade BEPCII, Proceedings of ECLOUD'02, Geneva 15-18 April, 2002, CERN-2002-001 (2002).
[48] K. Ohmi, F. Zimmermann, Head-Tail Instability Caused by Electron Cloud in Positron Storage Rings, PRL 85, 3821-3824 (2000).
[49] K. Ohmi, F. Zimmermann, E. Perevedentsev, Wake-Field and Fast Head-Tail Instability Caused by an Electron Cloud, Phys. Rev. E65, 016502 (2002).
[50] E. Perevedentsev, Head-Tail Instability Caused by Electron Cloud, Proceedings of ECLOUD'02, Geneva 15-18 April, 2002, CERN-2002-001 (2002).
[51] G. Rumolo, F. Zimmermann, Electron Cloud Instability with Space Charge or Beam Beam, Contribution of the SL-AP Group to the Two-Stream Instability Workshop, KEK, Tsukuba, September 11-14, and CERN-SL-2001-067 AP (2001).
[52] K. Cornelis, The Interplay between the SPS Impedance and the Electron Cloud, CERN Mini-Workshop on SPS Scrubbing Run Results and Implications for the LHC, 28th June 2002 (web site: *http://sl.web.cern.ch/SL/sli/Scrubbing-2002/Workshop.htm*).
[53] A. Ghalam et al., Electron Cloud Effects on Beam Evolution in a Circular Accelerator, submitted to PRST-AB (2003).
[54] Y. Cai, Emittance Growth due to Electron Cloud in Positron Ring, Proceedings of ECLOUD'02, Geneva 15-18 April, 2002, CERN-2002-001 (2002).
[55] E. Benedetto et al., Transverse 'Monopole' Instability Driven by an Electron Cloud?, PAC 2003, Portland (2003).
[56] K.V. Lotov, G. Stupakov, Single Bunch Instability of Positron Beams in Electron Cloud, Proc. EPAC2002, Paris (2002).
[57] T.-S. Wang, A Theoretical Study of the Electron-Proton Instability in a Long Proton Pulse, Proc. PAC 95, Dallas, p. 3140 (1995).
[58] M. Blaskiewicz et al., Electron-Cloud Instabilities in the Proton Storage Ring and Spallation Neutron Sources, PRST-AB 6, 014203 (2003).
[59] M. Blaskiewicz, Implications of the PSR Instability for the SNS, Proc. EPAC 2002 Vienna (2000).
[60] M. Blaskiewicz, The Fast Loss Electron Proton Instability, Proc. Workshop on Instabilities of High-Intensity Hadron Beams in Rings, Upton NY, June 1999, AIP Conf. Proc. 496 (1999).
[61] K. Ohmi, A. Chao, Combined Phenomena of Beam-Beam and Beam-Electron Cloud Effects in Circular e+e- Colliders, Proceedings of ECLOUD'02, Geneva 15-18 April, 2002, CERN-2002-001 (2002).
[62] M. Furman, A. Zholents, Incoherent Effects Driven by the Electron Cloud, PAC99, New York (1999).

[63] F. Zimmermann, Electron Cloud Simulations: An Update, Proc. Chamonix XI, CERN-SL-2001-003 DI (2003).
[64] J. Laskar, Astron. Astrophys. 198, 341 (1988).
[65] A. Ferrari, private communication (2003).
[66] P. Thieberger et al., Secondary-Electron Yields and their Dependence on the Angle of Incidence on Stainless-Steel Surfaces for Three Energetic Ion Beams, Physical Review A, 042901 (2000).
[67] F.-J. Decker et al., Impact of Microwaves on the Electron Cloud and Incoherent Effects, Proceedings of ECLOUD'02, Geneva 15-18 April, 2002, CERN-2002-001 (2002).
[68] F. Caspers, private communication (2003).
[69] F. Zimmermann, Accelerator Physics Studies for KEKB: Electron Trapping, Electron Cloud in the HER, Closed-Orbit Drift, Horizontal Instability and Tune Shift, SL-Note-2001-043 MD (2001).
[70] K.C. Harkay and R.A. Rosenberg, Properties of the Electron Cloud in a High-Energy Positron and Electron Storage Ring, PRST-AB 6, 034402 (2003).
[71] R. Macek, Possible Cures for Electron Cloud Problems, Proceedings of ECLOUD'02, Geneva 15-18 April, 2002, CERN-2002-001 (2002).
[72] K.C. Harkay et al., Simulations of Electron-Cloud Build Up and Saturation in the APS, Proceedings of ECLOUD'02, Geneva 15-18 April, 2002, CERN-2002-001 (2002).
[73] S. Heifets, Electron Cloud at High Beam Currents, Proceedings of ECLOUD'02, Geneva 15-18 April, 2002, CERN-2002-001 (2002).
[74] ECLOUD'02, Mini-Workshop on Electron Cloud Simulations for Proton and Positron Beams, Geneva, 15-18 April, 2002, CERN Yellow Report CERN-2002-001, web site: *http://wwwslap.cern.ch/collective/ecloud02/index.html* (2002).
[75] PAC 2003, 2003 Particle Accelerator Conference, Portland, Oregon, May 12-16, web site: *http://www-conf.slac.stanford.edu/pac03/Default.htm*
[76] S.Y. Zhang, BNL workshop, private communication, email: syzhang@bnl.gov
[77] M. Furman, ECLOUD'04, private communication, email: mafurman@lbl.gov

2.17 Machine parameters of e^+e^- colliders in the world. The Lepton Colliders DataBase

M.E. Biagini
mail to: biagini@lnf.infn.it

Laboratori Nazionali di Frascati - Istituto Nazionale di Fisica Nucleare
C.P. 13, I-00044 Frascati, Italy

2.17.1 Introduction

Storage rings are a beautiful reality since 40 years, but the idea of a database collecting the design and operational parameters for lepton colliders was born only in 1997 at the 14th Advanced ICFA Workshop on Beam Dynamics Issues for e^+e^- Factories in Frascati [1]. At that time there were many e^+e^- colliders in operation, and e^+e^- factories were just starting construction (as the B-Factories PEP-II and KEK-B) or commissioning (as the Φ-Factory DAΦNE), providing plenty of data in the following 5 years. This year the ICFA Beam Dynamics Sub-Panel on High Luminosity e^+e^- Colliders endorsed the idea to build the database and publish it on the ICFA website.

Planning the construction of a collider means first of all, once the energy range is chosen, to fix a goal value for the peak luminosity, and consequently choose a design strategy to reach that goal. In designing a storage ring the operational experience of similar, existent machines is a valuable hint for what nature has allowed in that field. In this respect, a catalogue of characteristics and performances can be a very useful tool when designing new colliders or comparing operating machines.

2.17.2 Machine parameters evolution

In the past 30 years the comprehension of the fundamental beam behavior in storage rings, together with the improved accelerator technology, allowed a big step forward in the design and operation of lepton colliders. While for the first generation of storage rings the goal was to study a specific energy region to discover new structures and improve the knowledge of the fundamental particle physics, in the second generation, the "Factory era", accelerators aimed to increase the number of collected events at a fixed energy, to perform precision measurements of very small physical quantities, quite difficult to extract from the events. To explore with high precision the physics of the decays of narrow vector mesons available in e^+e^- annihilation, a huge amount of events is necessary, which in turn demands for high average luminosity and reliable operation. The peak luminosity needs to be orders of magnitude larger than that achieved in the past. All the Factory projects have in common the request of a very large number of closely spaced bunches, with design total currents and beam-beam parameters often beyond the limits reached by previous colliders. For the asymmetric B-factories, with beams very different in energy, a further difficulty was the difference in lattice design and beam dynamics in the two rings. The technology had to improve at

the same time, providing vacuum systems, RF cavities, feedbacks, temperature controls, adequate to the number of bunches and stored currents.

A pictorial example of this progress [2] is shown in Fig. 1, where the peak luminosity versus energy is plotted. In the lower ellipse are the first generation storage rings, with LEP as a frontier of what technology can provide to increase the energy in a circular collider. The middle ellipse contains both present and in construction Factories. Their luminosities are an order of magnitude larger than the previous ones, at the same energies. The top ellipse contains the future: two orders of magnitude in luminosity will require new ideas and new technologies, rather than brute force.

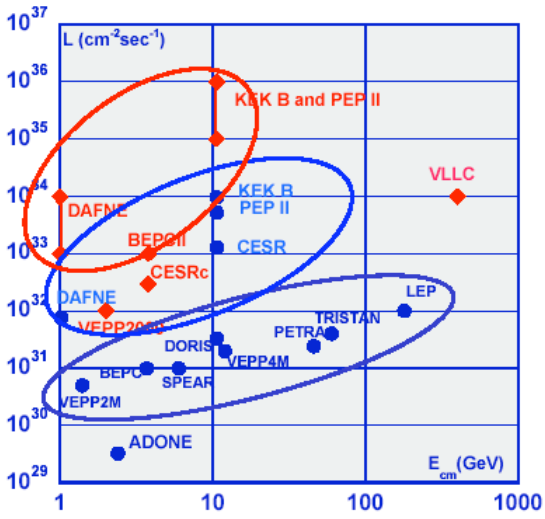

Fig. 1 – Luminosity vs. energy in lepton circular colliders. Past and present results (blue dots), future projects (red diamonds).

How do we increase the peak luminosity? Looking at the classical luminosity formula:

$$L = \frac{f N^2}{4\pi\sigma_x\sigma_y}$$

we could think that by squeezing the beams and increasing the beam current we can theoretically get an infinite luminosity, but this actually is impossible, since a limit is instead found. Let's look at the more complete formulation for flat beams, as those in all the operating storage rings:

$$L = \pi\left(\frac{\gamma}{r_e}\right)^2 f \frac{\xi^2 \varepsilon(1+\kappa)}{\beta_y}\sqrt{\frac{\kappa_\beta}{\kappa}}$$

Here: f is the collision frequency, r_e is the classical electron radius, γ is the beam energy in units of electron mass, ε is the beam emittance, β_y is the vertical betatron function at the Interaction Point (IP), k is the coupling parameter ($\varepsilon_y/\varepsilon_x$), κ_β is the ratio β_y/β_x and ξ is the beam-beam tune shift.

A limit to the maximum density achievable in single bunch comes straight from the beam-beam interaction, and it is expressed by the beam-beam tune shift:

$$\xi_{x,y} = \frac{r_e N \beta_{x,y}}{2\pi\gamma\sigma_{x,y}(\sigma_x + \sigma_y)}$$

For $\kappa = \kappa_\beta$, it is clearly:

$$\xi_{x,y} = \frac{r_e N}{2\pi\gamma\varepsilon}$$

Since the beam-beam interaction is highly nonlinear, a prediction of the maximum reachable tune shift can come from the simulation tools, and mostly by the study of the performances of similar machines. Indeed, the comprehension of the beam-beam limit is one of the major issues in the theory of e^+e^- storage rings. Many attempts to study the beam-beam limit have been done, among the others see Refs. [3], [4], [5], and [6]. This is why we think that DataBase will be very useful.

As an example, a parameter found to affect the tune shift limit is the damping time τ. From the LEP experience we can see that strong radiation by damping and quantum excitation, obtainable for example with wiggler magnets, can give an increase in ξ. In fact when the damping time, expressed in number of turns, decreases, the limit on ξ increases: LEP-1 at 100 GeV and LEP-2 at 200 GeV had a maximum vertical ξ value more than a factor of two different.

Looking again to the luminosity formula we can identify all the other parameters we can actually play with. The collision frequency plays a major role, in fact all the Factories have chosen to increase the number of bunches, that in most of the cases implied to introduce a crossing angle at the IP. How this configuration, which introduces coupling between transverse and longitudinal motion, limits the luminosity is not yet fully understood. Some machines, like the pioneer DORIS, observed a low limit, represented by the Piwinski angle. Others, like KEK-B, show a small or no effect on luminosity, for ξ values below 0.05.

With a large number of bunches, large currents have been stored, while keeping small the single bunch current. This solution, common to synchrotron light sources, has several drawbacks. Beam dynamics has become more and more complicated: any sort of instability has arisen, including the new electron-cloud affecting mostly the high energy B-Factories (the low energy Φ-Factory DAΦNE has not yet shown any threshold, in spite of almost 2 A of stored positrons in a single positron beam). To control instabilities a very careful impedance budget, including new designs of bellows and synchrotron radiation masks and RF with High Order Modes dampers, have been studied. Sophisticated multibunch feedbacks have been developed, ultra-vacuum has to be reached, and temperature control has become an issue that future high current colliders will have to solve with dedicated R&D programs.

When a collider is working close to the ξ limit, the luminosity is inversely proportional to the value of β_y at the IP. In fact, looking at the data we can see how this value decreased, from the first colliders to the new era Factories, to values close to millimeters. This change has also meant that the Interaction Region design has become more critical, focusing quadrupoles have to be installed closer to the IP to control the

chromaticity, with limitations for the detector solid angle and the need to study very compact, and powerful, elements as the permanent magnets or the superconducting quadrupoles.

However nature is not always a good mother: also in this case the smallest value of the IP β_y is limited by the hourglass effect, in fact for β_y values smaller than the bunch length there is actually a reduction of the luminosity. The limit, operationally found, is that the minimum β_y must be of the same order of magnitude of σ_l. In turn, to decrease the bunch length new RF technology has to be developed. New ideas under study [7], for example a bunch length modulation around the ring, a new regime where σ_l is maximum in the RF cavity and minimum at the IP, obtained with huge values of the RF cavity voltage and by working close to the half-integer synchrotron tune, could also represent a solution.

Very low coupling is up to now the solution chosen to decrease the beam area at the IP and maximize luminosity. Round beams operation, though theoretically capable to double the luminosity, has not been implemented yet. However, for low or intermediate energy colliders high beam density and small beam volume can represent a problem for the Touschek scattering in the bunch, a process limiting the beam lifetime and consequently the average luminosity.

Nonlinearities are also a source of problems, since the consequent dynamic aperture limitation brings to low beam lifetime. This is a problematic common to synchrotron light sources. Extreme care has to be taken in designing magnets, in particular the wigglers, with a low content of high harmonics in the magnetic field.

The receipt to increase the average luminosity, thus increasing the integrated luminosity, is hardware reliability, short injection times, long beam lifetimes. A possible solution seems the continuous or “trickle charge” injection, and of course the possibility to keep the detector data acquisition on during injection. The last item implies that the background rate is kept to a reasonable value, compatible with the detector’s components lifetime.

2.17.3 The Lepton Colliders DataBase: Past, Present and Future Colliders

The Lepton Colliders DataBase (LCDB) aims to collect information on the world e^+e^- storage rings, but it is especially intended to provide data for fits and parametric studies to compare performances and predict behaviours.

Many of the collider’s data are available in conference papers; but often the published data are not enough complete. Moreover, while data on the present and future projects are easy to obtain, it is difficult to gather information on the past accelerators. Unfortunately in the past years, let’s say before the ’90, complete and systematic data on performances and measurements where not always available. Conferences were not, as at present, scheduled every year, and performances were sometimes just summarized in internal reports or resting forever in Logbooks. This makes particularly hard to collect data for machine now dismantled or no more in operation as colliders, like Spear, DCI, PEP, Doris, Petra, Tristan, Vepp-2M. We hope anyway, with the help of accelerator physicists who worked for these storage rings, to be able to fill the gap soon. Some of the data are of course subject to change very fast, as the B-Factories luminosity vertiginous increase has proven. The more efficient way to proceed is probably that for each collider, or each Laboratory, there is a person in charge of keeping the “dynamical” data updated.

We also would like to encourage those designing new accelerators, or upgrading existing ones, to communicate the new data so that they can be included.

2.17.4 DataBase Structure

In this section we mention briefly the structure of the LCDB. In the following is a list of the accelerators whose data, even though not always complete, were available up to now. In parenthesis is their centre of mass energy in GeV:

- DAΦNE (1.02), ADONE (0.6 to 3.1), Frascati National Laboratories, Italy
- VEPP-2000 (2.), Budker Institute, Novosibirsk, Russia
- BEPC (2. to 5.), BEPC-II (2. to 4.2), Institute of High Energy Physics, Beijing, China
- CESR (10.6), CESR-c (3. to 11.), Cornell University, Ithaca, US
- PEP-II (10.58), Stanford Linear Accelerator Centre, Menlo Park, US
- KEK-B (10.58), KEK, Tsukuba, Japan
- LEP-I (88. to 95.), LEP-II (161. to 209.), CERN, Geneva, Switzerland.

An Excel worksheet, with four sheets, contains information on the different aspects. The colliders are arranged in order of increasing beam energy.

- **Sheet 1: General and luminosity parameters**. Here geometric and dynamical parameters are collected. The luminosity data are the most important but also the most critical. A key point is that there should be consistency between peak luminosity, currents and tune shifts. This means that sometimes is not the maximum ever reached tune shift that has to be listed, but the one relative to the peak luminosity quoted. The same for the currents, since the maximum luminosity is often reached at currents lower than the maximum storable. In this section also crossing angle, beam sizes in collisions (so called Σ) and injection parameters are recorded.

- **Sheet 2: Lattice parameters**. The magnetic layout, including fields and gradients, vacuum parameters, impedance and e-cloud instability observation are reported here.

- **Sheet 3: Optics parameters**. Here β, η, beam sizes, tunes, and the most important parameters, including bunch length, lifetimes and damping times, are listed.

- **Sheet 4: RF related parameters**, both RF hardware and dynamics, as the synchrotron frequency and tune, are in this section.

Each accelerator has two or more columns dedicated: the first is where "design" values are listed, the others are relative to the "operational" parameters, more than one column if the collider works in different modes of operation, as in DAΦNE for example, where 2 detectors share operation.

In Appendix B, a preliminary version of the LCDB is reported. For sake of simplicity every sheet has been cut in two parts. The complete LCDB will soon be available on the ICFA Working Group on High Luminosity e^+e^- Colliders web page [8]. Suggestions, comments and remarks are very welcome.

2.17.5 Acknowledgements

The first idea of the LCDB was conceived with H. Burkhardt from CERN. I wish to thank him for his encouragement and for collecting the LEP data for several years, until the DB became a reality.

Many scientists from many Laboratories around the world have contributed up to now to the LCDB. It is due to their good will if the LCDB exited from the Limbo it was confined for 5 years. They are:

- D. Rice (Cornell) for CESR and CERC-c;
- Huang Nan, Jiuqing Wang (IHEP) for BEPC and BEPC-II;
- Y. Cai, M.H. Donald, M. Placidi, J.T. Seeman, M.K. Sullivan (SLAC) for PEP-II;
- Y. Funakoshi, Y. Ohnishi (KEK) for KEK-B;
- A.A. Valishev (BINP) for VEPP-2000;
- E. Levishev (BINP) for VEPP-4, to be included soon;
- H. Burkhardt (CERN) for LEP-1 and LEP-2;
- M.A. Preger (INFN) for Adone, to be completed;
- C. Biscari, S. Guiducci, M. Zobov (INFN) for DAΦNE.

I'm also indebted with all the colleagues who will help in the future to complete the LCDB with data from past colliders and updates of the present or future.

Finally, I would like to thank C. Biscari, Chairman of the ICFA BD Panel Working Group on High Luminosity e^+e^- Colliders, for proposing me to actually build the LCDB for the ICFA sub-panel.

References

1. First idea from H. Burkhardt (CERN) and M.E. Biagini (LNF), see for example the "Letter to the Editor", ICFA Beam Dynamics Newsletter, No. 15, Dec. 1997, p. 5, http://icfa-usa.jlab.org/archive/newsletter/icfa_bd_nl_15.pdf
2. C. Biscari, "Future plans for e^+e^- factories", Proc. of PAC 2003, Portland,US, May 2003.
3. F. Amman, D. Ritson, "Space charge effects in e^-e^- and e^+e^+ colliding or crossing beam rings", Frascati Internal Report LNF 61/038 (1961).
4. A. Chao, "A summary of some beam-beam models", in "A review of beam-beam phenomena for the symposium on nonlinear dynamics and the beam-beam interaction", BNL 25703, Brookhaven, March 1979.
5. J.T. Seeman, "Observation of the beam-beam interaction", SLAC-PUB-3825, presented at the Joint US/CERN School on Particles Accelerators, Sardinia, Italy, Feb. 1985.
6. M. Bassetti, M.E. Biagini, "A beam-beam tune shift semi-empirical fit", Frascati Physics Series Vol. X (1998), pp. 289, presented at the 14th Advanced ICFA Workshop on Beam Dynamics Issues for e^+e^- Factories, Frascati, Italy, Oct. 1997.

7. A. Gallo, P. Raimondi, M. Zobov, "Strong RF Focusing for Luminosity Increase", DAFNE Technical Note G60, August 2003.
8. http://www.lnf.infn.it/icfa/

3 Recent Doctoral Theses

3.1 Direct Measurement of Resonance Driving Terms in the Super Proton Synchrotron (SPS) of CERN using Beam Position Monitors

Rogelio Tomas Garcia

mail to: rogelio.tomas@cern.ch

Affiliation: CERN (present affiliation: BNL (NY))
Title: Direct Measurement of Resonance Driving Terms in the Super Proton Synchrotron (SPS) of CERN using Beam Position Monitors
Name: Rogelio Tomas Garcia
Graduation date: Thesis successfully defended at the University of Valencia on 30th of May of 2003.
Supervisor1: Angeles Faus-Golfe, angeles.faus.golfe@cern.ch, IFIC (Spain)
Supervisor2: Frank Schmidt, frank.schmidt@cern.ch, CERN

Abstract:
In this thesis a beam based method is developed to measure the Hamiltonian terms of an accelerator by precise Fast Fourier Transform of turn-by-turn beam position data. The effect of beam decoherence on the turn-by-turn Fourier spectrum and the longitudinal variation of the resonance terms are studied analytically and via computer simulations. Experiments to validate the proposed technique are performed at the CERN SPS and at the BNL RHIC. The improvement of using an AC dipole instead of applying a single kick is also studied.

4 Workshop and Conference Reports

4.1 The XIIth ICFA Beam Dynamics Mini-Workshop on High Intensity and High Brightness Beams - Space Charge Simulation

Chris Prior, Frank Gerigk and Giulia Bellodi, CCLRC Rutherford Appleton Laboratory

c.prior@rl.ac.uk, f.gerigk@rl.ac.uk, g.bellodi@rl.ac.uk

The XIIth in the series of ICFA mini-workshops, devoted to Space Charge Simulation, was held at Trinity College, Oxford, England, from April 2nd-4th 2003. Around 40 people attended and faces both familiar and relatively new to the community were welcomed into the university setting. Either for political or financial reasons, no one was able to come from Japan or LANL, but there was otherwise a good representation from TRIUMF and most US and European laboratories.

The final day of the workshop marked the 80th birthday of Dr. John Lawson, FRS, whose health was toasted at the workshop banquet the evening before. Until his retirement from the Rutherford Appleton Laboratory about 15 years ago, John's career had spanned more than 40 years, and he is well known worldwide for his many important contributions in the fields of radar technology, accelerators and magnetic/inertial confinement fusion. Participants, to many of whom "John Lawson" was only a name from the list of accelerator greats, were delighted that he was able to lighten one of the workshop sessions by spending an hour reminiscing over his early life in science.

As with all small workshops of this kind, the programme was dictated by the attendees. Thus plans for a balanced agenda covering space charge effects in linacs and rings, experiments and comparison with theory, and recent developments in advanced computational techniques had to be revised in the run up to the meeting. However, we did achieve a fairly comprehensive picture of the simulation codes available, their current status, capabilities and plans for future development. Some experiments using the CERN PS were identified and a formal benchmarking programme was agreed.

The talks (pdf), list of participants, details of the benchmarking tests and a full spreadsheet of space charge simulation codes are available on http://www.isis.rl.ac.uk/acceleratortheory/workshop/workshop.htm.

Session I: Space Charge in Linacs (Chairman: R.D. Ryne)

Rob Ryne opened the first session by describing the philosophy behind IMPACT, which is emerging as the main code for modelling the latest generation of high intensity linacs. Run on banks of parallel processors, it benefits fully from recent advances in computational techniques and uses typically ~10^6 particles in its modelling. Frank

Gerigk went on to describe the use of IMPACT to try to understand halo formation in low and intermediate energy linear accelerating structures. He had carried out over 300 runs in a relatively short space of time to look at errors and their possible effects on halo generation (later reported at the ICFA HALO'03 meeting). Single-pass machines of a few hundred metres in length lend themselves to modelling such large numbers of simulation particles on many parallel processors. Extension to rings, where multiple passes mean that several hundred kilometres have effectively to be tracked, is a far more daunting task. Nevertheless, Rob Ryne gave a further talk explaining his group's plans to integrate some of the rings features of MaryLie into IMPACT. MaryLie is a Lie algebraic code using transfer maps and covers both linear beam transport systems and circular storage rings. In the same session, Ji Qiang, who has played a major role in the development of IMPACT and its MaryLie hybrid, gave an interesting theoretical talk on the calculation of space charge for a long bunch in a curved beam pipe.

Session II: Space Charge in Rings (Chairman: J. Holmes)

While there are many tools for modelling high intensity rings, the code that appears to be the most versatile is ORBIT, developed by Jeff Holmes and co-workers at Oak Ridge, initially for theoretical studies of the SNS. This can now tackle a wide range of tasks including H^- injection, foil heating, phase space painting, single particle transport through various types of magnets, effects of errors, closed orbit calculations and corrections, longitudinal and transverse impedances, collimation and feedback. There are plans to incorporate an electron cloud model to handle the possible e-p instability predicted for many high intensity proton machines under either construction or study. Since existing electron cloud codes tend not to use full lattices in their modelling, it would be an important development if predictions from a full particle tracking code could be achieved.

ORBIT appears to have spawned various offspring. The code has been adopted by Fermilab, where it is being used for Booster studies. Resources have been allocated for in-house development, resulting in incorporation of a Python shell along with other improvements for maintainability and usability. Similarly at Brookhaven, Alfredo Luccio has formulated a parallelised 3D version using various economies (for example, using longitudinal bunch slicing, 2D space charge solving and re-combination, and optical functions rather than transfer matrices) to run on a small local computing cluster. A talk by Weiren Chou described the use of FNAL-Orbit in an attempt to improve Booster performance by comparing simulation with experiment, though the results were inconclusive. Similarly comparison of FNAL-Orbit with a locally-written code, Synergia, shows a need for reconciliation, the codes predicting different patterns of emittance growth though the end results are the same. Sarah Cousineau also described work she had carried out on the PSR at Los Alamos in which ORBIT had been used in conjunction with experiments on the ring. Here there is quite good agreement between predictions and beam profile measurements. In particular, the observation that the beam profile does not depend on the specific painting technique above $3\ 10^{13}$ protons is understood, and modelling results, showing intensity limitation as the tune is depressed by space charge and the vertical envelope tune approaches the integer 4, have led to a study to produce a compensation scheme.

In this session, we also heard talks by Peter Lucas on ESME, a code of long-standing developed by Jim Maclachlan at Fermilab for 1D (longitudinal) studies, and by Jingyu Tang (FZJ), who has been using various codes to design a beam transfer system for the European Spallation Source (ESS) including non-linear elements to tailor the transverse beam distribution under space charge to the required profile at the target.

Session III: From Codes to Experiment (Chairman: I. Hofmann)

Session III was intended to move through the remaining talks that were basically describing codes and modelling techniques into the domain of experiments that could be performed on real machines.

In the former category was a presentation by Armando Bazzani (Univ. Bologna) on Particle in Core models in which Coulomb collisions are taken into account. He was particularly interested in halo formation and described a self-consistent set of equations from which he was able to show the different effects from matched and mismatched KV beams in a periodic FODO cell. Elias Metral (CERN) (who, indefatigably, gave three talks on this day of the workshop) described a simple theory of the longitudinal microwave instability in bunched beams including the effects of space charge. He suggested that in a high space-charge regime some kind of self-stabilization through the formation of a low-momentum tail might lead to beam halo, and tantalisingly left us with hints at possible experiments for discussion later in the day (Session IV).

An interesting feature of the morning's talks was a description of the code GPT developed by a group called Pulsar Physics mostly under contract from TESLA. Working in the time domain, this package is very efficient, with cpu time scaling as $N^{1.1}$ (N = number of macro-particles), and is able to handle the difficult problem of space charge calculations for bunch aspect ratios from 0.01 to 100. A large effort, mainly by Gisela Pöplau, has been put into developing a suitable methodology for the space charge routines, based on multigrid and preconditioned conjugate gradient techniques. In the workshop, we were treated to only a limited range of the code's capabilities, but full details of its versatility (for example, its use in designing collimation systems) are available on http://www.pulsar.nl.

A further code, GenTrackE, developed by Andreas Adelmann (LBL), whose PhD thesis was highlighted in ICFA Beam Dynamics Newsletter 29, was also presented. Aiming to model large scale machines with complicated 3D geometries, this code has been running on the US NERSC Seaborg parallel system with good performance and results. There are now plans to incorporate a full model for electron cloud studies.

A special feature of this session was the talk by Agust Valfells of the small (3.7m diameter) electron ring UMER being constructed at the University of Maryland. Being dedicated entirely to beam physics, this machine has a source with enough brightness to depress the tune over a wide range, making it possible, for example, to study the regime where most proton synchrotrons operate. It was appropriate that in the audience for this

talk was John Lawson, whose earlier pioneering work with Martin Reiser had been instrumental in the birth of the UMER project.

Session IV: Experiments and Simulation (Chairman R. Cappi)

In a series of talks, Elias Metral (CERN) and Ingo Hofmann (GSI) described experiments carried out at CERN with the aim of comparing theory, simulation and measurements.

The CERN group's aim was to measure transverse emittance increase due to space charge as a function of such parameters as tune, bunching factor and bunch intensity. The variations considered were sufficient to cause the beam to cross integer and half-integer resonances under space charge tune depression. Emittance increases up to a factor 3 on a time scale of 10-100 ms were recorded. The results, including all the necessary machine parameters, are to be published on a web page to provide data for code benchmarking tests (see below).

Ingo Hofmann, similarly, reported on a study comparing simulations and measurements on the CERN PS of emittance exchange in crossing the Montague resonance $2Q_h$-$2Q_v$=0. There is agreement on the level of emittance exchange but not on the width of the stop-band, which experimentally is much wider that predicted. Though study is needed to resolve the discrepancy – and help may be at hand with some simple emittance exchange formulae derived by Elias Metral - this work also provides scope for future benchmarking tests.

Other experimentally-related work included a talk by Marcus Kirk (GSI) on the advantages of phase space tomography against traditional longitudinal tracking codes such as ESME. His studies were instigated by plans for upgrading the GSI synchrotron to higher intensities and energies.

Finally in this session, Fred Jones (TRIUMF) presented a status report of the code ACCSIM. His opening suggestion, likening the code to a Swiss army penknife with a host of gadgets, seemed very apt since it now seems suitable for a wide range of applications. ACCSIM is used at many laboratories for modelling rings such as CERN's PS Booster, the Hitachi medical synchrotron, KEK-PS and the J-PARC 3GeV ring, generally providing good results (in terms of predictions v. measurements) for RMS matching, beam profiles, injection losses, coherent resonance losses etc.

Session V: Alternative Codes and Benchmarking (Chairman W. Chou)

The scope of the final session was planned to be Vlasov solvers and their use as an alternative to traditional PIC tracking codes. However, because of illness, the direct Vlasov presentations were reduced to a single talk in which Eric Sonnendrucker (Univ. Strasbourg) explained the principles behind such an approach, the advantages (such as effective use in regions of low phase space density) and the difficulties (extensions to other dimensions). While the provision as a tool for cross-checking PIC codes is

important, it is clear that extension to cover even 2D (transverse) space with reasonable cpu times remains a development for the future

Hong Qin (PPPL), also covering nonlinear Vlasov-Maxwell systems, described development of a code called BEST (Beam Equilibrium Stability and Transport) based on the δf method. As a consequence of this work, he suggested a number of theoretical predictions for benchmarking tests: 1D thermal equilibrium beam profiles, stable beam propagation, and eigenmodes in a space charge dominated beam. He proposed modelling of the two-stream instability and beam echo as additional tests.

As an introduction to the final discussion setting up a formal benchmarking programme, Chris Warsop (RAL) described his plans for an experimental study of space charge using the ISIS synchrotron. With a tune shift of about −0.4, several resonant lines are crossed during injection, including the half-integer line (3.5) in the vertical plane and the integer line (4.0) in the horizontal plane, and space charge plays a significant role in the total beam loss. Measurements have been made using a residual gas beam profile monitor and it is expected that parallel simulations will start soon.

Outcome of the Workshop

The workshop ended with the three main conclusions:

1. Tables were drawn up containing comparisons of code v. code (Table 1) and code v. experiment (Table 2) to date.

Codes	**Test**	**Result**
Accsim, Orbit, Simpsons	PSR, KV rms emittance	Good
Orbit, ESME	1D longitudinal	Good
Orbit, Synergia	FNAL booster, multiturn injection, emittance blow up	Discrepancy
Track1D, Long1D, Accsim	1D longitudinal, ISIS, SNS, ESS	Good
Track2D, Simpsons, Orbit	SNS ring modelling Fermilab PD injection	Good
Micromap, Impact	Octupole resonance with space charge	Good

Table 2: Code v. Code Comparison

2. The two experiments identified in Session IV (emittance growth v. various machine parameters and emittance exchange in crossing the Montague resonance) were chosen for benchmarking tests. All the relevant parameters are to be set up on a website

http://www-wnt.gsi.de/ihofmann/Benchmarking/Benchmarking.htm
and participation from all those interested is invited. Those agreeing to take part to date are: I. Hofmann and G. Franchetti (Micromap), W. Chou, J-F. Ostiguy and P. Lucas (FNAL-Orbit), H. Qin (BEST), F. Jones (ACCSIM), A. Luccio (BNL-Orbit), J. Holmes and S. Cousineau (ORBIT), A. Adelmann (GenTrackE), R. Ryne and J. Qiang (IMPACT, MaryLie-IMPACT), D. Johnson and F. Neri (SIMPSONS).

Code/Machine	**Measurement**	**Result**
Orbit, PSR	Profile	Good agreement
ESME/ Fermilab ESME/CERN PS	1D (long)	Good/fair Good/fair
Micromap/CERN PS	Montague resonance	Comparison in progress
Accsim/CERN PSB	1D profile	Fair
Accsim/KEK PS	1D profile	Good
Impact/LANL LEDA	Halo	Discrepancy when mismatched, good agreement when matched
Orbit/FNAL booster	Emittance blow up	Inconclusive
GPT/Felix	Emittance, radiation, profile	Good
BEST/PSR	Electron cloud effect	Fair
Track1D/ISIS	1D (long) profiles and loss	Good
Track2D/CERN PSB	Instability/emittance effect (Ph.D. Thesis)	Good

Table 3: Code v. Experiment Comparison

3. As is a tradition of ICFA Beam Dynamics mini-workshops, a spreadsheet was devised containing full details of all the space charge simulation codes and their general availability. For completeness this covers some codes that were not actually represented or discussed at the workshop. The spreadsheet (Appendix A) is published in the workshop proceedings and will also be posted on the ICFA working group web site http://www-bd.fnal.gov/icfa.

5 Forthcoming Beam Dynamics Events

5.1 ICFA Advanced Beam Dynamics Workshops

5.1.1 30th: e^+e^- Factories 2003

The 30th ICFA Advanced Beam Dynamics Workshop on Beam Dynamics Issues for e^+e^- High Luminosity Factories will be held October 13-16, 2003, at the Stanford Linear Accelerator Center, Menlo Park, California 94025, USA

This workshop will cover topics of e^+e^- colliders including electron-cloud effects, beam-beam interaction, high beam-loading RF systems, bunch-by-bunch feedbacks, interaction regions, impedances, instabilities, operation and status of present colliders, and potential future accelerators and upgrades.

e^+e^- Factories 2003 is the fourth workshop to advance the operation and luminosity of present colliders and discuss options for future higher luminosity accelerators, following Ithaca (2001), Tsukuba (1999), and Frascati (1997).

Time at the workshop will be divided equally between plenary sessions and working groups.

Working groups:
Beam-Beam Interaction
Interaction Region, Optics, and Magnets
RF, Feedbacks, and Collective Effects
Operations, Reliability, Instrumentation, and Injection

Registration and abstract deadline: September 1, 2003.

Housing reservation deadline: September 1, 2003.

Contact information:

The conference web site with registration is: www-conf.slac.stanford.edu/icfa03

Workshop: John Seeman (Chair) 1-650-926-3566, MS17, SLAC, 2575 Sand Hill Road, Menlo Park, CA 94025, USA and Seeman@slac.stanford.edu

Logistics: Regina Matter 1-650-926-3783, MS 17, SLAC, 2575 Sand Hill Road, Menlo Park, CA 94025, USA and Regina@slac.stanford.edu

5.1.2 31st: Electron-Cloud Effects "ECLOUD04"

Berkeley, April 19-22, 2004

The existence of electron cloud effects (ECEs), which include vacuum pressure rise, emittance growth, instabilities, heat load on cryogenic walls and interference with certain beam diagnostics, have been firmly established at several storage rings, including the PF, BEPC, KEK-B, PEP-II, SPS, PSR, APS and possibly RHIC, and is a primary concern for future machines that use intense beams such as linear collider damping rings, B factory upgrades, heavy-ion fusion drivers, spallation neutron sources and the LHC.

This ICFA workshop will review experimental methods and results obtained within the past few years on the ECE, along with progress on its understanding obtained from simulations and analytic theory, and the effectiveness of mitigation mechanisms, including active damping.

Proceedings will be published, and authors will be encouraged to submit their contributions to a special edition of PRST-AB.

As in previous workshops dealing with the ECE (KEK, July 1997; Santa Fe, February 2000; KEK, September 2001; CERN, April 2002), the focus of ECLOUD04 will be broad, covering all aspects of the phenomenon. Some of the topics to be covered are:

- Review of observations at the SPS, PSR, and the B factories.
- Experimental methods and e-cloud diagnostics.
- Lessons learned from simulation comparisons with experiments (effect of secondary emission yield, understanding of single-bunch instabilities, etc)
- Predictions for intense proton and heavy-ion machines.
- Progress in simulation codes and the physical model involved.
- Progress in analytical models.
- Various methods of mitigating ECE (e.g. Landau damping, e-suppression coatings, beam scrubbing, clearing fields, beam manipulation, and active damping)

Some of the goals that will guide the workshop are:

- Summarize our understanding, identify essential issues, and scope out future research avenues.
- Assess state of theory and simulations.
- Identify and assess mitigation mechanisms.
- Compile list of simulation codes and their features.
- Assess experimental methods and diagnostics.
- Strengthen and expand international collaborations.

ECLOUD04 preliminary committee membership

International Advisory Committee	Program Committee
S. Chattophadyay (JLAB)	R. Macek (LANL) (chairman) (*)
W. Chou (FNAL) (*)	A. Adelmann (PSI) (*)
R. Davidson (PPPL) (*)	M. Blaskiewicz (BNL) (*)
O. Gröbner (CERN) (*)	J. Byrd (LBNL) (*)
Z. Guo (IHEP) (*)	Y. Cai (SLAC) (*)
K. Harkay (ANL) (*)	W. Decking (DESY)
I. Hoffmann (GSI)	A. Friedman (VNL/LLNL) (*)
N. Holtkamp (SNS)	M. Furman (LBNL) (*)
S. Kurokawa (KEK)	T. Katsouleas (USC) (*)
S. Y. Lee (IUCF)	K. Ohmi (KEK) (*)
A. Molvik (LLNL) (*)	M. Pivi (SLAC)
C. Prior (RAL) (*)	H. Qin (PPPL) (*)
T. Raubenheimer (SLAC) (*)	J. Rogers (Cornell)
T. Roser (BNL) (*)	G. Rumolo (GSI) (*)
F. Ruggiero (CERN)	J. Q. Wang (IHEP) (*)
W. Turner (LBNL) (*)	A. Wolski (LBNL) (*)
J. Wei (BNL) (*)	S. Y. Zhang (BNL)
F. Willeke (DESY) (*)	F. Zimmermann (CERN) (*)

(*) confirmed

Local Organizing Committee
M. Furman
J. Byrd
T. Gallant (admin)

Miguel Furman, LBNL
John Byrd, LBNL
Robert Macek, LANL

Berkeley, California, August 18, 2003.

5.1.3 32nd: High Current, High Brightness Electron Injectors and Energy Recovering Linacs for Future Light Sources and Colliders

Topics will include: High average current electron sources and injectors, high average current polarized electron sources, high brightness photoinjectors, physics and technology of energy recovering linacs (ERLs). Potential applications include: ERL-based light sources, high average power FELs, SASE FELs, ERL-based electron cooling devices, electron-ion colliders.

Date: Late spring to early summer 2004
Chairpersons: Swapan Chattopadhyay and Lia Merminga, Jefferson Lab
Place: TBD
Proceedings will be published in an established journal (to be determined, e.g., AIP, NIMPR, PRST-AB).

5.2 ICFA Beam Dynamics Mini-Workshop

5.2.1 13th: Workshop of Beam Induced Pressure Rise in Rings

Time: December 9-12, 2003

Place: BNL

Scope of the Workshop:
Main sources of beam induced pressure rise include electron stimulated gas desorption, ion desorption, and beam loss/halo scraping. Beam induced pressure rise had limited beam intensity in CERN ISR and LEAR. Currently, it is a limiting factor in RHIC, AGS Booster, and GSI SIS. It is a relevant issue at SPS, LANL PSR, and B-factories. For projects under construction and planning, such as SNS, LHC, LEIR, GSI upgrade, and heavy ion inertial fusion, it is also of concern. In this workshop, the status of existing machines and various measurement results will be reported. Remedies to reduce secondary electron yield, electron and ion desorption rates, etc. will be discussed. These include beam scrubbing (both electron bombardment and ion sputtering), chamber coating and treatment, solenoid field, and beam bunch pattern.

Working Group:
1. Electron and ion desorption
2. Chamber coating and treatment
3. Electron cloud effect

Invited Talk (tentative):
F. Ruggiero - LHC concerns*
J. Wei - SNS concerns*
W. Fischer - RHIC concerns*
A. Molvik - HIF (Heavy Ion Fusion) concerns*
O. Boine-Frankenheim - GSI upgrade*
M. Chanel - LHC heavy ion injectors*
J.M. Jimenez - SPS issues*
R. Macek - PSR issues*
S.Y. Zhang - AGS Booster issues*
A. Kraemer - SIS experiments*
E. Mahner - LINAC3 measurement results*
P. Chiggiato - NEG coating*

A. Kulikov - PEP- II vacuum experience
Y. Suetsugu - KEKB observations*

* Confirmed

Organizing Committee:
M. Chanel, CERN
A. Chao, SLAC
W. Chou, FNAL
W. Fischer, BNL
B. Franzke, GSI
M.A. Furman, LBNL
K. Harkay, ANL
S. Henderson, ORNL
I. Hofmann, GSI
H.C. Hseuh, BNL
R. Macek, LANL
A. Molvik, LLNL
Y. Mori, KEK
T. Roser, BNL(Chair)
F. Ruggiero, CERN
J. Wei, BNL
S.Y. Zhang, BNL(Co-chair)
F. Zimmermann, CERN

5.3 Other Workshops

5.3.1 ICFA Beam Dynamics Mini-Workshop organized by the Working Group on High Luminosity e^+e^- Colliders

e^+e^- in the 1-2 GeV range: Physics and Accelerator Prospects Alghero, Italy, 10th - 13th September 2003

The Workshop, sponsored by Istituto Nazionale di Fisica Nucleare (INFN), will be jointly organized by INFN, Università di Cagliari, Università di Sassari and will be held on **10-13 September 2003** at Alghero (SS), Italy.

In the post-LEP era the high energy frontier is reachable only by large scale collaborations and laboratories, while the present lepton colliders operating at low and intermediate energies are planning major upgrades aimed at increasing substantially their luminosity, in order to meet the continous interest in precision physics.

The lowest energies are now represented by DAΦNE (1.02 GeV cm, operating at Frascati), VEPP-2000 (from 1 to 2 GeV, in construction at Novosibirsk), CESR

(presently operating at Cornell in the range 9.4 to 12 GeV, foreseen 3 to 12 GeV), BEPC (presently operating in Beijing in the range 2 to 5.6 GeV, foreseen luminosity upgrade).

The workshop will be dedicated to discuss both the physics issues and the strategies and problems towards higher luminosities in the energy range mainly but not only between 1 and 2 GeV. It is intended to clarify which experiments are more appealing to the physics community, and which is the way to proceed for obtaining the necessary luminosity. Physics topics include precision measurement of nucleon form factors, low energy spectroscopy, physics of hypernuclei, tests of fundamental symmetries through rare kaon decays, gamma-gamma physics. Eventually an indication for the future upgrades of DAFNE will be obtained.

Two working groups will participate to the workshop: the first will be dedicated to the physics and the second to accelerators. On the first and last day there will be two plenary sessions, to introduce the main issues and to make the concluding remarks in the presence of the whole community. On the two central days there will be separated sessions for each working group, in which the discussions will be more specialized.

All the information concerning the workshop can be found at:

http://www.lnf.infn.it/conference/d2/

Registration deadline is already over; more than 100 participants will attend the meeting. Advisory and Organizing Committees are listed below, and the Program main issues are listed in the Table.

International Advisory Committee

Bressani Tullio	tullio.bressani@to.infn.it
Brodsky Stanley	sjbth@slac.stanford.edu
Calvetti Mario	mario.calvetti@fi.infn.it
Close Frank	f.close@physics.ox.ac.uk
De Sanctis Enzo	enzo.desanctis@lnf.infn.it
Drechsel Dieter	drechsel@kph.uni-mainz.de
Franzini Paolo	paolo.franzini@lnf.infn.it
Guaraldo Carlo	carlo.guaraldo@lnf.infn.it
Jowett John	john.jowett@cern.ch
Lee Franzini Juliet	juliet@lnf.infn.it
Maiani Luciano	luciano.maiani@cern.ch
Perevedentsev Eugene	e.a.perevedent@inp.nsk.su
Petronzio Roberto	roberto.petronzio@roma2.infn.it
Rice David	dhr1@cornell.edu
Seeman John	seeman@slac.stanford.edu
Serci Sergio	sergio.serci@ca.infn.it
Solodov Evgeni	solodov@slac.stanford.edu
Zhang Chuang	zhangc@ihep.ac.cn

Organizing Committee

Baldini Rinaldo	rinaldo.baldini@lnf.infn.it

Bertolucci Sergio *(Chairman)*	sergio.bertolucci@lnf.infn.it
Biagini Marica	marica.biagini@lnf.infn.it
Biscari Caterina	caterina.biscari@lnf.infn.it
Bossi Fabio	fabio.bossi@lnf.infn.it
Bottigli Ubaldo	bottigli@uniss.it
Ferroni Fernando	fernando.ferroni@roma1.infn.it
Isidori Gino	gino.isidori@lnf.infn.it
Pancheri Giulia	giulia.pancheri@lnf.infn.it
Serio Mario	mario.serio@lnf.infn.it
Zobov Mikhail	mikhail.zobov@lnf.infn.it

Program

10th afternoon **Plenary Session**	Welcome and Opening Remarks QCD Studies in Low Energy e-e+ Annihilation Flavour Physics and K Decays Factories at Low Energies - Status and Upgrades	
	Working Group 1 - Physics	**Working Group 2 - Accelerators**
11th morning	Rare Kaon Decays	High Luminosity issues - beam-beam
11th afternoon	CPT-Tests & Interferometry Charged Kaon Decays	High Luminosity issues - single beam
12th morning	Hypernuclear Physics Nucleon Form Factors	Technological issues
12th afternoon	R Measurements Low Energy Spectroscopy	DAϕNE Upgrades
13th morning **Plenary Session**	Concluding remarks Working group 1 Working group 2 Conclusions	

5.3.2 Mini-Workshop on Communication Tools for a Global Accelerator Network

October 29-31 2003

Elettra Laboratory Trieste Italy

The concept global accelerator network (GAN) has found considerable interest in the accelerator community world wide. There have been two study groups initiated by ICFA which were followed by three workshops: Cornell in March 2002, Berkeley in August, 2002, and Brookhaven (Shelter Island) in September 2002. An ICFA working group on Remote Experiments in Accelerator Physics (REAP) under the Beam Dynamics Panel has been formed to foster further activities in this area, and the

progress on the topic has been presented at the major accelerator conferences in the last 3 years.

A number of activities have been started recently. A proposal has been worked out to create a novel, universal communication tool (MVL) to support collaborations to build, test, install, and test accelerator hardware and software which allows the virtual presence of the remote experts at the site of the activity. Activities have been started at Cornell to create a global accelerator seminar network.

In the context of these recent developments, the general goal of this mini-workshop is to determine adequate criteria for universal communication tools to support collaborations in the field of accelerators. In doing this a variety of collaboration and remote access tools relevant to remote operations and accelerator physics experiments will be examined. Reports on recent experience in remote operations will help in determining these criteria. Information will be exchanged with experts in the field of human-computer communications, networking and communication technology.

Programme Committee

Luca Chittaro Univ.Udine
Hans Frese DESY
Mattias Kasemann Desy,
Stephen Peggs, BNL
Roberto Pugliese, Elettra (chair local organizations)
Martin Einhoff, Frauenhofer-Gesellschaft
David Rice Cornell
Hermann Schmickler, CERN
Daniele Sertore, INFN Milano
Sergio Tazzari, Rome2
F. Willeke, DESY

contact: David Rice Cornell, mailto:dhr1@cornell.edu

6 Minutes of Beam Dynamics Panel Meetings

6.1 Minutes - ICFA Beam Dynamics Panel Meeting

Tuesday, May 13, 2003, 5:30 - 7:30 pm
Senate Suite, Hilton Hotel, Portland, Oregon, U.S.A.

1. Nine panel members or their designated representatives attended the meeting. They were: (in alphabetical order)
   Caterina Biscari (LNF-INFN)
   Weiren Chou (Fermilab)
   John Lewellen (ANL, for Kwang-Je Kim)
   Alessandra Lombardi (CERN)
   Lia Merminga (Jlab, for Swapan Chattopadhyay)
   Kazuhito Ohmi (KEK, for Susumu Kamada)
   David Rice (Cornell U.)
   Michael Sullivan (SLAC, invitee)
   Jie Wei (BNL)
   The meeting was chaired by W. Chou on behalf of J. Jowett.

2. W. Chou gave a brief report on the last ICFA meeting February 13-14, 2003 at Tsukuba, Japan. The details can be found on the web (http://www.fnal.gov/directorate/icfa/icfa_46thmtg.html). He also made the announcement about the retirement of three panel members: K. Hirata (Sokendai), C. Zhang (IHEP/China) and O. Napoly (CEA), and the addition of two new panel members: J. Urakawa (KEK) and J-Q. Wang (IHEP/China). The Panel thanked Prof. Hirata, Prof. Zhang and Dr. Napoly for their valuable contributions in the past years and welcomed Dr. Urakawa and Dr. Wang to join the Panel.

3. D. Rice gave a brief report on the Partial Panel meeting February 12, 2003 at the KEK. The details can be seen in the "From the Chairman" in the next issue of the ICFA BD Newsletter (No. 30, April 2003).

4. Report from working groups:
   - J. Lewellen, on behalf of K-J. Kim gave a report on the working group of Future Light Sources. A new web site has been established and will be linked to the panel main web page. It proposed a "full" workshop and a mini-workshop (see below).
   - C. Biscari gave a report on the working group of High Luminosity e+e- Colliders. A lepton collider database is being created and will be put on the web soon. It proposed a mini-workshop (see below).
   - W. Chou gave a report on the working group of High Intensity and High Brightness Hadron Beams. This group had a meeting on the day before.

Seventeen group members or their designated representatives attended the meeting. It proposed a "full" workshop and 3-4 mini-workshops (see below).

- D. Rice gave a report on the recently formed working group of Remote Experiments in Accelerator Physics (REAP). There are 23 members. A web site has been created and linked to the panel main web page. This group will have a meeting on the following day to plan for future activities, including remotely accessible seminars.

5. ICFA Advanced Beam Dynamics Workshops (ABDW):
   - Status of the proceedings: Publication of proceedings is a requirement of all ICFA workshops (except mini-workshops). Most of the ABDW proceedings are published. The status of the five unpublished proceedings is as follows: 23rd (D. Rice, to be published in two months), 24th (K-J. Kim, to be published on CD and web), 26th (F. Zimmermann, to be published in one month), 27th (C. Pellegrini, no information), and 28th (P. Chen, no information).
   - Plan for the upcoming workshops:
     - 29th - HALO03: This will take place May 19-23 at Montauk, Long Island, U.S.A. J. Wei reported that there are 90 registered participants, including 25 locals and 65 non-locals. There will be 4 working groups. The agenda has been finalized. The proceedings will be published by the AIP.
     - 30th - e+e- High Luminosity Factories: This will take place October 13-16, 2003 at SLAC. M. Sullivan reported the organizing work on behalf of J. Seeman, who is the chairman of the workshop. This is the 4th in the series. There will be 4 working groups, with the expected attendance of 60-80 people. The proceedings will be on CD.
   - Proposals for three future workshops:
     - 31st – "High current injectors and energy recovery linacs for future light sources and colliders," early spring of 2004, Jlab, U.S.A., co-chaired by S. Chattopadhyay and L. Merminga (Jlab).
     - 32nd – HB2004, early October 2004, Mainz, Germany, co-chaired by I. Hofmann (GSI) and J-M. Lagniel (CEA).
     - 33rd – FLS workshop, DESY, 2005.

     The Panel approved these proposals and will bring them to the next ICFA Committee meeting in August for approval.

6. ICFA mini-workshops:
   - The High Intensity and High Brightness Hadron Beams working group proposed 3-4 mini-workshops in the following two years:
     - "Vacuum," BNL, organizer T. Roser.
     - "Low level RF," CERN, organizers R. Garoby and T. Linnecar.
     - "Magnet fringe field," Fermilab, organizer W. Chou.
     - A mini-workshop in Korea or Japan, topic to be decided.
   - The Future Light Source working group proposed a mini-workshop:
     - "From start to end simulation for X-FELs," August 18-22, 2003, DESY, co-chaired by J. Galayda (SLAC) and J. Rossbach (DESY).

- The High Luminosity e+e- Colliders working group proposed a mini-workshop:
- "e+e- in the 1-2 GeV range: physics and accelerator prospects," September 10-13, 2003, Alghero, Italy, co-chaired by S. Bertolucci and C. Biscari (LNF-INFN).

The Panel approved these mini-workshop proposals.

(Note: After the Panel meeting, the Remote Experiments in Accelerator Physics working group proposed a mini-workshop at its group meeting on the following day:

- "Multipurpose Virtual Laboratory (MVL) project," November, 2003 in Trieste, Italy, chaired by F. Willeke (DESY).

This mini-workshop will be proposed to the Panel for approval.)

7. ICFA Beam Dynamics Newsletter:
   - Most of the issue editors for the next two years (6 issues) have been decided:
     - No. 31, August 2003, Y. Funakoshi
     - No. 32, December 2003, (TBD)
     - No. 33, April 2004, K. Ohmi
     - No. 34, August 2004, D. Rice
     - No. 35, December 2004, C. Biscari
     - No. 36, April 2005, A. Lombardi.
   - Printing: It has been decided to have three printing places for each issue: KEK (S. Kamada, Asia and Pacific), DESY (H. Mais, Europe and Africa), Fermilab (W. Chou, North and South America). There was a discussion on the two different paper sizes: A4 and Letter. This should not be a problem for most printers to print PDF files. Should this become a problem, a back off solution is to ask the editor to prepare two versions (A4 and Letter) for each issue.
   - Distribution: The editors-in-chief will send a request to the three regional distributors for an update of their mailing list. In particular, if some recipients are willing to read the Newsletter on line, the number of paper copies can be reduced.

6.2 Minutes - ICFA High Intensity Hadron Beams Working Group Meeting

Monday, May 12, 2003, 6:00 - 8:00 pm
Studio Suite, Hilton Hotel, Portland, Oregon, U.S.A.

1. Seventeen members or their designated representatives and invitees attended the meeting. They were: (in alphabetical order)
   Weiren Chou (Fermilab)
   Ron Davidson (PPPL)
   Miguel Furman (LBL, for Jonathan Wurtele)
   Roland Garoby (CERN)

Massimo Giovannozzi (CERN, for Roberto Cappi)
Stuart Henderson (ORNL, for John Galambos)
Ingo Hofmann (GSI, invitee)
Jean-Michel Lagniel (CEA, invitee)
Trevor Linnecar (CERN)
Bob Macek (LANL)
Ernie Malamud (Fermilab, invitee)
Won Namkung (POSTECH, invitee)
Chris Prior (RAL)
Thomas Roser (BNL)
Izumi Sakai (KEK, for Yoshiharu Mori)
Lee Teng (ANL, invitee)
Bill Weng (BNL)

The meeting was chaired by W. Chou. He made the announcement about the retirement of C. Zhang (IHEP/China), who will be replaced by J-Q. Wang (IHEP/China). The group thanked Prof. Zhang for his valuable contribution in the past years and welcomed Dr. Wang to join it.

2. There were brief reports on three construction projects and three future projects:
   - SNS project, S. Henderson (ORNL)
   - LHC project, M. Giovannozzi (CERN)
   - J-PARC project, I. Sakai (KEK)
   - GSI future facility, I. Hofmann (GSI)
   - High intensity hadron beams in Korea, W. Namkung (POSTECH)
   - CSNS project, C. Zhang (IHEP/China, presented by W. Chou)

   The "Big Three" construction projects (SNS, LHC and J-PARC) are proceeding well. Their completion dates are all scheduled around 2006. The GSI future facility has got the approval of the German government and is expected to start the construction in a few years (contingent upon 25% international funding). The total budget is about 700 M euros. Korea is working on a 1 GeV high intensity proton facility called KOMAC. The first stage is 1/10 of this project, namely, a 100 MeV, 20 mA, pulsed proton linac. The budget is about US$100 M. China has started the design work of a synchrotron based spallation neutron source called CSNS. The beam power is 100 kW and upgradeable to 400 kW.

3. ICFA mini-workshops:
   - In the past years, this working group has organized 12 mini-workshops. This type of workshops is gaining popularity also in other ICFA working groups because of its flexibility, efficiency and productivity.
   - C. Prior gave a report on the recent 12th mini-workshop on space charge simulation, held April 2-4, 2003 in Oxford, U.K. In particular, he introduced a code benchmarking agreement among a number of attendees at the workshop.
   - 3-4 new mini-workshops were proposed for 2003-2005:
     - "Vacuum," BNL, organizer T. Roser.
     - "Low level RF," CERN, organizers R. Garoby and T. Linnecar.
     - "Magnet fringe field." Fermilab, organizer W. Chou.

- A mini-workshop in Korea or Japan, topic to be decided.

These proposals will be submitted to the ICFA Beam Dynamics Panel for approval. (Note: At the Panel meeting on the following day, these mini-workshops were approved.)

4. ICFA "full" workshop:
   - The last "full" workshop organized by this working group, HB2002, April 12-15, 2002 at Fermilab was a success. There were about 150 registered participants. The proceedings have been published by the AIP in both hardcopy and CD.
   - The next one, HB2004, will take place in early October 2004, at Mainz, Germany. It will be co-chaired by I. Hofmann (GSI) and J-M. Lagniel (CEA). This proposal will be submitted to the ICFA Beam Dynamics Panel and ICFA Committee for approval. (Note: The Panel has approved this workshop. The Committee is expected to discuss this proposal at its August meeting.)

7 Announcements of the Beam Dynamics Panel

7.1 ICFA Beam Dynamics Newsletter

7.1.1 Aim of the Newsletter

The ICFA Beam Dynamics Newsletter is intended as a channel for describing unsolved problems and highlighting important ongoing works, and not as a substitute for journal articles and conference proceedings that usually describe completed work. It is published by the ICFA Beam Dynamics Panel, one of whose missions is to encourage international collaboration in beam dynamics.

Normally it is published every April, August and December. The deadlines are 15 March, 15 July and 15 November, respectively.

7.1.2 Categories of Articles

The categories of articles in the newsletter are the following:

1. Announcements from the panel.
2. Reports of Beam Dynamics Activity of a group.
3. Reports on workshops, meetings and other events related to Beam Dynamics.
4. Announcements of future Beam Dynamics-related international workshops and meetings.
5. Those who want to use newsletter to announce their workshops are welcome to do so. Articles should typically fit within half a page and include descriptions of the subject, date, place, Web site and other contact information.
6. Review of Beam Dynamics Problems: this is a place to bring attention to unsolved problems and should not be used to report completed work. Clear and short highlights on the problem are encouraged.
7. Letters to the editor: a forum open to everyone. Anybody can express his/her opinion on the beam dynamics and related activities, by sending it to one of the editors. The editors reserve the right to reject contributions they judge to be inappropriate, although they have rarely had cause to do so.
8. Editorial.

The editors may request an article following a recommendation by panel members. However anyone who wishes to submit an article is strongly encouraged to contact any Beam Dynamics Panel member before starting to write.

7.1.3 How to Prepare a Manuscript

Before starting to write, authors should download *the latest* model article file, in Microsoft Word format, from the Beam Dynamics Panel home page

http://wwwslap.cern.ch/icfa/

It will be much easier to guarantee acceptance of the article if the latest model is used and the instructions included in it are respected. These model files and instructions are expected to evolve with time so please make sure always to use the latest versions.

The final Microsoft Word file should be sent to one of the editors, preferably the issue editor, by email.

The editors regret that LaTeX files can no longer be accepted: a majority of contributors now prefer Word and we simply do not have the resources to make the conversions that would be needed. Contributions received in LaTeX will now be returned to the authors for re-formatting.

In cases where an article is composed entirely of straightforward prose (no equations, figures, tables, special symbols, etc.) contributions received in the form of plain text files may be accepted at the discretion of the issue editor.

Each article should include the title, authors' names, affiliations and e-mail addresses.

7.1.4 Distribution

A complete archive of issues of this newsletter from 1995 to the latest issue is available at

http://wwwslap.cern.ch/icfa/

This is now intended as the primary method of distribution of the newsletter.

Readers are encouraged to sign-up for to electronic mailing list to ensure that they will hear immediately when a new issue is published.

The Panel's Web site provides access to the Newsletters, information about Future and Past Workshops, and other information useful to accelerator physicists. There are links to pages of information of local interest for each of the three ICFA areas.

Printed copies of the ICFA Beam Dynamics Newsletters are also distributed (generally some time after the Web edition appears) through the following distributors:

Weiren Chou	chou@fnal.gov	North and South Americas
Helmut Mais	mais@mail.desy.de	Europe* and Africa
Susumu Kamada	Susumu.Kamada@kek.jp	Asia** and Pacific

* Including former Soviet Union.
** For Mainland China, Chuang Zhang (zhangc@bepc3.ihep.ac.cn) takes care of the distribution with Ms. Su Ping, Secretariat of PASC, P.O.Box 918, Beijing 100039, China.

To keep costs down (remember that the Panel has no budget of its own) readers are encouraged to use the Web as much as possible. In particular, if you receive a paper copy that you no longer require, please inform the appropriate distributor.

7.1.5 Regular Correspondents

The Beam Dynamics Newsletter particularly encourages contributions from smaller institutions and countries where the accelerator physics community is small. Since it is impossible for the editors and panel members to survey all beam dynamics activity world-wide, we have some *Regular Correspondents*. They are expected to find interesting activities and appropriate persons to report them and/or report them by themselves. We hope that we will have a "compact and complete" list covering all over the world eventually. The present *Regular Correspondents* are as follows

Liu Lin	liu@ns.lnls.br	LNLS Brazil
S. Krishnagopal	skrishna@cat.ernet.in	CAT India
Ian C. Hsu	ichsu@ins.nthu.edu.tw	SRRC Taiwan

We are calling for more volunteers as *Regular Correspondents*.

7.2 ICFA Beam Dynamics Panel Members

Caterina Biscari	caterina.biscari@lnf.infn.it	LNF-INFN, Via E. Fermi 40, Frascati, Italy
Swapan Chattopadhyay	swapan@jlab.org	Jefferson Lab, 12000 Jefferson Avenue, Newport News, VA 23606, USA
Pisin Chen	chen@slac.stanford.edu	SLAC, P.O. Box 4349, MS26, Stanford, CA 94309, USA
Weiren Chou	chou@fnal.gov	FERMILAB, MS 220, P.O.Box 500, Batavia, IL60510, USA
Yoshihiro Funakoshi	yoshihiro.funakoshi@kek.jp	KEK, Oho, Tsukuba, IBARAKI 305-0801, Japan.
Jie Gao	gao@lal.in2p3.fr	Laboratoire de L'Accélérateur Linéaire, B.P. 34, 91898, Orsay cedex, France
Sergei Ivanov	ivanov_s@mx.ihep.su	Institute for High Energy Physics, Protvino, Moscow Region, 142281 Russia
John M. Jowett (Chairman)	John.Jowett@cern.ch	CERN, CH-1211 Geneva 23, Switzerland
Kwang-Je Kim	kwangje@aps.anl.gov	Argonne Nat. Lab., Advanced Photon Source, Accelerator Systems Division, 9700 S. Cass Avenue, Bldg 401/C4265, Argonne, IL 60439
Alessandra Lombardi	Alessandra.Lombardi@cern.ch	CERN, CH-1211 Geneva 23, Switzerland
Helmut Mais	mais@mail.desy.de	DESY, Notkestrasse, 85 D-2000, Hamburg 52, Germany
Olivier Napoly	Olivier.Napoly@cea.fr	DAPNIA-SEA, CEA Saclay, 91191 Gif/Yvette CEDEX, France
David Rice	dhr1@cornell.edu	Cornell University, 271 Wilson Lab, Ithaca, NY 14853-8001, USA
Yuri Shatunov	Yu.M.Shatunov@inp.nsk.su	Acad. Lavrentiev prospect 11, 630090 Novosibirsk, Russia
Junji Urakawa	junji.urakawa@kek.jp	KEK, Oho, Tsukuba, IBARAKI 305-0801, Japan.
Jie Wei	wei1@bnl.gov	BNL, Bldg. 911, Upton, NY 11973- 5000, USA
JiuQing Wang	wangjq@mail.ihep.ac.cn	IHEP, CAS, BEPC National Laboratory, P.O. Box 918, 9-1, Beijing 100039, China

The views expressed in this newsletter do not necessarily coincide with those of the editors. The individual authors are responsible for their text.

8 Appendices

In the following, there are two kinds of spreadsheets. In Appendix A, shown are spreadsheets containing full details of all the space charge simulation codes and their general availability which were devised in the XIIth ICFA Beam Dynamics Mini-Workshop on High Intensity and High Brightness Beams - Space Charge Simulation (see section 4.1).

In Appendix B, we show spreadsheets for a lepton collider database which was created by the ICFA BD Panel Working Group on High Luminosity e^+e^- Colliders (see section 2.18).

Appendix A : Space Charge Simulation codes

Sheet 1

Code	Language	Platform	GUI	Parallel	1D/2D/3D	Particles	linacs/rings
IMPACT	F90	Unix/Linux	no	MPI	3D	>10^6	linacs
ML/IMPACT	F90	Unix/Linux/Mac	no	MPI	3D	>10^6	linacs, rings
ORBIT	C++, supercode (Python soon)	Linux/Unix	no	MPI	all	> 10^5 (2D) > 10^6 (3D)	rings & transport lines
BNL-ORBIT	C++	Linux,Unix	yes	MPI	all	10^6	rings
SIMPSONS	F77	any	no	in progress	2D/3D	>10^4 (2D) >10^5 (3D)	rings, transport
ACCSIM	F77	Linux, Unix	no	no	2.5D	>10^5	rings
PARMILA	F90	Windows	no	no	2D/3D	10^4 - 10^5	linacs, transfer lines
ESME	F77 with pointer extension	Unix, Linux	post, online	MPI (in progress)	1D longitudinal	10^7	rings, transfer lines
LONG1D	F77	DEC,Linux	screen menu	no	1D longitudinal	10^6	rings
Track1D	F77	any	no	no	1D longitudinal	~10^6	rings
Track2d	F77	any	no	no	2D transverse	~10^6	linacs, rings
Track3d	F77	any	no	no	3D	~10^6	linacs, rings

Sheet 2

Code	*Language*	*Platform*	*GUI*	*Parallel*	*1D/2D/3D*	*Particles*	*linacs/rings*
GPT	C,C++	Windows	yes	MPI scans	3D	10^6	linacs, transfer lines FEL
GenTrackE	C++	Unix, Linux (IBM)	no	MPI	3D	>10^9	rings, transfer lines, cyclotrons
BEST	F90	Unix, Linux	python, IDL	MPI, openMP	3D	>10^6	linacs, rings
VADOR	C++	Unix,Linux	no	MPI	2D	n/a	linacs
SPUNCH	F77	Linux	no		1D	10^4	LEBT
PATH	F90	Windows	yes	no	3D	10^5	linacs/rings
TRACE/WIN	C++	Windows	yes	no	2D/3D	10^5	linacs
DYNAC	F77	Linux, Unix, Windows	no	no	2D,3D	10^5	linacs
Synergia	F90/C+/Python	Unix(inc AIX,Linux)	no	MPI	3D	>10^6	linacs, rings
WARP	Python/F77/F90/C	Linux, Unix Mac OS X, Windows	Under dev.	MPI	3D, (r,z), (x,y)	any number so far up to ~10^8	linacs,rings,other bends

Sheet 3

Code	*Space Charge Solver*	*Boundaries/Images*	*Impedances*	*Field maps*	*Integration order*
IMPACT	spectral	combination of open, periodic, rectangular, circular pipes	no	yes	2nd order in z
ML/IMPACT	spectral	no	yes	no	2nd in z with 5th order maps
ORBIT	FFT, force or potential potential	open, conductive wall (elliptical, rectangular, circular, other shapes easily possible)	transverse, longitudinal	MAD beamline elements, Beamline, MXYZPLTK, symplectic elements	2nd in s
BNL-ORBIT	LU+SOR	conductive, automatic images	automatic or external	no	arbitrary 2nd in s
SIMPSONS	FFT in cylindrical coordinate	circular cond. wall	no	same as teapot	1st order symplectic
ACCSIM	hybrid FMM	none or any conducting boundary	no	no	1st, 2nd
PARMILA	SCHEFF, PICNIC	open	no	yes (superfish)	
ESME	smoothed dλ/dz	circular conductive wall	yes	no	n/a
LONG1D	smoothed dλ/dz		yes	n/a	2nd
Track1D	smoothed dλ/dz	variable g-factor	simple Z/n model	n/a	2nd
Track2d	FEM < 10th order	automatic treatment, open, periodic, elliptical, polygon	no	partly	leapfrog
Track3d	FEM < 6th order	automatic treatment, open, periodic, elliptical, polygon, lossy	no	yes	

Sheet 4

Code	*Space Charge Solver*	*Boundaries/Images*	*Impedances*	*Field maps*	*Integration order*
GPT	3D multigrid	open, conductive rectangular pipe, cathode	no	2D,3D	5th Runge Kutta
GenTrackE	FEM, multigrid	periodic, Dirichlet Neumann, mixed	no	no	any order Runge Kutta, leapfrog
BEST	spectral, FD	circular conductive wall	automatic/external	no	user specified
VADOR	FFT	conductive wall, any shape	no	no	2nd
SPUNCH	exact for disc-shaped particles	circular conductive wall	n/a	n/a	1st
PATH	Scheff, point to point	open	no	yes	?
TRACE/WIN	Scheff, PICNIC, Gaussup	open	no	no	?
DYNAC	Scheff, Scherm, Hersc	open	no	yes	3d order analytical
Synergia	spectral (from IMPACT)	combination of open, periodic, rectangular, circular pipes	no	yes	2nd order in z
WARP	FFT, Cap matrix, Multigrid, Adaptive Mesh Refined-MG	square pipe, round pipe, internal conductors, bent pipe, general	no (some ad-hoc)	no	2nd

Sheet 5

Code	time or s-tracking	Graphics	Portability	Source Code Available?	User Manual	Standard Test Cases
IMPACT	s	postprocessor	all Unix platforms with MPI	yes to collaborators	partial	yes
ML/IMPACT	s	postprocessor		yes to collaborators	partial	yes
ORBIT	s	Plplot or external	Linux, IBM, DEC, SUI Libraries included	yes	needs update	yes
BNL-ORBIT	s	GNUplot	fully portable	yes	old	yes
SIMPSONS	t	GNUplot, topdrawer, postprocessor	fully portable	yes	needs update	yes
ACCSIM	s	built in	any platform with CERN libraries	yes	needs updating	yes
PARMILA	s	external: Lingraf (Windows)	Windows	no	yes	yes
ESME	t	PGPLOT	yes	yes	yes	yes
LONG1D	revolution time	built in	?	yes	yes	yes
Track1D	revolution time	continuous and external (PGPLOT)	libraries included	yes	needs updating	yes
Track2D	s	continuous and external (PGPLOT)	libraries included	yes	needs updating	yes
Track3D	t	continuous and external (PGPLOT)	libraries included	no	not yet available	no

Sheet 6

Code	time or s-tracking	Graphics	Portability	Source Code Available?	User Manual	Standard Test Cases
GPT	t	built in	portable except user interface	all beamline components	yes, up to date	yes
GenTrackE	t/s	no	yes	yes	no	not yet
BEST	t	netcdf, IDL	any Linux,Unix	yes	no	yes
VADOR	s	GNUplot, openDX	any Linux, Unix	yes	almost	yes
SPUNCH	s	built in	fully portable	yes	no but commented	yes
PATH	s	built in	any DOS	yes	yes	?
TRACE/WIN	s	built in	any Windows	no	yes	?
DYNAC	t,s	GNUplot	fully portable	yes	yes	yes
Synergia	s	postprocessor (Octave), Root+OpenInventor in progress	all Unix platforms	yes, see IMPACT	in progress	not yet
WARP	t; s for (x,y) "slice" pkg	PyGist 2D, OpenDX 3D	portable	yes (with permission)	yes (online)	yes

Sheet 7

Code	Limitations	Other Features	Access	Price
IMPACT			jqiang@lbl.gov rdryne@lbl.gov	free to academia free to academia
ML/IMPACT		standardized input format (MAD and others)	Ji Qiang, Robert Ryne	
ORBIT	user manual incomplete	injection painting and foil, magnet errors, fringe fields, RF diagnostics, apertures and collimation, symplectic tracking, closed orbit correction, e-p under development	jzh@ornl.gov scousine@ornl.gov Sarah Cousineau/Jeffrey Holmes	free
BNL-ORBIT	in continuous revision	multi-turn injection and painting	luccio@bnl.gov Alfredo Luccio	free
SIMPSONS	bunch length >> beam size	TEAPOT input format, acceleration, multiturn injection w painting, apertures & collimation, variable charge, multipole errors, time dependance of parameters	shinji.machida@kek.jp Shinji Machida	free
ACCSIM	no symplectic higher order treatment	collimators, orbit bumps, painting, energy deposition, injection foils	fwj@triumf.ca Frederick Jones	free
PARMILA		magnet field map	htakeda@lanl.gov Harunori Takeda	free
ESME		gamma-t jump, mountain range plots, time/freq. domain, feedback, generate matched distributions	maclachlan@fnal.gov	free
LONG1D		synchrotron radiation and others	shane@triumf.ca Shane Koscielniak	free
Track1D		injection, dp/p ramping, gamma-t jump, mountain range plots, errors, variable charge	c.prior@rl.ac.uk Christopher Prior	free
Track2d		injection, run and optimization modes, errors	c.prior@rl.ac.uk	free
Track3d	needs much revision		c.prior@rl.ac.uk	free

Sheet 8

Code	Limitations	Other Features	Access	Price
GPT	no wakefield	position all elements in 3D space automatic scans, hierarchical data analysis	gpt@pulsar.nl Bas van der Geer	on request
GenTrackE		multiple particle species, optimizer framework for particle tracking	andreas.adelmann@psi.ch Andreas Adelmann	free
BEST	physics only	multiple species, low noise, delta-f	hongqin@princeton.edu Hong Qin	free
VADOR		Vlasov	sonnen@math.u-strasbg.fr Eric Sonnendrucker	free
SPUNCH	nonrelativistic	for bunching simulations with space charge	krab@triumf.ca Rick Baartman	free
PATH			alessandra.lombardi@cern.ch Alessandra Lombardi	free
TRACE/WIN		PARTRAN, TRACE3D, TOUTATIS, SCDYN & Monet Code from one surface, matching tools	npichoff@cea.fr, duriot@cea.fr Nicolas Pichoff, Didier Uriot	?
DYNAC			http://dynac.web.cern.ch/dynac/dynac.html Eugen Tanke, 4et@sns.gov	free
Synergia		3D space charge can be calculated at any position in any element; multiple charge states reads MAD files, programmable python interface	spentz@fnal.gov; amundson@fnal.gov Panagiotis Spentzouris	free (see IMPACT)
WARP	not map-based electrostatic	subgrid-scale conductor boundaries; non-paraxial; mixed straight-bent system; user-prog'able ("steering")	dpgrote@lbl.gov David Grote. Alex Friedman	free (permission needed)

Appendix B: Lepton Collider Database Sheet 1a – General Parameters

LEPTON COLLIDERS (e+/e-)		Units	DAFNE design	DAFNE KLOE best	DAFNE DEAR best	VEPP 2000 design	ADONE design	ADONE I generation	ADONE II generation	BEPC design	BEPC	BEPC-II design
Physics start date				1999	2001			1969	1990			
Physics end date					2002			1978	1993		2002	
Energy (center of mass) (e+/e-)	E_{cm}	GeV	1.02	1.02	1.02	2	.6/3.1	.6/3.1	2./3.1	2-5.6	2.-5.0	2.- 4.2
Energy per ring (e+/e-)	E	GeV	0.51	0.51	0.51	1	.3-1.5	.3-1.5	1./1.505	2.8/2.8	1.89/1.89	1.89
Lorentz factor (e+/e-)	γ		998.04	998.04	998.04	1957	587./2935.	587./2935.	1956./2935.	5479	3698	3698
Number of rings			2	2	2	1	1	1	1	1	1	2
Circumference	C	m	97.69	97.69	97.69	24.38	105	105	105	240.4	240.4	237.5
Number of IPs			2	1	1	2	6	6	1	2	2	1
Revolution time	T	μsec	0.3260	0.3260	0.3260	0.08	0.3500	0.3500	0.3500	0.8010	0.8010	0.792
Revolution frequency	F_{rev}	MHz	3.07	3.07	3.07	12.292	2.86	2.86	2.86	1.247	1.247	1.26
Time between collisions	Tc	nsec	2.7	5.4	2.7	40	58	58	350	801.0	801.0	8
Bunch spacing	s_b	m	0.81	1.62	0.81	24.38	35	35	105	240.4	240.4	2.4
Half crossing angle	$\phi/2$	mrad	15	12.5	14.5	0	0	0	0	0	0	11
Piwinski angle	$(\phi/2) * \sigma_l / \sigma_x^*$	rad	0.225	0.22	0.255	0	0	0	0	0	0	0.44
Number of Colliding Bunches	N_b		120	49	98	1	3	3	1	1	1	93
Particles per bunch (e+/e-) (10^{10})	N_{part}		8.9	4.7/3.1	2.1/1.7	10				32.5	23	4.9
Beam current (e+/e-)	I	A	5	1.14/.756	1./.8	0.196				0.065	0.045	0.91
Bunch current (e+/e-)	I_b	mA	42	23.3/15.4	10.2/8.2	196				65	45	9.8
Peak current (e+/e-)	I_{peak}	A	55	45./30.	20./16.	64				125	86	62
Peak Luminosity (10^{32})	L_{peak}	$cm^{-2} sec^{-1}$	2.5	0.8	0.66	1		0.003	0.0003	0.17	0.112	10
Specific Luminosity (10^{30})	L_{sp}	$cm^{-2} sec^{-1} mA^{-2}$	0.0012	0.0045	0.008	0.26				0.004	0.006	0.11
Luminosity lifetime		hr	0.6							6.5	7	2.7
Beam-beam tune shift per crossing (e+/e-)	horizontal		0.04	0.028	0.017	0.1				0.038	0.041	0.04
	vertical		0.04	0.02	0.017	0.1				0.02	0.029	0.04
Σ in collision	horizontal	μm	2828			117				926	869	379
	vertical	μm	28.3	6	10	117				101	52	5.7
Filling time (e+/e-)		min	5	5	5					40	30	12
Injection energy (e+/e-)	E_i	GeV	0.51	0.51	0.51	0.9	0.3		0.3	1.1-1.4	1.1-1.55	1.89
Acceleration period		sec								30	21	0
Ion/Abort Gap	Yes/No		No	Yes	Yes	No	No		No	0	0	yes
Integrated Luminosity		fb^{-1}		0.3	0.05							
NOTES				IP 1	IP 2						Best	

Sheet 1b – General Parameters

LEPTON COLLIDERS		Units	CESR	CESR	CESR-C	PEP-II	PEP-II	KEKB	KEKB	LEP	LEP I	LEP II
(e+/e-)			design		design	design	BaBar	design	Belle	design		
Physics start date				1979	2003		1999		1999	1984	1989	1996
Physics end date				2003	2006						1995	2000
Energy (center of mass) (e+/e-)	E_{cm}	GeV	16	10.6	3.0-11.0 (3.77)	10.58	10.58	10.58	10.58	40 - 200	88 - 95	161 - 209
Energy per ring (e+/e-)	E	GeV	8	5.3	1.55-5.6 (1.88)	3.12/8.97	3.1/8.99	3.5/8.0	3.5/8.0	20 - 100	44 - 47.5	80.5 - 104.5
Lorentz factor (e+/e-)	γ		15656	10371.8	3679	6103/17560	6103/17560	6850/15655	6850/15655		89237	191390
Number of rings			1	1	1	2	2	2	2	1	1	1
Circumference	C	m	768	768	768	2199	2199	3016	3016	26658.9	26658.9	26658.9
Number of IPs			2	1	1	1	1	1	1	4	4	4
Revolution time	T	μsec	2.56	2.56	2.563	7.336	7.336	10.1	10.1	88.9244	88.9244	88.9244
Revolution frequency	F_{rev}	MHz	0.39	0.39	0.39	0.136	0.136	0.099	0.099	0.011246	0.011246	0.0112455
Time between collisions	Tc	nsec	2.50E+03	14.0	14.0	4.2	6.3	2	8	2.22E+04	1.11E+04	2.22E+04
Bunch spacing	s_b	m	7.68E+02	4.2	4.2	1.26	1.89	0.6	2.4	6664.725	3332.363	6664.725
Half crossing angle	$\phi/2$	mrad	0	2.3	2.8	0	0	11	11	0	0	0
Piwinski angle	$(\phi/2) * \sigma_L/\sigma_x^*$	rad	0	0.1	0.07	0	0	0.57	0.69	0	0	0
Number of Colliding Bunches	N_b		1	45	45	1658	1034	5000	1284	4	8	4
Particles per bunch (e+/e-) (10^{10})	N_{part}		150	12.7/11.7	6.4	5.95/2.07	9.3/5.	3.3/1.4	7./5.2	41.6	11.8	40
Beam current (e+/e-)	I	A	0.1	.356/.329	.18/.18	2.155/0.75	1.55/1.175	2.6/1.1	1.376/1.049	3.00E-03	1.70E-03	2.88E-03
Bunch current (e+/e-)	I_b	mA	100	7.91/7.31	4.0/4.0	1.3/0.452	1.5/1.14	0.52/0.22	1.07/0.82	7.50E-04	2.13E-04	7.20E-04
Peak current (e+/e-)	I_{peak}	A	766	134./124.	123	95./34.	109/87	124/53	183/140			
Peak Luminosity (10^{32})	L_{peak}	$cm^{-2}\ sec^{-1}$	1	13	3	30	65.82	100	105.67	0.16	2.05E-01	1
Specific Luminosity (10^{30})	L_{sp}	$cm^{-2}\ sec^{-1}\ mA^{-2}$	0.01	0.5	0.42	3.06	3.74	17.5	8.5			
Luminosity lifetime		hr	1.4	2		1.55	3				10	3
Beam-beam tune shift per crossing (e+/e-)	horizontal		0.06	0.025	0.03	0.03	0.075/0.065	0.039/0.039	0.096/0.065		0.03	0.043
	vertical		0.06	0.06	0.03	0.03	0.06/0.048	0.052/0.052	0.069/0.052		0.033	0.079
Σ in collision	horizontal	μm	1110	470	400	221.8	140	109	157		197	178
	vertical	μm	72	3.6	6	6.7	6.8	2.7	3.1		3.4	3.3
Filling time (e+/e-)		min	6	6	6	10	7		10 (top off)		40	30
Injection energy (e+/e-)	E_i	GeV	8	5.3	1.5-5.5	3.1/8.99	3.12/8.97	3.5/8.0	3.5/8.0		22	22
Acceleration period		sec	0.08	0.08	0.08			0	0		300	300
Ion/Abort Gap	Yes/No		no	no	no	Yes (5%)	Yes (2.5%)	Yes	Yes		No	No
Integrated Luminosity		fb^{-1}					138		158.7		0.2	0.8
NOTES				Nov. 2000			July 2003		July 2003			

Sheet 2a – Lattice Parameters

LEPTON COLLIDERS		Units	DAFNE	DAFNE	DAFNE	VEPP 2000	ADONE	ADONE	ADONE	BEPC	BEPC	BEPC-II
(e+/e-)			design	KLOE	DEAR	design	design	I generation	II generation	design		design
Dipoles in ring (e+/e-)			8	8	8	8						
Dipole radius of curvature (e+/e-)		m	1.4	1.4	1.4	1.4						
Dipole magnetic field (e+/e-)		T	1.21	1.21	1.21	2.46						
Type of cell (e+/e-)			CG	CG	CG	FODO				FODO	FODO	FODO
Length of stardard cell (e+/e-)		m	/			24.36						
Phase advance per cell (e+/e-)		degrees	/			35						
Wigglers in ring (e+/e-)			4	4	4							
Wiggler radius of curvature (e+/e-)		m	1.94	1.94	1.94							
Wiggler magnetic field (e+/e-)		T	1.8	1.8	1.8							
Low-β quadrupoles (e+/e-)			6+8	6+6	6+6							
Max low-β quadrupole gradient (e+/e-)		T/m										
Quadrupoles in ring (e+/e-)			39	39	39	24						
Maximum quadrupole gradient (e+/e-)		T/m	12	12	12	50						
Sextupoles in ring (e+/e-)			16	15	15	12						
Maximum sextupole gradient (e+/e-)		T/m2	40			1960						
Octupoles in ring (e+/e-)			0	3	3							
Maximum octupole gradient (e+/e-)		T/m3	0									
Detector field (IR1/IR2/...)		T	0.6/1.1	0.6/0.	0.6/0.	1.5						
e-cloud instability observed	Yes / No		No	No	No					No	No	No
e-cloud solenoids (e+)	Yes / No		No	No	No					No	No	No
Machine impedance (e+/e-)	$Z_{//}/n$	Ω	0.2									4
Standard / minimum aperture (e+/e-)		mm				40						
Vacuum pipe material (e+/e-)			Al	Al	Al							
Antichamber (e+/e-)	Yes / No		Yes	Yes	Yes							
Number of vacuum pumps												
Type of vacuum pumps						IP						
Vacuum		nTorr				5						
Ion clearing electrods (e-)	Yes / No		Yes	No	No							
NOTES												

Sheet 2b – Lattice Parameters

LEPTON COLLIDERS		Units	CESR	CESR	CESR-C	PEP-II	PEP-II	KEKB	KEKB	LEP	LEP I	LEP II
(e+/e-)			design		design	design		design		design		
Dipoles in ring (e+/e-)			84	84	84			171/114	171/114			
Dipole radius of curvature (e+/e-)		m	32-140	32-140	32-140			16.3/104.5	16.3/104.5			
Dipole magnetic field (e+/e-)		T	.013-0.55	.013-0.55	.005-0.2			0.72/0.26	0.72/0.26			
Type of cell (e+/e-)			FODO	FODO	FODO	FODO	FODO	2.5π cell	2.5π cell			
Length of stardard cell (e+/e-)		m	8.2	8.2	8.2			68/68	68/68			
Phase advance per cell (e+/e-)		degrees	varies	varies	varies	90/60	90/60	450/450	450/450			
Wigglers in ring (e+/e-)			0	2	14	1/0	0/0	192/0	152/0			
Wiggler radius of curvature (e+/e-)		m		14.7	3			16.3/inf.	16.3/inf.			
Wiggler magnetic field (e+/e-)		T		1.2	2.1			0.72/0	0.72/0			
Low-β quadrupoles (e+/e-)			4	6	6			8/10	8/10			
Max low-β quadrupole gradient (e+/e-)		T/m	15.2	48.4	16			21/21	20.9/20.9			
Quadrupoles in ring (e+/e-)			100	108	108			462/454	462/454			
Maximum quadrupole gradient (e+/e-)		T/m	12.8	9	4							
Sextupoles in ring (e+/e-)			78	78	78			108/104	108/104			
Maximum sextupole gradient (e+/e-)		T/m2	272	150	100				234/310			
Octupoles in ring (e+/e-)			0	4	4			0/0	0/0			
Maximum octupole gradient (e+/e-)		T/m3	0					0/0	0/0			
Detector field (IR1/IR2/...)		T	1.5	1.5	1	1.5	1.5	1.45	1.45			
e-cloud instability observed	Yes / No		No	No	No	Yes	Yes	Yes	Yes	No	No	No
e-cloud solenoids (e+)	Yes / No		No	No	No	Yes	Yes	Yes	Yes	No	No	No
Machine impedance (e+/e-)	$Z_{//}/n$	Ω	0.5	0.22	0.25							
Standard / minimum aperture (e+/e-)		mm	90/50	90/50	90/50			94/-/50/-	94/~8/50/~8			
Vacuum pipe material (e+/e-)			Al	Al	Al			Cu/Cu	Cu/Cu			
Antichamber (e+/e-)	Yes / No		no	no	no			No	No			
Number of vacuum pumps												
Type of vacuum pumps			IP	IP/Ti sub	IP/Ti sub/NEG			NEG+IP	NEG+IP			
Vacuum		nTorr	16.0	1.0	1.0			1/1	0.73/0.96			
Ion clearing electrods (e-)	Yes / No		no	no	no	No	No	No	No			
NOTES							Wigg OFF					

Sheet 3a – Optics Parameters

LEPTON COLLIDERS		Units	DAFNE	DAFNE	DAFNE	VEPP 2000	ADONE	ADONE	ADONE	BEPC	BEPC	BEPC-II
(e+/e-)			design	KLOE	DEAR	design	design	I generation	II generation	design		design
β function @ IP (e+/e-)	horizontal	m	4.5	2.7	1.7	0.1					1.2	1
	vertical	cm	4.5	2.7	3	10					5	1.5
Dispersion (η) @ IP	horizontal	m	0	0	0	0						0
	vertical	m	0	0	0	0				0	0	0
Max β_x (Arcs)		m	16			7.14						
Max β_y (Arcs)		m	16			7.14						
Max η_x (Arcs)		m	2			0.95						
Max η_y (Arcs)		m	2			0.95						
Max β_x (IR)		m				7.14						
Max β_y (IR)		m				7.14						
Max η_x (IR)		m	0	0	0	0						
Max η_y (IR)		m	0	0	0	0						
Beam size @ IP (e+/e-)	horizontal	μm	2000	1440		117					700	370
	vertical	μm	20	7.9		117					27	5.61
Betatron tunes @ I = 0 (e+/e-)	horizontal		5.15/5.11	5.15/5.11		4.097					5.8	6.5
	vertical		5.21/5.14	5.21/5.14		2.097					6.7	7.61
Natural chromaticities Δν/(Δp/p) (e+/e-)	horizontal		-8	-8	-6	-8.77					-11.3	-11.9
	vertical		-16	-16	-14	-8.79					-26.1	-25.4
Operation chromaticities (e+/e-)	horizontal		0/0	0	0	0.073						
	vertical		0/0	+0.5/+2.	0	0.05						
Transverse emittances @ I = 0 (e+/e-)	horizontal	nm	1000	770	600	136					580	140
	vertical	nm	10	1.54/2.31		136					23	2.1
Beam aspect ratio @IP	r=σy/σx	%	1	1		1					3.9	1.5
Coupling factor (e+/e-)	κ=εy/εx	%	1	0.2/0.3	.2/.3	1					4	1.5
Betatron coupling factor (e+/e-)	κβ=βy/βx	%	1	1		2					4.2	1.5
Natural Bunch length @ I = 0 (e+/e-)	σ_L	cm	3	2	2	3					5	1.5
Relative energy spread @ I = 0 (e+/e-)	σ_E/E	$x10^{-4}$	4	3		7					5.1	5
Momentum compaction (e+/e-)	α_c		0.03	0.028	0.018	0.0359					0.043	0.024
Transverse damping times (e+/e-)	τ_x	ms	36	36	36	2.71					28	25
Longitudinal damping time (e+/e-)	τ_s	ms	18	18	18	1.226					14	12.5
Turns/damping time	$x10^3$		120	120	120	34					35	31
Touscheck lifetime		hr				1.4						
Beam gas lifetime		hr										
Quantum lifetime		hr										
Total lifetime		hr									6-8	2.7
NOTES											@1.89 GeV	@1.89 GeV

Sheet 3b – Optics Parameters

LEPTON COLLIDERS		Units	CESR	CESR	CESR-C	PEP-II	PEP-II	KEKB	KEKB	LEP	LEP I	LEP II
(e+/e-)			design		design	design	BaBar	design	Belle	design		
β function @ IP (e+/e-)	horizontal	m	1.8	0.96	0.7	0.5	0.35/.41	0.33/0.33	0.59/0.58			
	vertical	cm	10	1.8	1.1	1.5	1.1/1.1	1.0/1.0	0.58/0.70			
Dispersion (η)@ IP	horizontal	m	2.2	0	0	0	0	0	0			
	vertical	m	0	0	0			0	0			
Max β_x (Arcs)		m	36	36	40	40/38		29/36	40/38			
Max β_y (Arcs)		m	34	34	40	100/95		27/31	28/27			
Max η_x (Arcs)		m	2.6	3.5	3.7	1/1.8		1.0/1.0	1.16/1.07			
Max η_y (Arcs)		m	2.6	3.5	3.7	1/1.8		1.0/1.0	1.16/1.07			
Max β_x (IR)		m	130	70	52	88/523		394/796	221/431			
Max β_y (IR)		m	65	85	45	111/443		439/1029	562/1159			
Max η_x (IR)		m	2.2	0	0	±1.2/.2		-0.46/0.44	-0.46/0.44			
Max η_y (IR)		m	0	0	0	.12/0.		0/0.024	0/0.024			
Beam size @ IP (e+/e-)	horizontal	μm	1110	470	400	157	147	74	103/121			
	vertical	μm	72	3.6	6	4.7	5	1.9	2.9/2.9			
Betatron tunes @ I = 0 (e+/e-)	horizontal		11.38	10.53	10.52	38.57/24.62	38.52/24.52	45.52/44.52	45.511/44.513			
	vertical		11.4	9.62	9.6	36.64/23.64	36.63/23.57	44.08/42.08	43.553/41.582			
Natural chromaticities Δν/(Δp/p) (e+/e-)	horizontal		-18	-15.8	-17	-60/-43		-71/-80	-73/-69			
	vertical		-31	-21.5	-23	-70/-57		-108/-102	-120/-109			
Operation chromaticities (e+/e-)	horizontal		2	2	2	+2/+2		+1/+0.3	+1/+0.3			
	vertical		2	2	2	+2/+4		+1/+2.5	+1/+2.5			
Transverse emittances @ I = 0 (e+/e-)	horizontal	nm	160	206	180	49/49	33/49	18/18	18/24			
	vertical	nm		0.67	1	1.5/1.5	2/2.5	0.36/0.36	0.78/0.69			
Beam aspect ratio @IP	r=σy/σx	%		0.8	1.4	3	3.4	2.6	2.8/2.4			
Coupling factor (e+/e-)	κ=εy/εx	%		0.3	1.3	3	6/5.1	2	7.5/5.0			
Betatron coupling factor (e+/e-)	κβ=βy/βx	%	5.5	2.1	1.6	3	3/2.7	3.3	1.05/1.15			
Natural Bunch length @ I = 0 (e+/e-)	σ_L	cm	4	1.8	1	1.2/1.15		0.4	0.54			
Relative energy spread @ I = 0 (e+/e-)	σ_E/E	$x10^{-4}$	8.9	6.75	8	7.7/6.1		7.0/6.7	7.3/6.9			
Momentum compaction (e+/e-)	α_c		0.0087	0.0115	0.011	0.0012/0.0024		0.00019	0.00034			
Transverse damping times (e+/e-)	τ_x	ms	7	23.7	50	62/37		43/46	43/46			
Longitudinal damping time (e+/e-)	τ_s	ms	3.5	11.9	25	30/19		22/23	22/23			
Turns/damping time	$x10^3$		2.8	9	20	8.4/5		4.3/4.6	4.3/4.6			
Touscheck lifetime		hr			4			5/ -				
Beam gas lifetime		hr			25			45/45				
Quantum lifetime		hr			>50							
Total lifetime		hr			2			3.7/7.4	2.1/4.3			
NOTES				Nov.2000	@1.89 GeV	Wigg ON	Wigg OFF					

Sheet 4a – RF Parameters

LEPTON COLLIDERS		Units	DAFNE	DAFNE	DAFNE	VEPP 2000	ADONE	ADONE	ADONE	BEPC	BEPC	BEPC-II
(e+/e-)			design	KLOE	DEAR	design	design	I generation	II generation	design		design
RF frequency		MHz	368.40	368.40	368.40	172				199.533	199.533	499.77
Harmonic number			120	120	120	14				160	160	396
Energy loss / turn (e+/e-)	U_o	MeV	0.009	0.009	0.009	0.0632				0.121	0.121	0.11
Energy loss / turn from wigglers (e+/e-)		MeV	0.005	0.005	0.005							
Number of cavities (e+/e-)			1./1.	1./1.	1./1.	1				1	1	1
Number of cells per cavity (e+/e-)			1./1.	1./1.	1./1.	1						
Max accelerating voltage (e+/e-)		MV	0.25	0.25	0.25	0.15						
Accelerating voltage (e+/e-)		MV	0.25	0.12/0.1	0.12/0.1	0.12				0.6-1.6	0.6-1.6	1.5
Cavity parameters (e+/e-)	R_S	(normal) MΩ	2	2	2	0.247						
	Q_0		33000	33000	33000	8800						
	β		4.5	4.5	4.5							
Number of klystrons (e+/e-)			1/1	1/1	1/1							
Cavity temperature regulation	Yes / No		Yes	Yes	Yes							
HOM dampers	Yes / No		Yes	Yes	Yes	Yes						
Harmonic cavity	Yes / No		No	No	No					No	No	No
Synchrotron frequency @ I = 0 (e+/e-)		kHz		28/30	28/30	30.73						
Synchrotron tune (e+/e-)	ν_s			0.008/0.01	0.008/0.01	0.0026				0.02	0.02	0.034
Synchrotron power/beam		kW				1.2						
NOTES												

Sheet 4b – RF Parameters

LEPTON COLLIDERS		Units	CESR	CESR	CESR-C	PEP-II	PEP-II	KEKB	KEKB	LEP	LEP I	LEP II
(e+/e-)			design		design	design	Babar	design	Belle	design		
RF frequency		MHz	499.77	499.77	499.77	476	476	508.9	508.9			
Harmonic number			1281	1281	1281	3492	3492	5120	5120			
Energy loss / turn (e+/e-)	U_o	MeV	6	1.14	0.2	0.8/3.6			1.64/3.48			
Energy loss / turn from wigglers (e+/e-)		MeV			0.2				0.82/0			
Number of cavities (e+/e-)			2	4	4	2/5		20/ 12(NC)+8(SC)	20/ 12(NC)+8(SC)			
Number of cells per cavity (e+/e-)			14	1	1	2		1	1			
Max accelerating voltage (e+/e-)		MV	8	10	10	3.4/14		10/18	10/18			
Accelerating voltage (e+/e-)		MV	12	6.28	10				8/13			
Cavity parameters (e+/e-)	R_S	(normal) MΩ	120									
	Q_0		32000	2.0E+09	2.0E+09			1.1E5(NC) 2E9(SC)	1.1E5(NC) 2E9(SC)			
	β		26.5					2.7(NC)	2.7(NC)			
Number of klystrons (e+/e-)			2	3	2			10/14	10/14			
Cavity temperature regulation	Yes / No		Yes	Yes	Yes			Yes	Yes			
HOM dampers	Yes / No		Yes	Yes	Yes			Yes	Yes			
Harmonic cavity	Yes / No		No	No	No	No	No	No	No	No	No	No
Synchrotron frequency @ I = 0 (e+/e-)		kHz	26	20	40	3.7/6.1			2.5/2.1			
Synchrotron tune (e+/e-)	ν_s		0.067	0.053	0.1	0.027/0.045	.0278/.0398		0.025/0.021			
Synchrotron power/beam		kW	500	390	36	1600/2600		4000/3800	2260/3660			